Synthesis, Characterization and Testing of Oxygen-Free Copper (OFC) Reinforced with NiTi/Graphene/Ti_3AlC_2 (Max Phase) and Prediction of Optimum Conditions

Yeshambel Yeshewendm Goshu

A Thesis Submitted to the Department of Mechanical Engineering

School of Mechanical, Chemical and Materials Engineering

Presented in Partial Fulfillment of the Requirement for the Degree of Master's in Manufacturing Engineering

Office of Graduate Studies

Adama Science and Technology University

May, 2024

Adama, Ethiopia

Synthesis, Characterization and Testing of Oxygen-Free Copper (OFC) Reinforced with NiTi/Graphene/Ti_3AlC_2 (Max Phase) and Prediction of Optimum Conditions

Yeshambel Yeshewendm Goshu

Main Advisor: Dr. Devendra Kumar Sinha

Co-Advisor: Dr. Getinet Asrat

A Thesis Submitted to the Department of Mechanical Engineering

School of Mechanical, Chemical, and Materials Engineering

Presented in Partial Fulfillment of the Requirement for the Degree of Master's in Manufacturing Engineering

Office of Graduate Studies

Adama Science and Technology University

May, 2024

Adama, Ethiopia

DECLARATION

First, I hereby declare that this Master Thesis entitled **"Synthesis, Characterization and Testing of Oxygen-Free Copper (OFC) Reinforced with NiTi/Graphene/Ti_3AlC_2 (Max Phase) and Prediction of Optimum Conditions"** is my original work. That is, it has not been submitted for the award of any academic degree, diploma or certificate in any other university. All sources of materials that are used for this thesis have been duly acknowledged through citation.

Yeshambel Yeshewendm Goshu

______________________ ______________________ ______________________

Name of Student Signature Date

RECOMMENDATION

We, the advisors of this thesis, hereby certify that we have read the final version of the thesis entitled **"Synthesis, Characterization and Testing of Oxygen-Free Copper (OFC) Reinforced with NiTi/Graphene/Ti_3AlC_2 (Max Phase) and Prediction of Optimum Conditions"** Prepared under our guidance by Yeshambel Yeshewendm Goshu submitted in partial fulfillment of the requirements for the degree of Mater's of Science in Manufacturing Engineering. Therefore, we recommend the submission of the final revised version of the thesis to the department following the applicable procedures.

Dr. Devendra Kumar Sinha

Main Advisor	Signature	Date
Co-Advisor	Signature	Date

APPROVAL PAGE OF THE THESIS

We, the advisors of the thesis entitled **"Synthesis, Characterization and Testing of Oxygen-Free Copper (OFC) Reinforced with NiTi/Graphene/Ti_3AlC_2 (Max Phase) and Prediction of Optimum Conditions"** and developed by Yeshambel Yeshewendm Goshu, hereby certify that the recommendation and suggestions made by the board of examiners are appropriately incorporated into the final version of the thesis.

__________________	__________________	__________________
Main Advisor	Signature	Date
__________________	__________________	__________________
Co-advisor	Signature	Date

We, the undersigned, members of the Board of Examiners of the thesis by Yeshambel Yeshewendm Goshu have read and evaluated the thesis entitled **"Synthesis, Characterization and Testing of Oxygen-Free Copper (OFC) Reinforced with NiTi/Graphene/Ti_3AlC_2 (Max Phase) and Prediction of Optimum Conditions"** and examined the candidate during open defense. This is, therefore, to certify that the thesis is accepted for partial fulfillment of the requirement of the degree of Master of Science in Manufacturing Engineering.

__________________	__________________	__________________
Chairperson	Signature	Date
__________________	__________________	__________________
Internal Examiner	Signature	Date
__________________	__________________	__________________
External Examiner	Signature	Date

Finally, approval and acceptance of the thesis/dissertation is contingent upon submission of its final copy to the Office of Postgraduate Studies (OPGS) through the Department Graduate Council (DGC) and School Graduate Committee (SGC).

__________________	__________________	__________________
Department Head	Signature	Date
__________________	__________________	__________________
School Dean	Signature	Date
__________________	__________________	__________________
Office of Post Graduate Studies	Signature	Date

ACKNOWLEDGEMENT

In the first place, I would like to express my deepest gratitude to the Almighty Lord for his countless blessings and unwavering patience, which sustained me throughout the completion of this thesis. I am particularly grateful to my advisor, Dr. Davendra Kumahar Sihn, for his invaluable guidance, support, encouragement and patience throughout my studies at Adama Science and Technology University. I would also like to extend my sincere appreciation to Dr. Getinet Asrat, my co-advisor, for his insightful discussions and support, and helpful suggestions. I would like to extend my sincere appreciation to the mechanical engineering department head Mr. Sntayoh Zeleke for his endless support. I would like to thank the Material Science and Engineering Department of Adama Science and Technology University for providing experimental work. Special thanks to Mr. Demeke Tesfaye, Mr. Kanate Sanbaba and Mr. Biruk Sisay from the material science and engineering department for their technical support and encouragement during experimental work.

Finally, I would like to express my immense gratitude and profound thanks to everyone who, in any way, supported me during my Master's studies at Adama Science and Technology University. If I have unintentionally omitted any names, please accept my sincere apologies.

TABLE OF CONTENTS

LIST OF TABLES

LIST OF FIGURES

LIST OF ACRONYMS AND SYMBOLS

ASTM	American Society for Testing and Materials
BH	Biker Hardness
CMC	Ceramic Matrix Composite
CNT	Carbon Nano Tube
Cu	Copper
CuMMC	Copper Metal Matrix Composite
GA	Genetic Algorithm
Gn	Graphene
HCI	Hydro chloric acid
MMC	Metal Matrix Composite
MPa	Mega Pascal
Ni	Nickel
NiTi	Nickle Titanium (nitinol)
OFC	Oxygen Free copper
OFHC	Oxygen Free Higher Conduction
OM	Optical Microscope
PMC	Polymer Matrix Composite
RAC	Refrigeration and Air-conditioning
RSM	Response Surface Methodology
SEM	Scanning Electron Microscope
SiC	Silicon Carbide
Ti	Titanium
Ti_2AlC	Titanium Aluminum Carbide
Ti_3AlC_2	Titanium Aluminum Carbide
TiC	Titanium Carbide
TiO_2	Titanium Oxide
UTM	Universal Testing Machine
Wt%	Weight percentage
XRD	X-ray Diffraction

ABSTRACT

*Oxygen-free copper (OFC) matrix-based composites are regarded as favorable materials for manufacturing and industrial applications due to their high electrical and thermal conductivity. However, pure copper has a low modulus of elasticity, poor strength and limited high-temperature applications. The main aim of this thesis work was to investigate experimentally the mechanical and metallurgical behavior of reinforced Oxygen Free Copper (OFC) metal matrix composite with a different weight percentage of reinforcement particles such as nitinol (5,10,7.5,5,0)wt%, Ti_3AlC_2 (10, 5, 7.5, 0, 5)wt% and Graphene (4)wt% fabricated through the Powder Metallurgy route at blending time of (24h), compaction pressure (60MPa) and Sintering temperature of (800 ℃. The microstructural behaviors of the developed sample were characterized through an Optical microscope (OM), Scanning Electron Microscope (SEM) and X-ray diffraction(X-RD)microscopy. The homogenous distribution of reinforcements was shown in the OM micrograph and some voids and grooves were observed in the SEM image. The physical, mechanical and tribological properties (density, porosity, hardness, compression strength, corrosion resistance, wear resistance and coefficient of friction) of the Cu/NiTi/Ti_3AlC_2 were investigated. The experimental test result shows that the density of OFC was decreased from 8.90 to 8.021g/cm^3, the hardness value was (168.6HV) improved by 104.4% by the addition of 10% NiTi, 5% Ti_3AlC_2 and 4% Graphene, the maximum compression strength was 403.34MPa at the 5%NiTi, 10% Ti_3AlC_2 and wear rate 7.518*10^{-6} mm^3/Nm with coefficient of friction of 0.29. From the experimental results, optimum properties of the OFC was obtained by the addition of NiTi/Ti_3AlC_2/Graphene. S1(Cu-10%Ti_3AlC_2-5%NiTi-4% Graphene) was selected using Grey Relational Analysis (GRA) for the prediction of optimum condition. The optimum result of Extrusion load 4.3575x10^8KN and Damage value 6.8061 were obtained at the optimum parameters of extrusion ratio 2, ram speed 1.5m/s and billet temperature of 850 ℃. through DEFORM 3D, Response Surface Methodology (RSM) and Genetic Algorithm (GA). This research work is expected to solve different industrial and engineering problems.*

Keywords: DEFORM-3D, Response Surface Methodology, Genetic Algorithm, Oxygen Free Copper, Extrusion, Max Phase particles

CHAPTER ONE

1. INTRODUCTION

1.1. Background of the study

Starting from the past few decades the need for economical, strong, lightweight, efficient and stiff materials has shifted the research trend from base alloy to composite materials (Sahu & Banchhor, 2016). Composites are materials produced from two or more materials having their own physical and mechanical properties and exhibiting a good combination of properties like strength, hardness, stiffness, ductility and toughness that are hard to obtain by a monolithic material (D. K. Sharma et al., 2019). Based on their matrix composite materials are classified into Metal Matrix Composites (MMCs), Ceramic Matrix Composites (CMCs) and Polymer Matrix Composites (PMCs) (Anil Kumar et al., 2016).

Metal Matrix Composites (MMCs) are the most promising materials and find their usage in a wide range of industrial applications such as automotive, aerospace, defense, marine, and electronics (Samal et al., 2023). Metal Matrix Composites (MMCs) based on steel, copper, magnesium, aluminum, bismuth, bronze, and titanium can be found in a wide range of industries. Of these, copper matrix composites are widely used because of their attractive combination of low cost, easy manufacturing, and good physical and mechanical properties (Şap et al., 2021).

Copper is a valued material due to its outstanding thermal and electrical conductivity, as well as its extraordinary ductility in a variety of applications. Copper and its alloys are a popular choice for many industrial and engineering applications because of these beneficial qualities. Copper and its alloys are widely employed in a wide range of applications, including air conditioning and refrigeration systems, automobile parts, sanitary pipes (including subterranean and underwater drinking water lines), and even lead frame materials in integrated circuits. Copper and its alloys do have one major disadvantage, though, which is that in some extreme situations, they are susceptible to corrosion and can quickly lose their mechanical strength. Copper-based equipment may completely fail as a result of this deterioration, which could result in very dangerous situations. Hince it is important to improve its mechanical and tribological properties (Kumar Singh et al., 2018).

Reinforcements are materials that possess excellent bonding capabilities and effectively enhance the strength of the base materials due to their remarkable physical and mechanical properties while maintaining low weight. And also reinforcement can be categorized as continuous or discontinuous fibers and particles (Selvam et al., 2021). These reinforcement materials are selected based on physical, mechanical and tribological properties, corrosion resistance, cost-effectiveness, availability and compatibility with the base material (Henry Ononiwu et al., 2019). Currently, the most widely used reinforcement materials for CMCs are the Carbides (Example, SiC, TiC, NbC, WC, TaC, B_4C), Oxides (Example, Al_2O_3, Y_2O_3, SiO_2, Cr_2O_3, TiO_2) and Borides (Example, TiB_2, ZrB_2)(Hamada et al., 2016).

Currently, three main fabrication techniques of metal matrix composites have been utilized. These techniques include liquid state, solid state, and in-situ fabrication. The solid state fabrication technique encompasses powder metallurgy and diffusion bonding.(A. Kumar et al., 2020). The fabrication process is selected based on matrix materials, reinforcement particles and their properties. And from those fabrication methods powder metallurgy is the most promising one for MMCs. (Sahu & Banchhor, 2016).

The production, processing, and shaping of different kinds of materials is referred to as powder metallurgy (PM) (Novak, 2020). The press and sintered method, which is used to create ferrous alloys, is the most popular PM technology. Copper (Cu) is commonly sinter-infiltrated into ferrous PM to enhance its mechanical properties. Molten copper penetrates the naturally porous PM structure during sinter-infiltration, filling pores and forming a denser, less porous material residue. One prevalent flaw in PM parts with copper penetration is Cu or incomplete infiltration. (Schotz, 2018). Powder production, mixing, compaction and sintering are the four main steps in powder metallurgy. Because powder metallurgy produces complicated shapes with good surface finish, near dimensional accuracy and efficient material utilization, it is an efficient method of producing copper metal matrix (Geethendra Kumar et al., 2018).

Secondary operations, such as plastic deformation and heat treatment, were employed to enhance the mechanical and tribological properties of the for metal matrix composite (Hamada et al., 2016). Hot extrusion, rolling, and forging are among the plastic deformation operations that can be utilized for metal matrix composites (M. K. Singh & Gautam, 2018).

Hot extrusion is performed at around 50-75% of the melting point of the metal to address defects or porosity that may have occurred during the initial fabrication. The primary objective is to enhance the strength, porosity, poor wettability and electrical conductivity of the copper-based composite (Tokutomi et al., 2015). The utilization of finite element modeling and simulation techniques has become necessary for assessing the impact of variable factors on the metal forming process before its actual implementation, to minimize the need for experimental trials. This is primarily due to the cost and time efficiency associated with these approaches. A wide range of commercial finite element codes, such as Forge, Hyper extrude, LS-DYNA, SUPERFORM, DEFORM, and ABACUS, among others, are available for simulating the metal forming process. Among these options, the DEFORM 3D Finite Element Analysis (FEA) has proven to be the most effective simulation method for metal forming. DEFORM -3D software for steady-state deformation using rigid plastic material. The extrusion load, stress, strain, strain rate, temperature and velocity distribution have been determined. A FEM-based program DEFORM 3D software consists of three special features Preprocessor, FEM simulation and Postprocessor (Workie & Tesfaye, 2021).

The focus of this work was on enhancing the mechanical and tribological properties of OFC material by Nitinol powder, graphene and max phase fabricated via powder metallurgy, characterized through (XRD, SEM and OM) and experimentaly investigated by various physical and mechanical tests. primarily to increase corrosion resistance, wear resistance and to improve compression strength. And to determine their post-deformation characteristics.

1.2. Application area of copper-based composite

The properties of high electrical and thermal conductivity, low density, improved fatigue strength, high hardness, non-magnetism, and high ductility make copper-based matrix widely used in a variety of industries (Şap et al., 2021). The excellent electrical and thermal, high plastic formability and ease of manufacturing of copper matrix composite inspire its usage in automotive, aerospace, construction and electrical and electronics industries (Zheng *et al.*, 2022). Copper-based materials possess strong electrical and thermal conductivity. Copper and its alloys are widely used in various engineering and industrial applications, such as air conditioning, refrigeration, automobiles, sanitary systems (underwater drinking water pipes), and lead frame materials for integrated circuits, because of these practical reasons.

Copper and its alloys have all of the aforementioned qualities, but in some harsh situations, they quickly lose their mechanical strength and corrosion resistance. This could result in the appliances made of copper completely failing, which could have negative effects. Hence, it becomes important to improve their anti-corrosion and mechanical strength in active working environments (Kumar Singh *et al*., 2018). Enhancing the mechanical and tribological properties of Oxygen-free copper material increases its fatigue life, corrosion resistance and service life of refrigeration and heat exchanger piping systems.

1.3. Motivation of this research

Currently, the worldwide annual copper production stands at approximately 24.8 million tons. In Ethiopia, the annual copper consumption is estimated to be 0.9 million tons, owing to its favorable mechanical properties, electrical conductivity, and ease of manufacturing. However, the limited strength, inadequate wettability, and reduced service life under high temperatures and corrosive environments have imposed restrictions on its utilization in diverse industrial applications. To address these challenges, the enhancement of mechanical, physical, and tribological properties of oxygen-free copper materials can be achieved through the incorporation of various ceramic reinforcements. Additionally, optimizing process parameters pertaining to the fabrication process and employing secondary operations can contribute to improve the overall performance of these material. Many research's use different ceramic-based reinforcement fabricated through powder metallurgy manufacturing techniques. To improve its mechanical and tribological properties such as hardness, compressive strength and wear resistance of the base materials. Also, secondary operations like heat treatment and plastic deformation are recommended by different researchers to improve the interfacial bonding, density, porosity level and electrical conductivity of the copper metal matrix composite. This thesis work looked at reinforcing oxygen-free copper with NiTi/Ti_3AlC_2/Graphene developed by powder metallurgy processing technique and simulated the developed sample via DEFORM 3D to determine the process parameter of hot extrusion to improve its mechanical, physical and tribological properties. The primary objective is to develop innovative materials that exhibit enhanced properties, enabling their utilization across a wide range of industrial sectors, including refrigeration, heat exchanger, aerospace, automotive, maritime and electronics.

1.4. Problem statement

To ensure the comfort of individuals and industrial sectors in different applications, such as residential buildings, industrial plants, electrical and electronic facilities, mining operations, and power generation stations, the usage of air conditioning units and refrigeration systems has become increasingly prevalent. Copper is often used in freezers and air conditioners for residential and public buildings and industrial sectors despite of its various advantages, including its thermal conductivity, economical, formable and ease of of manufacturing. Nevertheless, the continuous flow of fluids such as carboxylic acids, air, moisture and other organic refrigerants can lead to various issues with oxygen-free copper-made piping systems, including corrosion, pinhole formation, and cracking. These problems can result in refrigerant leakage, pipeline failure and equipment malfunction limiting the service life of the materials. In light of the challenges associated with OFC pipe for refrigeration and air conditioning systems, prompted to look for solutions that would enhance the material's mechanical and tribological characteristics while preserving its original functionality. The second major problem of pure copper is the limited service under high-temperature environments that restrict the usage of copper-made materials. The main goals of this study were to improve the mechanical and tribological characteristics of OFC-based materials used in refrigeration and air conditioning systems, to increase their shelf life and to improve their corrosion and wear resistance. This problem was solved by improving its physical, mechanical and tribological properties by introducing different ceramic reinforcements, optimizing the processing parameters and treating the fabricated material through post-deformation techniques.

1.5. Objectives

The study was designed to achieve the following general and specific objectives.

1.5.1. General objective

The general objective of this thesis work was Synthesis, Characterization and Testing of Oxygen-Free Copper (OFC) Reinforced with NiTi/Graphene/Ti_3AlC_2 (Max Phase) and Prediction of Optimum Conditions for the Post Deformation Behaviours of the developed material through DEFORM 3D.

1.5.2. Specific objective

To achieve the general objective of this research. The following specific objectives were designed:

- To fabricate Oxygen Free Copper reinforced with nitinol (NiTi), MAX phase (Ti_3AlC_2) and Graphene powders through a powder metallurgy manufacturing technique.
- To study the particle distribution, phase, morphology and crystal structure of the developed sample through Optical Microscope(OM), X-ray diffraction(X-RD) and Scanning Electron Microscopy(SEM).
- To determine the physical properties (density and porosity) and mechanical properties (hardness and compressive strength) of the developed material.
- To investigate the Tribological properties (wear rate and coefficient of friction) of the prepared material.
- To determine the corrosion resistance of the developed material.
- Numerical simulation of developed composite material for prediction of extrusion load, effective stresses and damage value.
- To determine the optimum value of hot extrusion process parameters for the minimum value of extrusion load, effective stresses and damage value.

1.6. Significance of the thesis

This thesis work was focused on the Synthesis, Characterization and Testing of Oxygen-Free Copper (OFC) Reinforced with NiTi/Graphene/Ti_3AlC_2 (Max Phase) and Prediction of Optimum Conditions of the post-deformation behavior of the fabricated sample through powder metallurgy. As a result, the work improved the mechanical and tribological properties, including compression strength, hardness, corrosion and wear resistance and increased the service life of Oxygen Free Copper materials. Therefore, it has crucial benefits in many industrial sectors such as refrigeration systems, air-conditioning, aerospace, automotive and manufacturing industries, and lead frame materials for integrated circuits. As well as it is important for individuals as well as other stakeholders at the national and international levels both academically and practically. It will improve the theoretical and applied knowledge of the research field for present and upcoming researchers.

1.7. Scope of the study

This thesis concentrates on the Synthesis, Characterization and Testing of Oxygen-Free Copper (OFC) Reinforced with NiTi/Graphene/Ti_3AlC_2 (Max Phase) and Prediction of Optimum Conditions for the post-deformation behavior of the fabricated sample. The sample was fabricated through the powder metallurgy manufacturing technique. Mechanical properties (hardness, compression strength) and tribological (wear and coefficient of friction) properties of the developed sample were investigated. A variety of experiments and testing were planned to be conducted for this study including investigation of hardness test, compression strength test, wear test and corrosion test and characterization of the materials particle distribution, phase, the morphology of the developed sample was also conducted through OM, X-RD and SEM respectively. Numerical simulation for the investigation of the deformation behavior of the developed sample was performed using the finite element analysis tool, DEFORM 3D. The best sample for the secondary operation was selected using the S/N ratio and Gray Relational Analysis Multi-objective optimization system. The Response Surface Method (RSM) and Genetic Algorithm (GA) determined the optimum input process parameter for the post-deformation process.

1.8. Thesis organization

This research paper comprises five chapters. The first chapter focuses on the introduction and background of the study, the problem statement, the study's objectives, the significance of the study, the scope of the study, and the organization of the thesis. The second chapter is about the theoretical and empirical review of copper-based reinforced MMC, providing a literature summary and identifying any gaps in the existing research. The third chapter covers the materials and methodologies employed, including the composition of the copper matrix and the weight percentages of NiTi, Ti_3AlC_2, and Graphene reinforcements, as well as the fabrication method and investigation process. The fourth chapter entails a comprehensive discussion and analysis of the experimental results of the mechanical and tribological properties, the microstructural behavior of the developed materials, and the simulation result of the post-deformation characterstics. Finally, the fifth chapter presents the conclusion of the study along with recommendations for future research endeavors.

CHAPTER TWO

2. LITERATURE REVIEW

2.1. Introduction to composite materials

Composites are materials produced by combining two or more materials having their own physical and mechanical properties that result in a better property than the individual materials used alone (Geethendra Kumar *et al*., 2018; Nagavally, 2016). Composite materials offer a unique advantage – they combine properties like strength, hardness, stiffness, ductility, and resistance to wear and corrosion that are hard to obtain with a monolithic material (D. K. Sharma et al., 2019). Composite materials are structural materials having a matrix phase and reinforcement phase (Sajan & Philip Selvaraj, 2021). Due to their promising attributes, they are well suited for a vast array uses across industrial sector, including aerospace, automotive, construction, sports, bio-medical, and numerous other fields (Rajak et al., 2019).

2.1.1. Classification of composite

Composite materials can be classified into two main categories such as composite based on their matrix and based on their geometry of reinforcement (Nagavally, 2016).

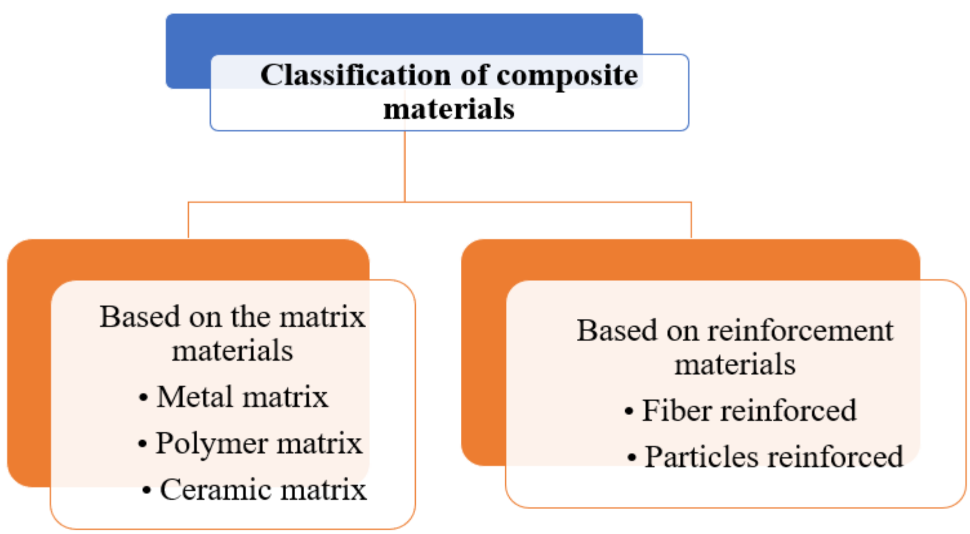

Figure 2.1: Classification of composite materials

2.1.2. Metal matrix composites(MMCs)

MMCs are the main type of composites in which the base material is metals including (Copper, Steel, Magnesium, Aluminum, Bismuth, Bronze, and Titanium) and the reinforcing elements are ceramic and organic materials including (SiC, TiC, NbC, WC, TaC, B_4C) (Sahu & Banchhor, 2016).

MMCs have received considerable attention in the fields of automotive, aerospace, defense, marine, and electronics as they are characterized by high strength, low density, and greater wear resistance, and they withstand elevated temperatures at corrosive media(Anil Kumar *et al*., 2016). Reinforcing materials like carbon nanotubes, carbides, oxides, and nitrides are incorporated into the metal matrix to give it significant performances in mechanical strength, wear resistance, and even damping properties. (Casati & Vedani, 2014).

MMC materials possess the following properties:

- High toughness and high impact strength
- High thermal and electrical conductivity
- Excellent machinability
- High strength
- Good specific stiffness

2.1.3. Copper metal matrix composite

Copper is a metallic substance having outstanding thermal and electrical conductivities and It is characterized by properties such as being soft, malleable and ductile comes at a cost. Copper finds abundant applications in various engineering fields and electrical applications such as power lines, electrodes and even aircraft and electronics packaging. unfortunately, the soft nature of copper can lead to a significant increase in wear rate at high temperatures, as well as poor strength and low hardness. These limitations typically restrict the utilization of copper in advanced engineering applications. (K. Singh *et al*., 2023). To address these challenges, copper-based metal matrix composites were developed by adding different ceramic reinforcements such as SiC, B_4C, Ti_2O, Graphene and carbon nanotube (M. K. Singh & Gautam, 2019). the reduced density, improved fatigue strength, strong corrosion resistance and increased specific strength of these composites make them desirable for various applications. (Gautam *et al*., 2018) Copper metal matrix materials are crucial in numerous engineering applications that demand higher temperature resistance and excellent microstructural stability (Jamwal *et al*., 2020). Copper finds a broad spectrum of applications, including heating and ventilation systems, solar energy systems, heat exchangers, condensers, bearings and in the automobile and marine industries (Karuppiah *et al*., 2017).

2.2. Fabrication process

There are numerous techniques for manufacturing composite materials (Nagavally, 2016). This fabrication process is selected based on matrix materials, reinforcement particles and their properties (Sahu & Banchhor, 2016). MMCs can be prepared by solid-state methods, liquid-state methods and in-situ fabrication techniques (S. Kumar *et al*., 2020).

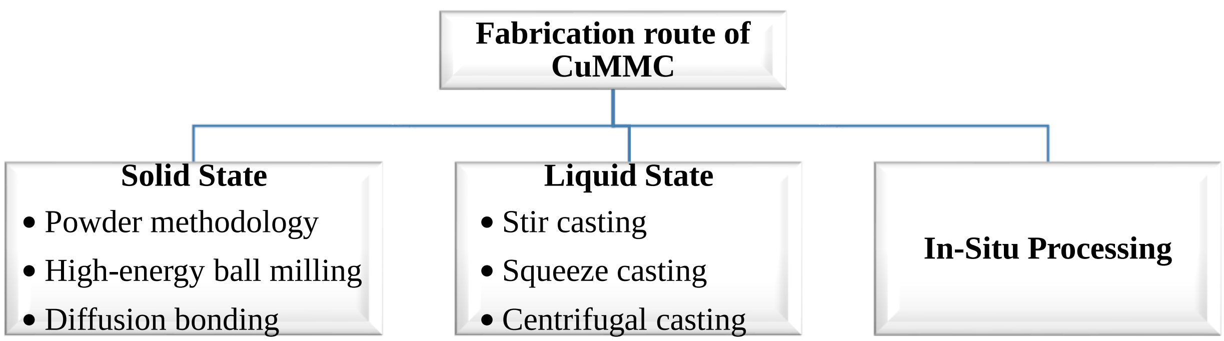

Figure 2.2: Fabrication Techniques of Metal Matrix

2.3.1 Liquid state processing method

It is a fabrication technique, in which the continuous phase (the base material) is found in the liquid state and then the discontinuous (reinforcement) is incorporated into it (Panwar & Chauhan, 2018). Liquid state fabrication is a crucial method for low-cost MMC preparation to improve wettability. However, a problem of reinforcement dispersion to attain homogenous matrix microstructure. Stir casting, squeeze casting and compo casting are the main categories of liquid state processing (A. K. Sharma et al., 2020).

2.3.2 Solid state fabrication of composite

The solid-state processing technique is the fabrication of particulate-reinforced MMCs done by mixing the powder of the matrix and reinforcements in several steps followed by consolidation (Panwar & Chauhan, 2018). To overcome the limitation of the liquid-state fabrication technique MMC composites are prepared using a solid-state fabrication technique below the melting point of the mixing materials (D. K. Sharma et al., 2019). Powder metallurgy, diffusion bonding, and friction stir processing are the major processing types of solid-state fabrication techniques (Patel et al., 2021).

2.3. Powder metallurgy

Powder metallurgy is the method by which finely powdered materials are compressed into a die of the intended shape. The particles of powder bind together to create a green compact. This compact is then removed from the die and subjected to high temperatures during sintering in a controlled atmosphere, which can be either neutral or reducing. This process is carried out to achieve the desired properties in a component (Geethendra Kumar et al., 2018). This technique is used for the preparation of discontinuous reinforced metal matrix with reinforcement (particulate, fiber, or whiskers) and metal as matrix material (Patel et al., 2021). This approach is economically advantageous when it comes to manufacturing intricate components with precise dimensional tolerances, resulting in minimal waste. However, it is not suitable for mass production due to the high expense associated with the powder used in the process (Sahu & Banchhor, 2016). There are four major steps involved in the powder metallurgy process (Geethendra Kumar et al., 2018).

2.3.1. Steps involved in powder metallurgy

There are four major steps involved in the powder metallurgy process(N. Kumar *et al*., 2020). They are:

- Powder Production
- Blending
- Compaction
- Sintering

2.3.2. Powder production

Powder is the basic material used in the powder metallurgy fabrication method and it can be found as pure elements, elemental blends and pure alloyed powders which were produced via atomization, electrolysis and chemical vapor deposition methods (Meignanamoorthy & Ravichandran, 2018).

2.3.3. Blending

Blending is the process of mixing powder to create a uniform distribution of particles and minimize porosity even if the powder has varied particle sizes. mixing was done through ball milling, bowl milling and pastel electric motor (Yoganandam *et al*., 2020).

2.3.4. Compaction

The next step after the blending powder is compacting the mixed powder which was done to give the necessary strength and shape for the blended mixture. Green compact is obtained by pressing the powder using hydraulic and mechanical presses on a suitable die and punch. The green compact strength and porosity are determined by compaction pressure. Consequently, raising the compaction pressure can decrease the porosity.

2.3.5. Sintering

In sintering, the green compacts are heated in a furnace under controlled atmospheric conditions to fuse the particles. This process is driven by material diffusion within the pores, which reduces voids and creates both physical and chemical bonds between the particles. These mechanisms significantly enhance the strength of the final material. Sintering was carried out at temperatures between 0.8 and 0.9 times the melting point of the base material (Venkatesh & Harish, 2015)

2.4. Reinforcement for CuMMCs

Reinforcing materials play a critical role in enhancing base materials properties, such as mechanical properties, thermal properties, electrical properties and tribological properties of the composite. The properties of metal matrix composite enhanced are corrosion properties, wear properties, and strength properties, and some of the reinforcement researchers identified are TiO_2, SiC, $TiB2_2$, WC, B_4C, AlN, fly ash and carbon nanotubes(Bharat & Bose, 2021).

Reinforcement Nano or Micro size ceramics can improve the base metals predominantly Al, Mg and Cu wear resistance, damping and mechanical properties (Casati & Vedani, 2014).

2.4.1. Graphene-reinforced copper matrix composite

The three-dimensional graphene network is the most crucial material for enhancing both mechanical and physical properties of a copper-based matrix owning to its fascinating properties such as high strength and elastic modulus, excellent thermal conductivity, good mechanical flexibility and large specific surface area (X. Zhang et al., 2020). The dispersion of graphene and its oxide greatly affects the mechanical and physical characteristics of copper-based metal matrix composite (Gao *et al*., 2016). To enhance the mechanical, physical, and thermal properties of metals like Al, Ni, Mg, Zn, Cu, and Ti, or their alloys, graphene was employed as a reinforcing material. (Guler & Bagci, 2020).

Huanchao Liua and Xinying Tenga (2018) investigated the addition of graphene to copper-based composite used in electrical contacts to solve the problem of interfacial bonding. The Cu/Gr composite is fabricated through powder metallurgy. SEM and EDS were used to determine its microstructure as well as particle distribution. Its mechanical, and physiochemical properties, hardens and relative density oxidation resistance were also tested. The result of this study showed that the maximum graphene additive is 0.2 wt%, the relative density is 90.0% and the hardness is 53.4HB.

Nazeer *et al*. (2019) investigated the powder metallurgy production method for the graphene and graphene oxide utilized in copper graphite composite. XRD and SEM were used to investigate the microstructure, surface morphology and phase analysis. The composite's Vickers hardness and thermal conductivity were also measured. The results of this investigation showed that using graphite and reduced graphene oxide with a Cu matrix in different mesh sizes led to a significant improvement. Cu-GP and Cu-RGO have hardness values of 67.58 HV and 71.2 HV, respectively, which are 54% and 61% greater than pure Cu's (44HV) hardness value. The best result is obtained at 1wt% and 3500µm of reduced graphene oxide and graphene. (Albartouli & Uzun, 2023) investigated the mechanical and electrical properties of graphene-reinforced copper matrix composite at wt% of (0, 0.5, 1 and 1.5) fabricated through powder metallurgy at different pressures (500, 600 and 700 MPa) and sintered in an argon atmosphere at different temperatures (850, 900 and 950°C).

The result showed a decrease in relative density up to 87.4%. The highest electrical conductivity was 76.59 IACS (0% GNS-500 MPa-950°C), while the lowest was 43.49 IACS (1.5% GNS-500 MPa-850°C) and hardness was increased up to 1%.

2.4.2. Nitinol(NiTi) reinforced copper matrix composite

Nitinol(NiTi) is one of the promising materials having the shape memory effect and best elastic properties which make it used in many applications such as aerospace, automotive and biomedical (Farber et al., 2019). Nitinol or shape memory alloy is one of the newest smart materials which can recover its original shape when heated above the critical temperature (Bellah et al., 2023).

R. Singh *et al*. (2021) focused on the fabrication of crack-free, dense Nitinol (NiTi) by a newly developed uniaxial compaction die and tested by solid work software simulation and investigated the effect of compaction pressure on mechanical properties and microstructure of nitinol. The sample was fabricated without a micro crack at 1910.82MPa compaction pressure. The microstructural characterization is done through Field Emission Scanning Electron Microscope (FESEM), EDS, and XRD. The results show that porosity is reduced (17.04% to 8.75%) by increasing compaction pressure (1273.88 to 1910.82 MPa). The density of 5.50 g.cm–3 at 1910.82MPa. Young's modulus and ultimate compressive strength increased from 4.07 to 6.93 GPa and 57.21 to 94.36 MPa, respectively, due to increased compaction pressure from 1273.88 to 1910.82 MPa.

Wang *et al*. (2019) were conducted to examine the relationship between the Cu/Ni coatings' microstructure and isothermal diffusion behavior, offering recommendations for creating high-performing surface coatings. To determine how isothermal diffusion affects surface performance, the coating's microstructure and isothermal diffusion behavior were thoroughly examined. Tribological characteristics and corrosion resistance were also assessed. Cu/Ni double coatings on TC4 alloy were created by diffusion bonding for 1, 3, 5, and 7 hours at 700 °C under isothermal treatment. Overall, this work shows that by utilizing an adequate diffusion period of 3 hours, the production of continuous refined laminar multiple layer and microstructure may considerably boost the surface performance, including the coating's resistance to wear and corrosion.

2.4.3. MAX phase (Ti_3AlC_2) reinforced oxygen-free copper

Ti_3AlC_2 is a member of a family of ternary carbides and nitrides, referred to as MAX phases, that all share a common chemical formula Mn+1AXn (where M is early transition metal, A is mostly group 13 and 14 elements, X is C or N, and N=1,2 or 3)(Benitez *et al.*, 2020). MAX phases display the distinctive combination of both metallic and ceramic encompassing exceptional resistance to wear and oxidation, thermal stability and remarkable thermal and electrical conductivity(Ali *et al*., 2023).

Mazaheri *et al*. (2021) investigated the microstructure of copper composite reinforced with max phase (Ti_2AlC) and MoS_2 using SEM and OM. Vickers hardness and dry wear tests were also used to determine the hardness and wear of the sample. The result of this study shows that the microhardness of the sample increases 38%-55% more than the pure copper substrate. The ultimate tensile strength of Cu/Ti_2AlC increases by 175%. Also, the average friction coefficient is decreased by 20%

Krinitcyn, (2022) Ti_3AlC_2 Nano Cu composites with a weight-to-AlC_2 ratio of 1:1 or roughly 4:1 by volume were investigated. Examine the effects of sintering temperature on the microstructure, density, mechanical properties, and electrical conductivity of the resultant material. The study's conclusion showed that a sintering temperature of 1050 °C yields the best possible balance of electrical conductivity, density, and strength. After sintering at 1050 °C, composites with 310 HV hardness, 4.67 g/cm3 density, 75% IACS electrical conductivity, and 573 MPa compressive strength were produced.

Jahani *et al*. (2023) The effects of the Ti_2SnC reinforcement and the friction stir welding setting on the mechanical, electrical, tribological, and microstructure characteristics of the Cu-Ti_2SnC composite were examined. This study's use of MAX phase reinforcing particles and execution of the extrusion process has improved the hardness, tensile strength, and wear resistance of the copper matrix by 128, 99, and 84%, respectively. Furthermore, the contribution of the adhesive wear mechanism decreases as the Cu-5 vol% Ti_2SnC composite hardness increases.

2.5. Effect of reinforcement on mechanical properties of copper

Karthick *et al*. (2019) prepared ceramic-reinforced pure copper metal matrix composite at different volume friction of SiC (5%, 10% and 15%) and constant volume friction of Graphite of (5%) through advanced wave sintering technique with varying temperature of 850 ℃ and 950 ℃. and the result of this study shows that optimum compressive strength is found at 15% of SiC and 5% Gr sintered at 850 ℃. The Vickers hardness test and the theoretical density were increased with increasing sintering temperature. Also, the mixing of composite powder results very fine homogenous distribution of the reinforcement throughout the matrix.

Tanaka *et al*. (2021) were conducted to look at how heat treatment affected OFC's low fatigue and tensile qualities for use in electric power equipment. For 20 minutes, the heat treatment is applied at 850 °C. A fatigue damage investigation using electron back-scattered diffraction (EBSD) was performed on heat-treated oxygen-free copper. The outcome shows that heat treatment increases grain size, relaxes strain through recrystallization, and lowers OFC's residual and tensile stresses. When the degree of compression increases..

Jomah *et al*. (2022) examined the mechanical properties and production characteristics of oxygen-free copper (C10200) produced by friction-crushing welding. All of the tests on the welded tubes were completed with the use of several tools, including tensile and hardness testers and microstructural characteristics were conducted via SEM and optical microscopy. Because the copper granules were coarse, the crush zone was found to have the lowest hardness. The sample's maximum hardness and tensile strength were 62HV and 105 MPa, respectively, at a tool rotation speed of 1500 rpm and a feed rate of 130 mm/min. The primary cause of failure, according to the results, is ductile fracture.

Özgün & Bulut (2020) focused on copper composite reinforced with different ratios of carbon Nanotube is studied. The hot pressing technique was used to fabricate the sample. The fabricated composite was characterized by different microstructural examinations and mechanical tests. The result showed that the carbon Nanotube was distributed homogenously, and the relative density of the sample decreased with increasing carbon Nanotube rate. A higher hardness value is obtained by adding a chromium specimen.

Alawadhi *et al*. (2020) Oxygen-free Cu was processed by ECAP for 1, 4, and 8 passes at room temperature and then further deformed by dynamic testing at 298 K using a strain rate of 10 s−1. The initial grain sizes after ECAP for 1, 4, and 8 passes were 16, 4.4, and 2.9 µm, respectively, and these values were reduced to 400, 330, and 300 nm by dynamic testing. were studied the effect of the initial microstructures induced by equal-channel angular pressing on the subsequent grain refinement and determined after test mechanical properties.

Lomakin *et al*. (2019) investigated aging kinetics for both coarse-grained and nanostructured by severe plastic deformation of Cu 2 wt% Be alloy. Differential scanning calorimetry (DSC) analyses were performed to determine the thermal analysis. XRD and TEM studies are carried out to determine the microstructure of the sample. As a result of this study, a significant hardening up to 450HV was observed in the nanocrystalline alloy after aging at 275 ℃ for 30 minutes. Annealing at 275℃ during 10 hours leads to further strengthening (yield stress up to 1300 MPa) attributed to the formation of a nanoscale dual-phase structure. A good thermal stability in the nanostructured alloy was also noticed.

2.6. Effect of reinforcement on tribological properties of copper

Chen *et al*. (2016) The mechanical, electrical, thermal, and friction properties of Cu/Ti_2AlC, which was produced by hot pressing at 900 °C for one hour, were examined. To determine its microstructural and phase distribution, XRD, SEM, and EDS are employed. The study's findings indicate that the relative density is greater than 96%. The resistivity of the surface increases progressively from 1.381×10^{-7} Ωm to 1.918×10^{-7} Ωm. The friction coefficient drops to roughly 0.15 from above 0.20. and solutions with 4% NaOH or 6.5% HNO3 have the highest corrosion rate.

J. Kumar & Mondal (2018) examined copper-based composite reinforced with graphite (5, 10, 15 wt%) prepared through the powder metallurgy technique. The samples were pressed at 637MPa and sintered at (900, 950, and 1050 ℃) for 2h. the microstructure of the sample was investigated using OM, SEM, and EDS. As a result of this study, The SEM picture from this investigation showed that the copper matrix phase and the graphite reinforcement phase with 5 weight percent had good interfacial bonding. The sintered density of the developed sample was slightly higher for the sample sintered at 1000 ℃. Wear rate and friction coefficient decreased with increasing graphite concentration. And the compression strength with 5% of graphite reinforcement.

Wang *et al*. (2019) examined the effects of Cu/Ni coating microstructure on isothermal diffusion to create standards for high-performing surface coatings. The isothermal diffusion behavior, microstructure, tribological characteristics (wear resistance), and corrosion resistance of the coatings were all thoroughly examined. On a TC_4 alloy, Cu/Ni double coatings were diffusion bonded using isothermal treatment at 700°C for 1, 3, 5, and 7 hours. The results show that by encouraging the development of a continuous, finely tuned, multi-layered microstructure, a suitable diffusion time of three hours in this case can greatly enhance surface performance, including wear and corrosion resistance.

Şap *et al*. (2021) carried out study on a copper hybrid composite reinforced with Ti-B-SiCp powder. Their mechanical properties and microstructural behaviors were investigated. The powder metallurgy method technique was used at a 2-8 wt% mixing ratio and sintered at 950-1050 ℃. EDX analysis is used to prove the existence of powder particles. As a result, the hardness increases at 6wt% reinforcement and sintered at 1050 ℃ and the maximum hardness was 77.517 HB. Relative density was obtained at 93%. And also wear resistance increased compared to pure copper.

2.7. Effect of reinforcement on corrosion properties of copper

Situmorang & Kawai (2018) explored the surface and cross-sectional perspectives for Cu_2O and H_2O, and the anti-nest corrosion on copper tubes in terms of variable potential and PH value. Using a polarization resistance curve, the ANC attack is further classified as a quick reaction system from an electrochemical perspective. In the steady state, the ant nest corrosion mechanism was controlled by the diffusion limiting current of Cu $(HCOO)_2$, iCu $(HCOO)_2$, and oxide film resistance. Ultimately, the amount of ANC on the copper tube shrank as a result of the pH solution dropping. Cu2O and H2O were the stable chemical species of the copper tube in the 103 ppm Cu (HCOO)2 solution at pH 5.5. The mechanism of ant nest corrosion is significantly influenced by the comproportionation and disproportionation response.

Lachowicz. (2020) presented the result of corrosion damage that occurred inside of the copper tube of a heat exchanger caused by carboxylic acid. and the corrosion occurring on the inner surface of the tubes made of Cu-DHP taken from a shell and tube heat exchanger has been described. Optical Microscope and Scanning Electron Microscope were used to investigate the anti-nest corrosion of copper tubes. The result of the investigation showed that the presence of internal stress facilitates the formation of surface cracks and promotes the development of corrosion. Then the risk of corrosion is reduced by smoothing the internal surface and minimizing contamination, especially carbon content.

Saber *et al*. (2022) investigated the impact of TiO_2 reinforcement and its effect on the mechanical and tribological properties of Cu Nano-composites. The powder metallurgy fabrication method was used to fabricate the Cu/TiO_2 Sample with (0, 4, 8, 12) wt%. The corrosion behavior was studied using a potentiodynamic polarization curve and electrochemical spectroscopy (EIS). Therefore, the hardness of the fabricated Cu/TiO_2 Sample increased from 53HV to 91HV by adding 12wt% and the experimental density of the fabricated sample was lower than the theoretical density of the sample. The corrosion current density (Icorr) of the test specimens made of copper nanocomposites was greater than the Icorr of pure copper.

2.8. Fabrication process of the Cu/NiTi/Ti_3AlC_2/graphene

Selection of the production route of metal matrix composite depends on many factors including the type and size of the matrix and reinforcement, the degree of microstructural integrity desired, and their mechanical, electrical, and thermal properties (Garg *et al*., 2019). Fabrication of the composite materials is focused on obtaining new material with improved mechanical and tribological properties compared to the monolithic material (A. K. Sharma *et al*., 2020). Many processes are used to fabricate metal matrix composite and these processes are classified into liquid-state processes and solid-state processes based on the temperature of the metallic matrix during processing (Sahu & Banchhor, 2016).

Powder metallurgy is the most flexible and versatile manufacturing technique in which powder particles are compacted into a die having the desired shape to produce semi-finished and finished products (Meignanamoorthy & Ravichandran, 2018). Powder production, mixing, powder compaction, and sintering are the four major steps of P/M (N. Kumar *et al*., 2020). The powder metallurgy method is efficient in producing copper metal matrix due to efficient material utilization, close dimensional tolerance, good surface finish, complex shape and suited moderate to high volume components (Geethendra Kumar *et al*., 2018).

N. Kumar *et al*. (2020) investigated the impact of powder metallurgy process parameters on the mechanical and electrical properties of SiC/Gr/Graphene with copper reinforcement and a weight fraction of (4-6)%.

Superior mechanical and electrical properties are obtained from matrix material (Cu) with small particle sizes of 3-5 µm. Cu-based composites were shown to exhibit improved mechanical and electrical properties in the ideal compaction pressure range of 550–650 MPa. Better mechanical and electrical properties of Cu-based composites are ensured by sintering temperatures between 800 and 900 °C and times between 60 and 90 minutes.

R. Singh *et al*. (2021) focused on the fabrication of crack-free, dense Nitinol (NiTi) by newly developed uniaxial compaction die and tested by solid work software simulation and investigated the effect of compaction pressure on mechanical properties and microstructure of nitinol. The sample was fabricated without a micro crack at 1910.82MPa compaction pressure. The microstructural characterization was done through Field Emission Scanning Electron Microscope (FESEM), EDS, and XRD. The results show that porosity is reduced (17.04% to 8.75%) by increasing compaction pressure (1273.88 to 1910.82 MPa). the density of 5.50 g.cm–3 at 1910.82MPa. Young's modulus and ultimate compressive strength increased from 4.07 to 6.93 GPa and 57.21 to 94.36 MPa, respectively, due to increased compaction pressure from 1273.88 to 1910.82 MPa.

2.9. Finite element analysis

Finite element analysis is a mathematical modeling technique for determining structural stress and analyzing for a specific result using a complex system unit (nodes) and elements that make a grid called a mesh (Srirekha & Bashetty, 2010). The analysis of structures and/or structural components with complicated geometry, materials, and loading conditions is a suitable application for finite element modeling (FEM), a flexible and universal numerical technique. (Mahapatra et al., 2016).

FEM is important to consider composites in some particular future such as material constative law, modeling and failure criteria (Reza Rezaie et al., 2020). In recent times, there has been an increased need for the utilization of finite element modeling and simulation techniques to predict the impact of variable parameters on the metal-forming process before actual production. This is primarily driven by the desire to reduce the number of experimental trials due to their associated costs and time constraints. To facilitate the simulation of the metal forming process, several commercial finite element codes are currently accessible, including Forge, Hyper extrude, LS-DYNA, SUPERFORM, DEFORM, and ABACUS, among others (Mohapatra & Maity, 2016).

2.9.1. DEFORM 3D

DEFORM-3D is an effective and efficient process simulation system specifically developed for the analysis of complex manufacturing processes involving three-dimensional (3D) flow. It serves as a valuable tool for accurately predicting material flow in processes characterized by significant deformation, thereby eliminating the need for costly and time-consuming shop trials. The simulation process involves a sequential execution of the pre-processor, run-engine, and post-processor, which collectively enable a comprehensive analysis. The pre-processor phase entails the creation of a new problem by arranging objects, defining the mesh, and specifying thermal and mechanical boundary conditions. The pre-processor utilizes these inputs to generate a database file that is subsequently processed by the simulation engine. In the run-engine phase, all numerical calculations about the generated database are performed. The time required to solve the problem depends on factors such as the number of elements and the numerical method employed. Finally, in the post-processor phase, the results obtained from the simulation run can be analyzed using a user-friendly graphical interface. This step allows for the visualization of the progressive changes in various factors within the material model through graphical presentations (Mohapatra & Maity, 2016).

2.10. Response Surface Methodology (RSM)

RSM comprises a group of mathematical and statistical techniques used in the development of functional relationships between some associated input variables and a respective output or responses of the interest (Khuri & Mukhopadhyay, 2010).

Response Surface Methodology employs a blend of metamodeling, specifically regression, and sequential procedures, such as iterative optimization. RSM encompasses a set of mathematical and statistical techniques that are instrumental in the modeling and analysis of various problems. Through meticulous experimental design, the primary aim is to optimize a response, which represents the output variable, that is influenced by multiple independent variables, also known as input variables. RSM is presented in Central Composite Design (CCD) and Box-Behnken Design according to continuous factors (Adiloğlu et al., 2016). Box-Behnken Design is a particular class of three-level fractional factorial designs used for studying quantitative variables. BBD is the most economical and efficient of than other three factorial designs (Riswanto et al., 2019).

Malghan et al. (2017) analyzed the process parameters of aluminum matrix composite for milling operation using response surface methodology central composite face-centered design to study the relationship between the input and output responses. The multiple regression technique was utilized to identify the interaction between the process parameters. The analysis demonstrated that spindle speed had a significant influence on all the responses, with feed rate and depth of cut following closely in terms of their contribution.

Aliemeke & Oladeinde (2020) investigated the process parameter of sand casting using response surface methodology box-Behnken design by conducting 27 experiments. The mathematical model for hardness was developed by multi-linear regression model. The results of the Statistical ANOVA test conducted showed that the mathematical model was adequate with an R2 value of 81.02% and an R2 (adjusted) value of 60.07%. The developed model has a p-value of 0.016 which indicates that the model was significant. The optimal values obtained for pouring temperature, vibration frequency, vibration time, and runner size are 700oC, 31.52Hz, 59.998sec, and 469.69mm2 respectively.

2.11. Genetic Algorithm (GA)

The genetic algorithm (GA) is a powerful optimization technique inspired by the principles of natural selection. It works with a population of potential solutions, mimicking the concept of "survival of the fittest." GA dynamically guides the search process by adjusting the probabilities of crossover, mutation, and selection.

This allows GA to modify the encoded information (genes) of candidate solutions, evaluate multiple individuals simultaneously, and potentially generate multiple optimal solutions (Katoch et al., 2021). In GAs, three operators are employed selection, crossover, and mutation. The selection operator involves the creation of a new population of individuals based on the fitness values of individuals from the previous generation. During crossover, specific parts of individuals are typically exchanged between two selected individuals. Mutation, on the other hand, involves randomly changing the values of particular genes (Slowik & Kwasnicka, 2020). The algorithms are straightforward to understand and the necessary computer code is relatively simple to write. Like the conventional approach, GA is selected due to its best to solve numerous complex problems that other approaches struggle with. GA is effective in reducing the computational workload. It has achieved successful applications in image processing, laser technology, aeronautics, robotics, and various other practical problem domains (Zainuddin & Samad, 2020).

Tiwari et al. (2024) used the Genetic Algorithm (GA) optimization tool in combination with the linear regression analysis to determine the best combination of hardness and tensile strength of AZ-61-graphene nanoplate (GNP) composite to correctly predict the effect of rolling process variable on to the hardness and tensile strength of the composite. The experimental results show that the maximum achievable hardness value happens to be 106.6 VHN and is very close to that predicted by GA, ~107.41 VHN. Similarly, the maximum experimental tensile strength is found to be 266.82 MPa whereas, the corresponding GA predicted value is seen to be 253 MPa.

Rajeswari & Amirthagadeswaran (2018) to determine the machining process parameters, multi-objective optimization employing the genetic algorithm was carried out. Using 27 experimental runs, the response surface approach box-Behnken design was used to create the mathematical model. A multi-objective genetic algorithm was used to determine the ideal parameter settings. Through confirmation studies, the expected best parameters were confirmed, and the outcomes were validated.

2.12. Literature summary

The surveyed literature shows that copper-based metal matrix composites have been reinforced with various ceramic materials, such as SiC, TiC, NbC, WC, TaC and B_4C materials. By adjusting the weight composition of the reinforcements and modifying different process parameters, both the physical properties (density and porosity), mechanical properties (compression strength, hardness and stiffness) and tribological properties(wear and coefficient of friction) of the base material were observed to change. These studies demonstrated that ceramic additives are materials that possess excellent bonding capabilities, and effectively enhance the properties of copper-based materials. Further research can be undertaken to investigate the impact of reinforcement composition, fabrication techniques, and input process parameters on the mechanical and metallurgical properties of copper-based metal matrix composites.

2.13. Research gap

Many studies have been conducted on copper-based metal matrix composites, which are known for their high electrical and thermal conductivity with good ductility. However, their limited application attributed to the low strength, porosity, poor wettability and limited high-temperature service motivated to reinforce copper with different ceramic materials. Existing literature has extensively explored on synthesis, testing and characterization of oxygen-free copper reinforced with various powdered reinforcements. Notably, there is no more research has been carried out on reinforcing oxygen-free copper with nitinol(NiTi), MAX-phase (Ti_3AlC_2) and Graphene powder particles and limited work was conducted on the simulation and parametric optimization of post-deformation behavior of copper-based composites. This study aimed to address the gaps by reinforcing oxygen-free copper with nitinol, graphene and Max phase for various applications particularly in refrigeration and air-conditioning. Additionally, prediction of Damage value, effective stress and extrusion load were conducted through the DEFORM 3D numerical simulation process and optimization of the input process parameter (Extrusion ratio, Ram speed and Billet temperature) was done through the Response Surface Methodology and Genetic Algorithm optimization technique.

CHAPTER THREE

3. MATERIALS AND METHODOLOGY

3.1. Introduction

This chapter covers the materials and their specifications utilized in the thesis work, the procedure for the powder metallurgy fabrication methods, the experimental procedures followed during sample testing, sample characterization and post-deformation analysis. The device and equipment used, the data analysis and process optimization techniques for the post-deformation process parameters were also assessed in this chapter.

3.2. Materials

It is essential to comprehend the characteristics and application of the matrix and reinforcing materials used in the research to guarantee the suitable selection of these materials for the proposed study. It is important to understand the necessary properties of the material used in refrigeration, air conditioning and other industrial applications. All mechanical, physical and thermal properties of the materials used in the analysis should be listed. After determining the required properties for the proposed application, (oxygen-free copper (C10200)) as a metal matrix and Nitinol (NiTi), graphene (Gr) and max phase (Ti_3AlC_2) powder as reinforcing materials were utilized to get the required properties under the consideration of applicability, availability, mechanical and physical properties and ease of manufacturing. The particle size of all the materials employed for this work was below 74µm. all the powders were obtained from NANO RESEARCH ELEMENTS, India.

3.2.1. Oxygen-Free Copper (OFC)

Copper is known as oxygen-free high conductivity copper, or OFC for short. It has less than 10 parts per million (ppm) of oxygen and at least 99.95% copper. The OFHC classification applies to several copper grades in the ASTM/SAE unified numbering system (UNS), including C10100, C10200, C10400, C10500, and C10700. Because of its exceptional ductility, high heat transfer capacity, and superior thermal and electrical conductivity, C10200 copper was the focus of this specific investigation.

The OFC concentration of the copper powder utilized in this study ranged from 81 to 91 weight percent (wt%), and its average grain size was less than 74μm. The purity of the powder was 99.99%. A range of advantageous mechanical and thermal characteristics are displayed by OFC, as detailed in the following section.

Table 3.1: Chemical composition of Oxygen Free Copper (C10200)(Alloys, 2014)

	Elements									
	Cu	Pb	Zn	Fe	P	Ag	As	O	Sb	Te
Min%	99.99									
Max%		0.0005	0.0001	0.0010	0.0003	0.0025	0.0005	0.0005	0.0004	0.0002

Table 3.2: Mechanical, physical and electrical properties of C10200 oxygen-free copper (according to ASTM/UNS(C10200 2.6., n.d.))

Properties	Value in metric
Code	C10200
Ultimate Tensile Strength	264-441MPa
Yield Tensile Strength	49-78MPa
Modulus of Elasticity	117MPa
Poisson’s Ratio	0.31
Specific Heat capacity	0.385J/g ℃
Thermal Conductivity	383-391W/m-k
Density	8.90g/cm^3
Hardness, Vickers	70-90HV
Melting Point	1083 ℃

3.2.2. Nitinol (NiTi) Reinforcement

Nitinol is a unique alloy belonging to the class of shape memory alloys (SMAs). It's composed of nearly equal amounts of nickel and titanium, with an atomic ratio of nickel to titanium close to 50:50. This remarkable material falls under the category of "smart materials" due to its exceptional ability to "return" its original shape and recover from plastic deformation. It possesses remarkable thermomechanical properties and good corrosion and shock resistance (Matli *et al*., 2020; Rondelli & Vicentini, 2002). For this work 5-10 wt% of nitinol powder with an average grain size of 74µm was utilized. It is found in powder form. It boasts the following mechanical properties.

Table 3.3:Summary of properties of nitinol (Jaronie Mohd Jani et al., 2013)

Mechanical Properties	Metric system
Ultimate tensile strength	895MPa
Tensile Yield Strength	70-140MPa
Young's Modulus	28-41MPa
Poisonous Ratio	0.33
Density	6.45g/cm^3

3.2.3. Graphene

Graphene is a 2D hexagonal lattice of carbon atoms extracted from graphite via chemical vapor deposition. It improves the mechanical properties of a base material while preserving the electrical conductivity. It is a self-lubricating material that easily enhances the wear of the composite. despite its electrical, thermal, and chemical properties, it has been gaining a unique interest in electronics, mechanical, and tribological systems (Hidalgo-Manrique *et al*., 2019). Moreover, it is the main material to enhance interfacial bonding between matrix and reinforcement. and for this work, 4 wt% of graphene powder was used. In general, graphene exhibits the following properties.

Table 3.4: Summary of properties of graphene (Guler & Bagci, 2020)

Properties	Value Metric System
Tensile Strength	125GPa
Elastic Modulus	1100GPa
Transparency	97.7%
Electrical Conductivity	$2.5x10^5$ S/m
Thermal Conductivity	5300W/mk
Density	2.25g/cm^3
Surface area	2600 m^2/g

3.2.4. MAX phase (Ti_3AlC_2)

Ti_3AlC_2 is a member of max phase families, exhibiting a unique blend of metallic and ceramic properties. The MAX phase exhibits high stiffness, strength, and good electrical and thermal properties all while maintaining a low density. Its electric and thermal conductivities are also good. Due of these special qualities, it has a large range of possible uses in the high-tech industry, such as parts of chemical equipment and abrasion-resistant components. and the most crucial material for structural application at high temperatures due to its high oxidation and corrosion resistance(Ali *et al*., 2023). For this work, 5-10 wt% max phase powder having an average grain size of 74µm was employed. It has the following properties.

Table 3.5:Summary of properties of MAX phase (Ti_3AlC_2) (Cai et al., 2017)

Properties	Metric system
Compressive Strength	670MPa
Flexural strength	432MPa
Density	4.25g/cm^3
Vickers Hardness	3.5GPa
Youngs modulus	297GPa
Shear modulus	124GPa

3.2.5. Die material (H13 Tool Steel)

H13 Tool Steel is a chromium-molybdenum hot-worked steel known for its versatility in various hot and cold work tooling applications. Its hot hardness allows it to withstand thermal fatigue cracking resulting from the repeated heating and cooling cycles in hot work tooling applications. H13 is frequently utilized in hot work tooling applications due to its good combination of high toughness and resistance to thermal fatigue cracking, which is also referred to as heat checking (Marashi *et al*., 2017).

Table 3.6: Elemental composition of die steel H-13 (Lei et al., 2022)

Element	Cr	Mo	V	Mn	Si	C	Fe
Wt%	5.12	1.26	1.03	0.39	0.98	0.42	Bal

Table 3.7: Properties of die steel H-13 (Markforged, 2018)

Properties	Value
Ultimate tensile strength	1420-1500MPa
Yield strength	800-1250MPa
Hardness	40-45HRC
Density	7.80g/cm^3
Melting Point	1427℃

3.3 Flow chart of the methodology

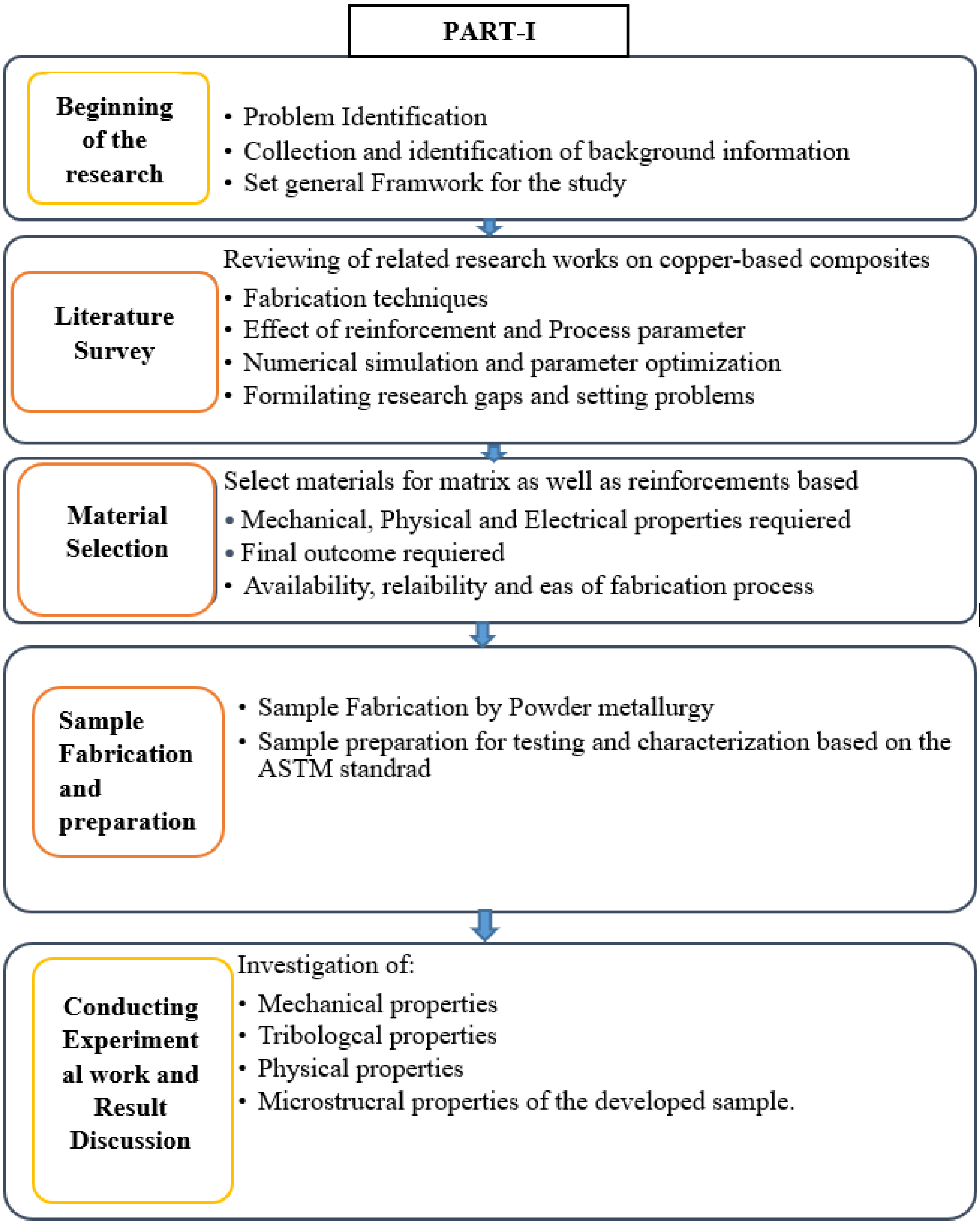

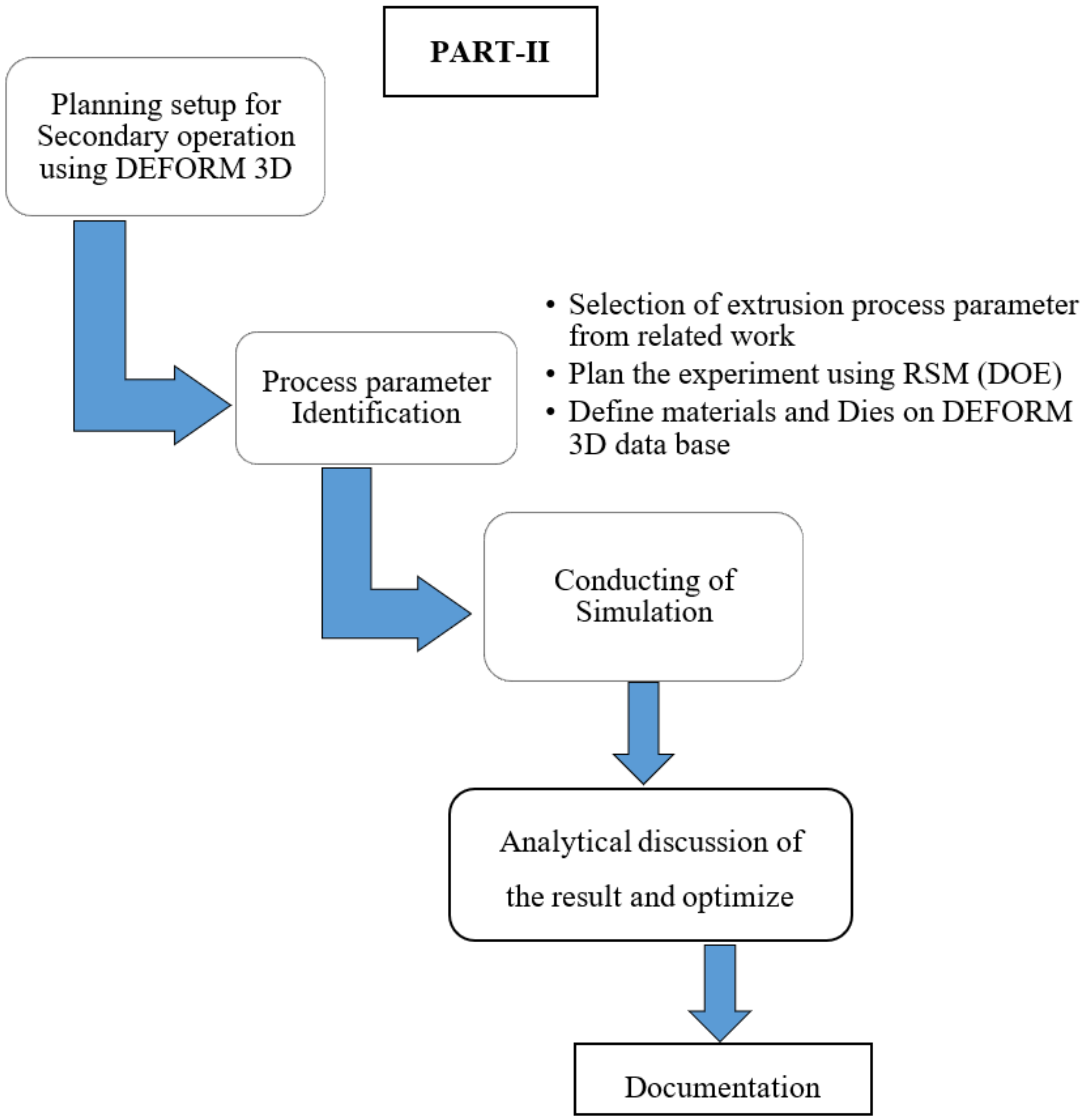

Figure 3.1: Flowchart of methodology

3.3.1. Materials selected for matrix and reinforcement

Oxygen-free copper (C10200) was selected as a matrix material for the composite despite its thermal and electrical conductivities, area of application, mechanical properties and ease of manufacturing. Nitinol (NiTi), Graphene, and Max phase (Ti_3AlC_2) were selected as reinforcement materials due to their special properties, such as, nitinol possesses remarkable characteristics such as superelasticity, shape memory, good corrosion and shock resistance. Graphene exhibits high electrical and thermal conductivities and it is the main material to enhance interfacial bonding between matrix and reinforcement. Ti_3AlC_2 exhibits both metallic and ceramic properties which possess high stiffness, strength and good electrical and thermal properties with low density.

3.3.2. Experimental design for sample fabrication

The developed sample was prepared using a solid-state powder metallurgy fabrication technique by compacting the mixed powder via a hydraulic press. There are three basic process parameters such as (compaction pressure, sintering temperature and sintering time) according to a number of research papers the optimum values of these process parameters are (60MPa, 800 ℃ and 60 min) respectively. The physical, mechanical and application of the developed composite depends on the weight composition of the matrix and reinforcement materials. The weight composition of the powders was selected based on the previous research papers the matrix was 81-91% and Powdered nickel-titanium (Ni-Ti) and Ti_3AlC_2 were added as a reinforcing material in different proportions of up to 10% each by weight. Graphene was added 4% to each sample.

Table 3.8: Experimental design for sample fabrication

Samples	Composition	Weight percentage
S1-Sample 1	Oxygen-free copper(C10200)	81%
	Nitinol (NiTi)	5%
	Graphene	4%
	Max phase (Ti_3AlC_2)	10%
S2-Sample 2	Oxygen-free copper(C10200)	81%
	Nitinol (NiTi)	10%
	Graphene	4%
	Max phase (Ti_3AlC_2)	5%
S3-Sample 3	Oxygen-free copper(C10200)	81%
	Nitinol (NiTi)	7.5%
	Graphene	4%
	Max phase (Ti_3AlC_2)	7.5%
S4-Sample 4	Oxygen-free copper(C10200)	91%
	Nitinol (NiTi)	0%
	Graphene	4%
	Max phase (Ti_3AlC_2)	5%
S5-Sample 5	Oxygen-free copper(C10200)	91%
	Nitinol (NiTi)	5%
	Graphene	4%
	Max phase (Ti_3AlC_2)	0%

Table 3.9: Powder metallurgy process parameters and their values

Parameters	Unit	Value
Compaction pressure	MPa	60
Sintering Time	min	60
Sintering Temperature	℃	800

3.3.3. Estimation of total amount (mass) of matrix and reinforcements

The amount of materials utilized to fabricate the Cu/NiTi/Graphene/Ti_3AlC_2 composite used for mechanical tests (hardness and compressive strength), wear test, microstructural tests, corrosion test and post deformation (hot extrusion) were estimated based on the ASTM standard of material tests. All the samples were fabricated with a diameter of 20mm and a length of 30cm. the weight fraction of the matrix and reinforcements were changed to determine their effect on the mechanical properties, physical properties and microstructural behavior of the developed samples. Based on the report of many scientific researchers the total amount of wt% was less than 30% to produce composites with low porosity and enhance the tribological and mechanical properties of the base materials. The wt% of all the reinforcements employed in this research work was determined according to various research surveys. Therefore, the maximum reinforcement for this research work was 19% (4% Graphene, 5-10% NiTi and 5-10% Ti_3AlC_2) which is less than 30% (Kalepu & Nallu, 2021).

The total volume of the cylindrical materials for this research work was determined according to eqn (3.1):

$$V = \frac{\pi D^2}{4} * L \tag{3.1}$$

where,

V= volume of the material in mm^3

D = diameter of the sample in mm

L= length of the sample in mm

Based on the ASTM standard the size of samples for various testing and characterization were given by Table(3.10).

Table 3.10: Dimension of samples each test based on ASTM

Tests	Diameter required	Length required
Hardness	12mm	15mm
Microstructural	12mm	15mm
Compressive strength	12mm	18mm
Wear rate	6mm	12mm
Hot extrusion	12mm	100mm
Clearance	12mm	10mm

From this table total length is given by:

=15mm(Hardness)+15mm(microstructure)+18mm(compression)+12mm(wear)+100mm(extrusion)+10mm(clearance)

= 170mm

D=20mm

V_T = Total volume of the material required

$V_T = \frac{\pi * 12^2}{4} * 170$ = 19226.547mm^3 or 19.227cm^3

For five samples V_T = 5*19.227cm^3 = 96.135cm^3

The total weight (in mass) of the matrix and each reinforcement were calculated according to eqn(3.2):

$$\text{Total mass } (m_x) = V_T * \rho_x * wt\% \qquad (3.2)$$

Total mass of Graphene($m_{Graphene}$) = 96.135cm^3*2.25g/cm^3*0.04 = 8.652g

Sample 1

Mass of OFC (m_{OFC}) = 19.227cm^3 * 8.90g/cm^3*0.81 = 138.607g

Mass of NiTi (m_{NiTi}) = 19.227cm^3*6.45g/cm^3*0.05 = 6.201g

Mass of Ti_3AlC_2 ($m_{Ti3AlC2}$) = 19.227cm^3*4.25g/cm^3*0.1 = 7.902g

Sample 2

Mass of OFC (m_{OFC}) = 19.227cm3*8.90g/cm^3*0.81 = 138.607g

Mass of NiTi (m_{NiTi}) = 19.227cm^3*6.45g/cm^3*0.1 = 12.401g

Mass of Ti_3AlC_2 ($m_{Ti3AlC2}$) = 19.227cm^3*4.25g/cm^3*0.05 = 3.951g

Sample 3

Mass of OFC (m_{OFC}) = 19.227cm^{3*}8.90g/cm^3*0.81 = 138.607g

Mass of NiTi (m_{NiTi}) = 19.227cm^3*6.45g/cm^3*0.075 = 9.301g

Mass of Ti_3AlC_2 ($m_{Ti3AlC2}$) = 19.227cm^3*4.25g/cm^3*0.075 = 5.927g

Sample 4

Mass of OFC (m_{OFC}) = 19.227cm^{3*}8.90g/cm^3*0.91 = 155.71g

Mass of NiTi (m_{NiTi}) = 19.227cm^3*6.45g/cm^3*0 = 0g

Mass of Ti_3AlC_2 ($m_{Ti3AlC2}$) = 19.227cm^3*4.25g/cm^3*0.05 = 3.951g

Sample 5

Mass of OFC (m_{OFC}) = 19.227cm^{3*}8.90g/cm^3*0.91 = 155.71g

Mass of NiTi (m_{NiTi}) = 19.227cm^3*6.45g/cm^3*0.05 = 6.201g

Mass of Ti_3AlC_2 ($m_{Ti3AlC2}$) = 19.227cm^3*4.25g/cm^3*0 = 0g

The total mass of the matrix and reinforcements of all the samples are calculated as:

Total mass of OFC(m_T(s_1+s_2+s_3+s_4+s_5)) = 138.607g +138.607g +138.607g +155.71g +155.71g =729.241g

Total mass of NiTi (m_T(s_1+s_2+s_3+s_4+s_5)) = 6.201g+12.401g+9.301g+6.202g =34.104g

Total mass of Ti_3AlC_2 (m_T(s_1+s_2+s_3+s_4+s_5)) = 3.951g+7.902g+5.927g+3.951g = 21.731g

3.3.4. Tools and equipment required

Table 3.11: Tools and equipment required

Equipment and Tools Needed	
Compaction Press	To fabricate the sample
Lath machine	To prepare samples for testing as per the ASTM standards.
Grinder/polisher	To prepare flat and smooth surface
Abrasive cutter	To section samples for testing
Chemicals	For etching and polishing
X-Ray Diffraction Microscope	To investigate the phase of the developed sample.
Scanning Electron Microscope	To determine the surface morphology of the developed sample
Optical Microscope	To investigate the microstructure of the developed sample
Universal Testing Machine	To determine the compressive strength of the developed composite
Vickers Hardness machine	To investigate the hardness of the developed
Pin On Disk apparatus	To determine the wear rate of the developed sample
Design Expert software	To develop the RSM experimental design
Minitab 21 software	It is a software package used to analyze and optimize various possess parameters and set the appropriate regression model for further analysis

MATLAB software	To solve the regression model and to provide the optimum solution
Potentiometer	To determine the corrosion behavior of composite

3.3.5. Fabrication of Cu/NiTi/Ti_3AlC_2/Graphene composite and procedure

3.3.5.1. Powder metallurgy fabrication technique

Appropriate procedures must be followed to develop a sample to achieve optimum mechanical properties, physical properties and tribological properties such as hardness, compressive strength, porosity, wear resistance and corrosion resistance of the sample.

The following steps were followed during Cu/NiTi/Ti_3AlC_2/Graphene sample fabrication by powder metallurgy process:

The powder particles dried in an electric oven at 100 ℃ and electronic weighing was used to measure the appropriate amount of each powder. zirconia milling balls are used to homogenously mix the matrix and reinforcement powders for 60min, A Compaction press (hydraulic press) was used to compact the mixed powder to produce a green compact, muffle furnace was employed to sinter the green compact at 800 ℃ to improve its density, porosity and enhance the bonding between the matrix and reinforcements. Oxygen-free copper (C10200) With minimum copper content of 99.95% and 74μm particle size powder was employed as a matrix material and NiTi consisting of nearly equiatomic proportion of Nickel and Titanium (i.e. 50:50 at. % Ni and Ti) with average grain size of 74μm, Graphene powder purity 99.9% and 74μm particle size and max phase (Ti_3AlC_2) purity of 99+% powders were utilized as reinforcement for the fabrication of the composite materials. Initially, the blended power was filled in the dies with the desired shape compacted at a compaction pressure of 60MPa and the green compact was ejected for the next process, the green compacts were sintered at a temperature of 800 ℃ the muffle furnace for 60min sintering time.

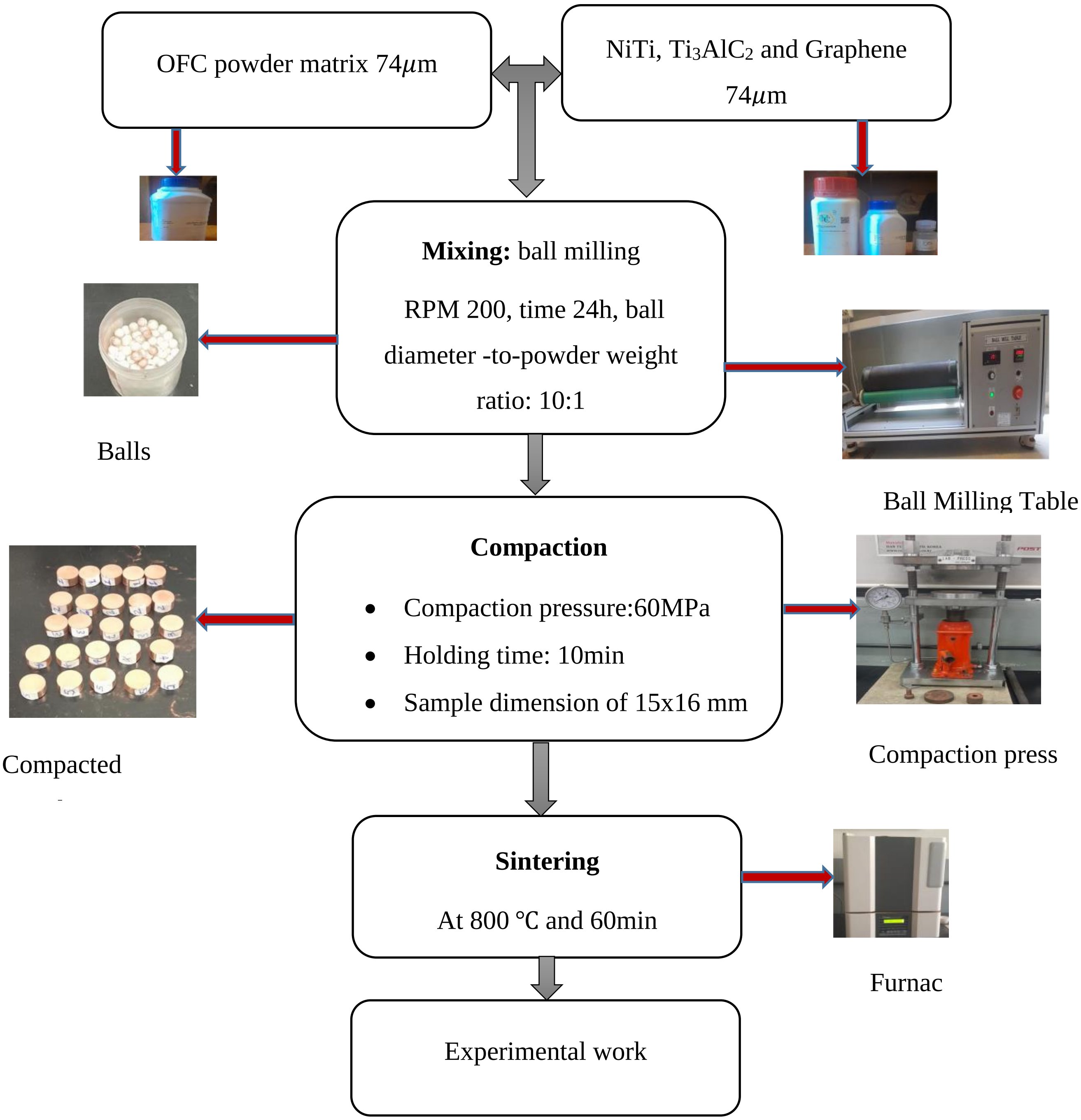

Figure 3.2: Flow chart of powder metallurgy

3.3.6. Specimen preparation for testing

All the specimens were prepared according to ASTM standards before conducting testing. The following procedures were followed:

3.3.7. Specimen preparation for microstructural characterization

The microstructural characterization was conducted on every fabricated sample using an Optical microscope to determine the distribution of the reinforcements and the grain size of the developed sample, A Scanning Electron Microscope was employed to determine the morphology of the developed sample and an X-ray Diffraction Microscope was employed to investigate phase, sample purity and crystalline size of the sample. This characterization provides information about grain size and shape, and the presence of micro defects. The steps followed to prepare the specimens are:

Figure 3.3: Specimen preparation (a) abrasive cutting (b) grinding and (c) Lath turning

I. Sectioning

Sectioning is the process of cutting the sample into the appropriate size and reducing the cross-section of the samples computable to the microscope stages. According to the sample size and shape sawing, grinding and machining techniques were employed at the suitable media to minimize the heat generation to avoid altering the material's microstructure.

II. Mounting

Mounting is placing the sectioned sample into epoxy resin material to provide support during subsequent grinding and polishing steps.

III. Grinding

Grinding is the process of smoothing the specimen to be examined to remove surface irregularity and the damage caused during sectioning. This process was conducted using coarse-graded media and then fine-graded girt. Synthesized copper matrix hybrid composites are ground using the sandpaper of gradually increasing scales of 400, 800, and 2000 grits.

IV. Polishing

In order to further refine the specimen's surface and eliminate grinding marks, a process known as polishing is used. To do this, the sample is rubbed with a diamond suspension while gradually reducing pressure to prevent the specimen from plastically deforming. The RB 204 Metpol-II Model polishing process was used.

V. Etching

Etching is a chemical procedure that targets several phases or material elements in the microstructure of the specimen to increase contrast between them. Additionally, it regulates the corrosion that happens on the sample's surface. Because of the variations in the electrochemical potential between the surface areas that display differences, chemicals (etchants) can dissolve certain areas of the specimen surface selectively. An etchant of 25 milliliters NH4(OH)2, 10 milliliters H2O2, and 25 milliliters distilled water was suggested for the polished Cu/NiTi/Ti_3AlC_2/Graphene hybrid composite. The specimen was immersed for 30 seconds.

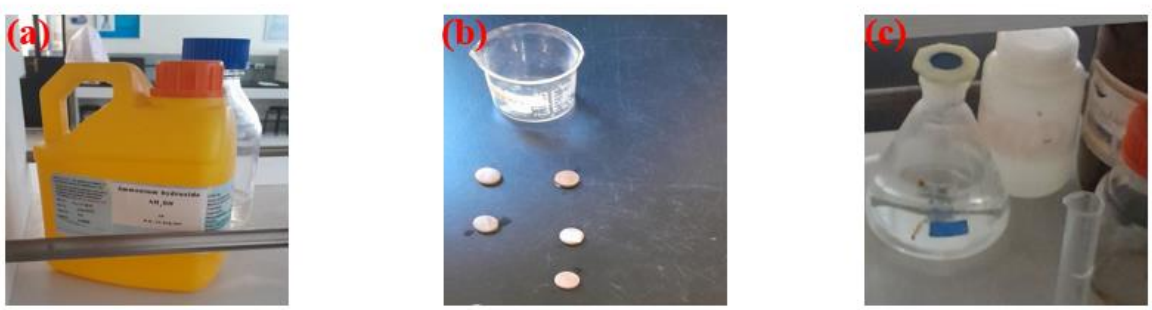

Figure 3.4: Photos of etching process (a) ammonia hydro oxide, (b) etched sample and (c) hydrogen peroxide

3.3.8. Measurement of physical properties (density and porosity)

The Experimental density theoretical density of each sample was calculated using a digital weighing balance with a tolerance of 0.0001. The theoretical density of the developed samples was calculated according to mixture law eqn(3.3)(Karthick *et al.*, 2019).

$$\rho_{theo} = (\rho_{matr}*V_{matr})+(\rho_{rein}*V_{rein}) \quad (3.3)$$

Where, $V_{matr,}$ and V_{rein} represent volume frictions of matrix and reinforces respectively. ρ_{theo} , $\rho_{matr,}$ and ρ_{rein}, are represents the theoretical density, matrix density and reinforcement density respectively.

The experimental density for the Cu/NiTi/Ti_3AlC_2/Graphene hybrid composite was calculated according to the Archimedes principle. First, the sintered sample was weighed in air (W_{air}) and then weighed in distilled water (W_{water}). The experimental density of the fabricated sample was calculated according to Archimedes principle equation (3.4) (Şap et al., 2021).

Figure 3.5: Photos of weighing balance (a) weight in air (b) weight in suspended water

$$\rho_{Exper} = \frac{m_{air}}{m_{air} - m_{water}} * \rho_{water} \quad (3.4)$$

Where m_{air} is the mass of the composite in air and m_{water} is the mass of the composite in distilled water, and ρ_{water} is the density of distilled water at 25 °Cwhichis 1g/cm^3.

The porosity of the developed composite was calculated using theoretical density eqn(3.3) and experimental density eqn(3.4) by eqn(3.5)(Saber *et al*., 2022).

$$P= 1- \frac{\rho_{Exper}}{\rho_{theo}} \tag{3.5}$$

Where P is porosity, ρ_{Exper} and ρ_{theo} are the experimental and theoretical density of the developed composite.

3.3.9. Hardness test

The resistance properties of the material to indentation and deformation under the applied load were measured using the Vickers hardness tester to determine the suitability of a material for various engineering applications. The Vickers hardness tester was employed, with a square-base diamond pyramid serving as an indenter. The sum of the angles between the pyramid's opposite faces is 136°. When the load is divided by the surface area of the indentation, the result is the diamond-pyramid hardness number (DPH), which is also referred to as the Vickers hardness number (VHN or VPH). In the Vickers hardness test, a diamond indenter and a small force are used to create an indentation on the material under examination. The depth of the indentation is then converted into the hardness value of the object. The vicker hardness value was calculated using equation (3.6).

$$HV = \frac{0.102*2F(\sin\frac{136^{\circ}}{2})}{D^2} \tag{3.6}$$

Where HV= Vicker hardness value in kgf/mm, D= is the average diagonal length of (d1 and d2) and F applied load for indentation.

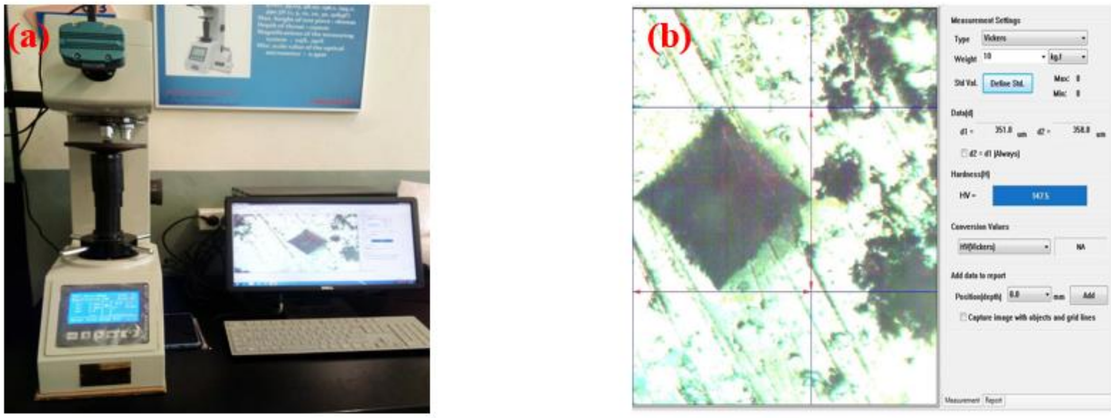

Figure 3.6: Vicker hardness test set up and (b) displayed results

3.3.10. Compression test

Compression strength is the mechanical properties of a material or structure to resist load that causes size reduction. Using a universal testing machine (UTM), the sample's compression strength was examined. Following the ASTME-9 standard, the specimen was prepared in a cylindrical shape with a length-to-diameter ratio of 2:1, or a diameter of 9 mm and a length of 18 mm, for the compression test. Then testing was conducted using UTM (WDW-100s) from AASTU. and the sample was compressed up to buckling deformation takes place.

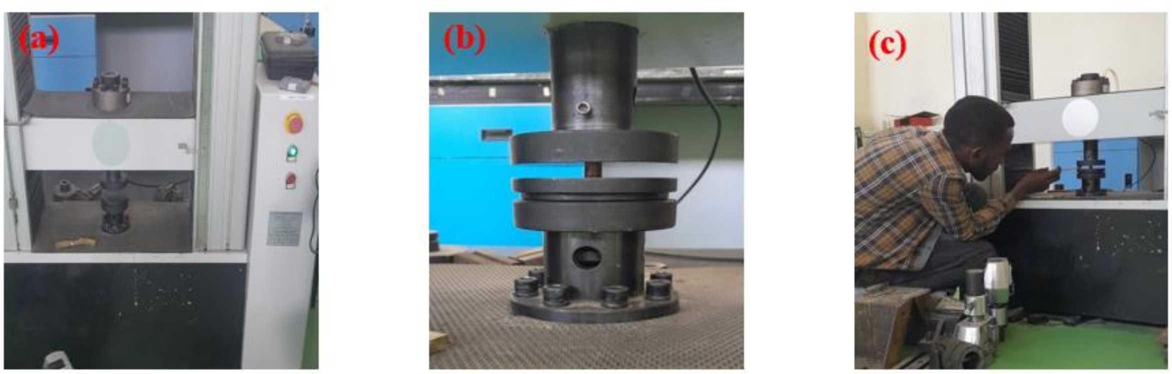

Figure 3.7: (a) UTM and (b) and (c) Sample setup

3.3.11. Corrosion test

The corrosion test of the developed sample was conducted by immersing the specimen in a 3.5% NaCl bath for 30 minutes. The specimens for the testing were 15mm in diameter and 7mm in length. First, the specimen was polished to remove any stray on the surface to make it mirror polished using 800 girt polishing emery paper and 12m diamond past on a double disc polishing machine. The working electrode was a copper-based composite specimen with an exposed area of 1cm2, an auxiliary electrode was graphite, and a reference electrode was a standard coamel electrode (SCE) or mercury. Tafel polarization curves offer electrochemical information, including corrosion potential (Ecorr), corrosion current density (Icorr), and corrosion rate (Cr). The corrosion potential (Ecorr) and corrosion current density (Icorr) were determined by analyzing the anodic and cathodic regions of the Tafel plots. By extrapolating the linear segments of the anodic and cathodic curves, the corrosion potential and corrosion current densities (Icorr) were obtained. The corrosion rate was subsequently calculated using a conversion formula (3.6).

$$\text{Corrosion rate(mpy)} = \frac{CEwIcorr}{\rho} \quad (3.7)$$

Where C= is the conversion constant (0.129), Ew = is the equivalent weight of the specimen (g) and = ρ is the density of the specimen (g/cm3).

Figure 3.8: Corrosion resistance test setup (a) Instrumental setup (b) Prepared ample

3.3.12. Wear test

Wear is a tribological discipline that measures the removal of material when two materials slide each other under an applied load. The amount of wear is determined by measuring the linear dimension of a specimen or by weighing the specimen before and after the test. Wear rate is the amount of material removed per unit of time. For this work pin on disk testing technique was used to test the wear mechanism of the developed copper hybrid composite under the recommended process parameters such as load, sliding speed and sliding distances(20N, 200rpm) (Thankachan *et al*., 2018). The procedure followed during the wear test.

Remove all dirt and foreign particles using nonchlorinated and cleaning agents

- Measure speciemen weight using balance to the nearest weight of 0.0001g
- Insert the disc perpendicular to the holding device
- Insert the pin specimen securely in its holder and adjust the specimen to 61° to the disc surface
- Add the proper mass to the system lever
- Start the motor and adjust the process parameter (load, rpm and distance)
- Finally, reweigh the specimen to the nearest 0.0001g.

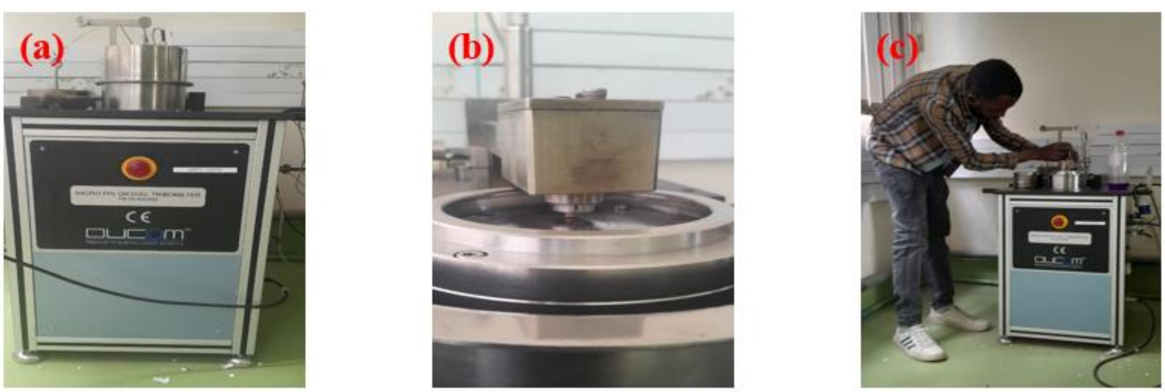

Figure 3.9: (a) Pin-on-Disc machine (a) and (b) Sample setup for wear test

Weight loss (ΔW), wear rate and sliding distance of $Cu/NiTi/Ti_3AlC_2$ were calculated using equations (3.8, 3.9 and 3.10).

$$\Delta W = W_f - W_i \quad (3.8)$$

$$W_R = \frac{\Delta W}{\rho * N * D_{sd}} \quad (3.9)$$

$$D_{sd} = 2\pi rNt \quad (3.10)$$

Where, ΔW= weight loss, W_f = final weight, W_i = initial weight, W_R = wear rate of the speceimen, ρ = density, N = applied loa, D_{sd} = sliding distance of the specimen, r = tracking radias, and t = holding time.

The coefficient of friction was calculated using equation (3.10).

$$\text{COF } (\mu) = \frac{\boldsymbol{F}}{\boldsymbol{f}} \quad (3.10)$$

3.4. Selection of best sample for secondary operation

One best sample was selected by using S/N ratio and Gray Relational Analysis(GRA):

3.4.1. Signal-to-noise ratio analysis

The Taguchi technique uses the signal-noise ratio (S/N) as a performance criterion for evaluating optimal sample attributes based on primary experimental findings and identifying process dependability in order to determine the best sample. S/N performance analysis The best equations are the nominal (3.12), the greatest (3.12), and the smaller (3.11).. In Taguchi optimization, the S/N ratio serves as a measurement for quality features and is determined in the following manner (Jebarose Juliyana & Udaya Prakash, 2020):

$$\frac{S}{N} = -10\log\left[\frac{1}{n}\sum_{i=1}^{n} Y_i^2\right] \quad (3.11)$$

$$\frac{S}{N} = -10\log\left[\frac{1}{n}\sum_{i=1}^{n} \frac{1}{Y_i^2}\right] \quad (3.12)$$

Where Y_i = i^{th} response n = total number of observation

The first equation is utilized for smaller is the better like corrosion rate and wear rate and the second equation is larger is the better employed for compression strength, hardness and electrical conductivities of copper-based hybrid composite.

3.4.2. Grey relational analysis

There are three main steps in the GRA analysis, the first step is normalizing or transformation done on a single input to uniformly distribute and scale the data into an acceptable level.

The followings are an equation for this: The equation was utilized in case of the larger is the better and smaller is the better respectively.

$$Z_{ij} = \frac{Y_{ij} - Y_{min}}{Y_{max} - Y_{min}} \quad (3.13)$$

$$Z_{ij} = \frac{Y_{max} - Y_{ij}}{Y_{max} - Y_{min}} \quad (3.14)$$

where Y_{ij} = the value obtained from experimental data Y_{max} = the maximum value from the experiment and Y_{min} = the minimum value from the experiment.

Compute the Grey Relation Coefficient for the normalized data using the following equation:

$$GRC_{ij} = \frac{\Delta_{min} + \partial\Delta_{max}}{\Delta_{ij} + \partial\Delta_{max}} \quad (3.15)$$

Where, i= 1, 2, ..., n-experiments and j== 1, 2, ..., m-responses GRC_{ij} = GRC for the ith experiment/trial and = absolute difference between Yoj and Yij, min = minimum value of and max = maximum value of is the distinguishing coefficient which is defined in the range $\mathbf{0 \leq \partial \leq 1}$.

Compute the Grey Relational Grade (GRG_i):

$$GRG_i = \frac{1}{m}\sum GRC_i \quad (3.16)$$

Where m is the number of response

The best sample with optimum properties was determined by selecting the maximum average GRG_i and the first-rank

3.5. Finite element analysis of hot deformation (Hot Extrusion)

The extrusion process is a secondary forming process to enhance the mechanical properties and microstructural behavior of metal matrix composite. However, modeling of an extrusion process parameter punch pressure, extrusion ratio, stress and strain distribution and material flow pattern is critical to manufacturing process design. To overcome these limitations and to obtain improved design and process parameters FEA based program DEFORM 3D V11 software was utilized to implement the simulation. It was typically intended to be used to analyze the forming process as well as for heat treatment for any metal forming process. This simulation was currently utilized for the process of hot extrusion of the developed sample (Cu/NiTi/Ti_3AlC_2/Graphene) hybrid composite. DEFORM -3D software for steady-state deformation using rigid plastic material. The extrusion load, stress, strain, strain rate, temperature and velocity distribution have been determined. A FEM-based program DEFORM 3D software consists of three special features such as Preprocessor, FEM simulation and Postprocessor (Workie & Tesfaye, 2021).

Pre-processor: used to build, compile, and alter the data needed for simulation analysis and to produce the necessary database files. A simulation engine reads the database file, does the real solution computation, and is utilized for the numerical calculations needed to assess the process and generate the result. When needed, the automatic mesh generation system in conjunction with the simulation engine creates a new FEM mesh on the workspace. Post-processor: used to read the simulation engine's database file, present the outcome graphically, and extract numerical data. This study applies commercial FEM-based software DEFOR-3D V11 to simulate the plastic deformation behavior during the copper hybrid composite hot extrusion process.

3.5.1. Input material data for DEFORM 3D

Accurate mechanical, thermal and physical parameters, such as density, elastic modulus, Poisson's ratio, specific heat capacity, thermal conductivity, and other appropriate data, are necessary for carrying out numerical simulations with DEFORM-3D software. Getting accurate flow stress and strain data for the materials being simulated is especially dependent on this. To assure the accuracy and dependability of the data it includes, it is imperative to make sure the material database being used is extensive and reliable (He & Bin, 2012). The simulation is conducted in a condition of plastic workpiece and rigid dies and follow stress is determined for the workpiece only as per the DEFORM 3D guideline. A compression test yields the flow stress data for the selected composite. For metals, the room temperature flow stress usually shows a dependence on the applied strain. Holloman's equation was developed based on empirical findings and provides an effective description of the flow stress's strain dependency.

$$\bar{\boldsymbol{\sigma}} = K\dot{\boldsymbol{\varepsilon}}^{\boldsymbol{n}} \tag{3.16}$$

Where $\bar{\boldsymbol{\sigma}}$ = flow stress $\dot{\boldsymbol{\varepsilon}}$ = true strain K= is material constant and n = is strain hardening constant

Generally, the flow stress is driven by the strain rate above the recrystallization temperature and approximated by the equation (3.11).

$$\bar{\boldsymbol{\sigma}} = C\dot{\boldsymbol{\varepsilon}}^{\boldsymbol{n}} \tag{3.17}$$

DEFORM 3D gives several equations of flow stress for new material of metal matrix composite and for copper-based hybrid composite power low equation is utilized as constitutive equation to determine flow stress during hot extrusion.

$$\bar{\boldsymbol{\sigma}} = C\bar{\boldsymbol{\varepsilon}}^{\boldsymbol{n}}\dot{\bar{\boldsymbol{\varepsilon}}}^{\boldsymbol{m}} + \boldsymbol{y} \tag{3.18}$$

Where, $\bar{\boldsymbol{\sigma}}$ = flow stress, $\bar{\boldsymbol{\varepsilon}}$ =effective plastic strain, $\dot{\bar{\boldsymbol{\varepsilon}}}$ = effective strain rate, n = strain exponent, m = strain rate exponent, C = is material constant and y = initial yield stress.

The initial yield stress is a point of limit at which the ending of elastic behavior and beginning of plastic behavior were generated from the stress-strain curve through a compression test. The true stress and strains were calculated by the following equation and the data obtained from the compression test.

$$\sigma = S(1+e) \tag{3.19}$$

$$\varepsilon = \log(1 + e) \tag{3.20}$$

Where $\boldsymbol{\sigma} =$ true stress, $\boldsymbol{\varepsilon}$ = true strain and S = engineering stress and e = engineering strain value

The strain hardening exponent and strain rate hardening exponent were calculated based on the following equation.

$$n = \frac{d\log(\sigma)}{d\log(\varepsilon)} \tag{3.21}$$

$$m = \frac{d\log(\sigma)}{d\log(\bar{\varepsilon})} \tag{3.22}$$

and strength coefficient was calculated by the equation of:

$$\log(\sigma) = \log(K) + n\log(\varepsilon) \tag{3.23}$$

3.5.2. Experimental design for simulation

The post-deformation (extrusion) process parameter was chosen with consideration for the desired end product attributes, processing effect, convenience of processing, and cost-effectiveness. A multi-objective optimization strategy based on the Response Surface Methodology (RSM) Box-Behnken approach method was used to analyze the effects of three hot extrusion process parameters on the intended sample size using Design Expert software. Extrusion temperature, extrusion ratio, and extrusion speed were among these variables. The die length was kept constant at 20 mm, and each die's and the billet's mesh size were determined using equation (3.17). Evaluating these parameters' impact on damage and the necessary load for extrusion was the goal.

$$\text{Mesh size} = \frac{Total\ volume\ of\ bar}{Volume\ of\ single\ element} \tag{3.24}$$

Table 3.12: List of mesh size of each element

Objects	Mesh size
Workpiece	58,177
Dies	35,255

Table 3.13: Process parameters of hot extrusion

Parameter	Unit	Levels		
		Level 1	Level2	Level3
Extrusion speed	m/sec	1	2	3
Extrusion ratio		2	3	4
Temperature	℃	750	800	850

3.6. Simulation of the post-deformation process

3.6.1 Design of die parts using solid work software

This round die was designed using mathematical cosine law for extruding material into a cylindrical shape.. Dies were designed based on a cosine die profile through solid work software and converted into STL file format. The die profile is given by the following cosine equation (3.18) (Endra & Pachalasiya, 2013).

$$F(X) = \frac{R_i+R_f}{2}+\frac{R_i-R_f}{2}\cos(\frac{\pi X}{L}) \quad (3.25)$$

Where, R_i = initial radius, R_f = final radius, L= die length and X = axis of extrusion.

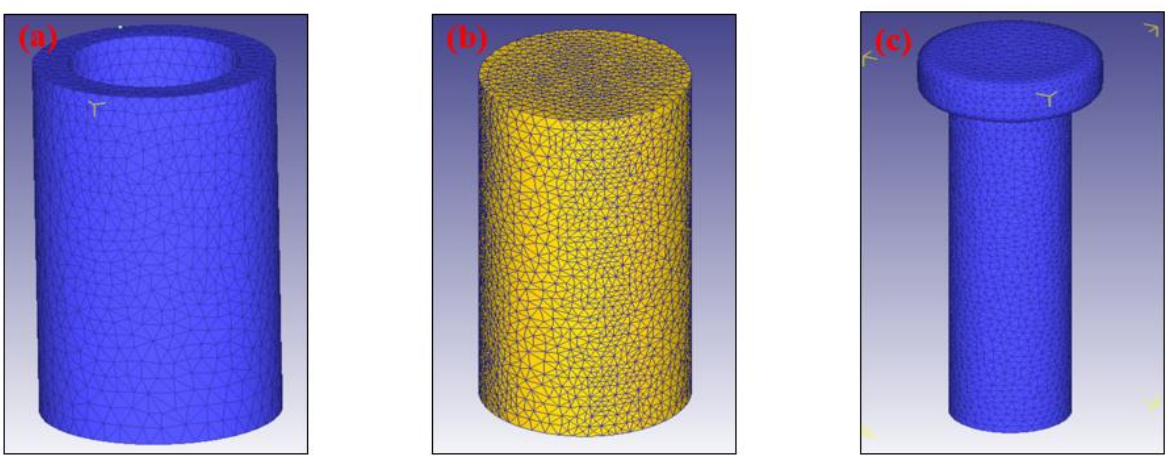

Figure 3.10: Meshed elements of a) Bottom die b) Work piece c) Top die

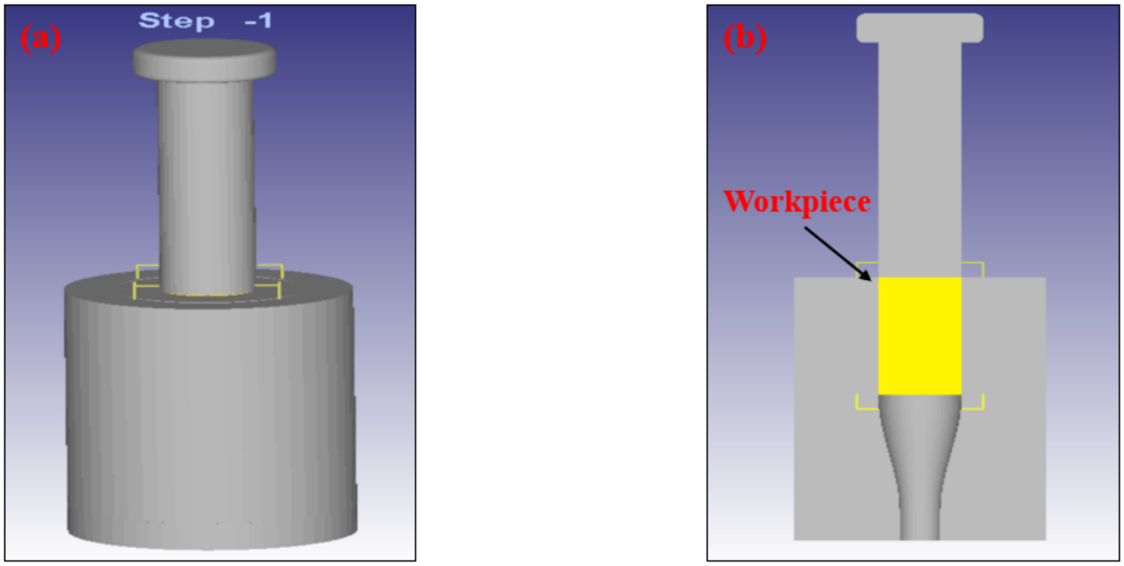

Figure 3.11: Simulation setup before extrusion a) 3D view b) Sectional view

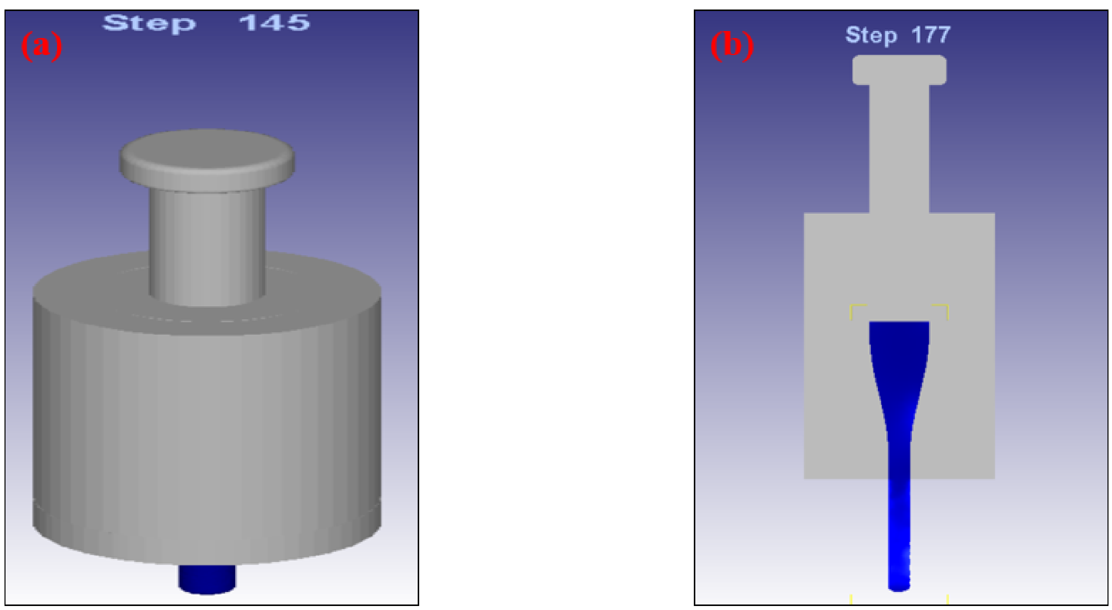

Figure 3.12: Simulation setup after extrusion a) 3D view b) Sectional View

3.7. Analysis and optimization of material behavior using Response surface methodology(RSM) and Genetic Algorithm(GA)

3.7.1. Response surface methodology (Box-Behnken)

Response Surface Methodology is an empirical optimization technique employed to assess the correlation between experimental outputs (or responses) and input variables denoted as X1, X2, X3, and so on. Typically, this approach is employed in conjunction with factorial design techniques like Box-Behnken designs and central-composite designs. RSM (box-Behnken design) is an experimental design of mathematical technique and statistical tool used to maximize or minimize or analyze variables interaction effect and optimize the output of the multi-variable process. RSM and BBD have the advantage of performing of analysis of several parameter process operations with fewer experimental trials, without having laborious and uneconomically run processes with all possible combinations. Box Behnken Design is one of the best RSM used to optimize the process parameters of the hot extrusion process variables (Nwobi-Okoye & Uzochukwu, 2020). The input variables are extrusion ratio, extrusion temperature and extrusion speed. Table () shows that the experimental design for those process parameters using Design Expert Software.

Table 3.14: Experimental design of all the process parameters

Runs	Extrusion ratio	Ram Speed (m/sec)	Billet Temperature (℃)	Responses (Damage value and Extrusion Load)
1	4	1	800	---
2	4	2	850	---
3	2	3	800	
4	3	1	850	
5	3	2	800	
6	2	2	850	
7	2	2	750	
8	4	2	750	
9	3	3	850	
10	4	3	800	

11	3	2	800	
12	3	3	750	
13	3	1	750	
14	3	2	800	
15	2	1	800	---

To predict the response, a mathematical model incorporating interaction terms, following a second-order polynomial as shown in equation (3.19) was utilized. From a geometric perspective, the response surface aligns with a response function.

$$Y = \beta_0 + \sum_{i=1}^{k} \beta_i X_i + \sum_{i,j=1}^{K} \beta_{ij} X_i X_j + \sum_{i=1}^{k} X_{ii}^2 + \ldots \tag{3.26}$$

Where, β_0, β_i, β_{ij}, β_{ii} are theoretical regression or polynomial coefficients.

Based on experimental values, the real regression coefficients are estimated as:

$$Y = b_0 + \sum_{i=1}^{k} b_i X_i + \sum_{i,j=1}^{K} b_{ij} X_i X_j + \sum_{i=1}^{k} b_{ii} X_{ii}^2 + \ldots \tag{3.27}$$

Where, Y= predicted-calculated response value, and b_0, b_i, b_{ij}, b_{ii} = real regression coefficients

3.7.2. Analysis of Variance (ANOVA)

The analysis of variance (ANOVA) was employed to ascertain which parameters exert a significant influence on the quality attribute. The statistical methodology of ANOVA is utilized to determine the impact of all control values. The percentage contributions of each control factor are employed to quantify their respective effects on the performance characteristics during the analysis of variance. In this analysis, a significance level of 5% was employed, corresponding to a 95% level of confidence. The ANOVA results indicate whether there exists a statistically significant variation in the output characteristics. In the ANOVA analysis, values less than 0.05 are considered significant, while values greater than 0.05 are deemed non-significant (Thankachan *et al*., 2018).

3.7.3. Genetic Algorithm (GA)

A search heuristic that mimics the process evaluation is the genetic algorithm. utilized to produce practical optimization results. A population of strings referred to as chromosomes, that represent potential solutions to an optimization problem grows toward better solutions in a genetic algorithm. The University of Michigan in Ann Arbor's Professor John Holland originally came up with the concept for these algorithms. Genetic algorithms (GAs) provide a number of benefits (Goldberg et al., 1989). GAs are very suitable for solving multi-objective problems (Nwobi-Okoye & Uzochukwu, 2020).

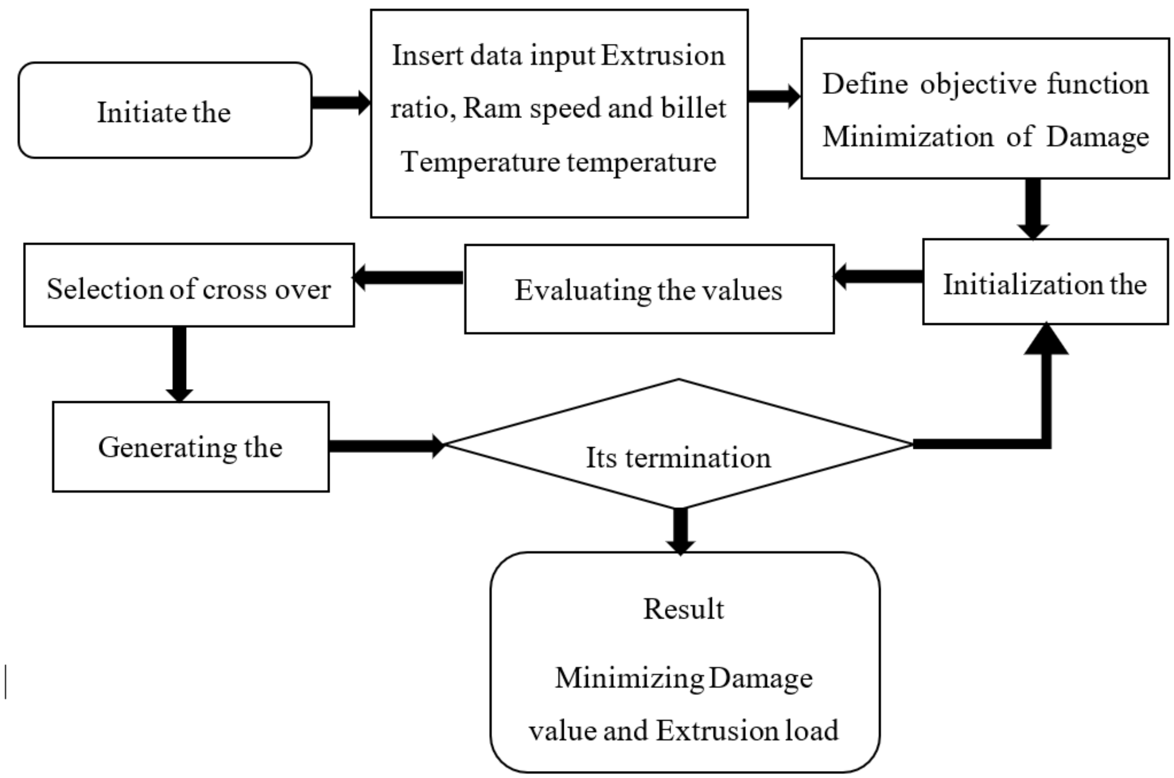

Figure 3.13: Conceptual model of GA optimization technique

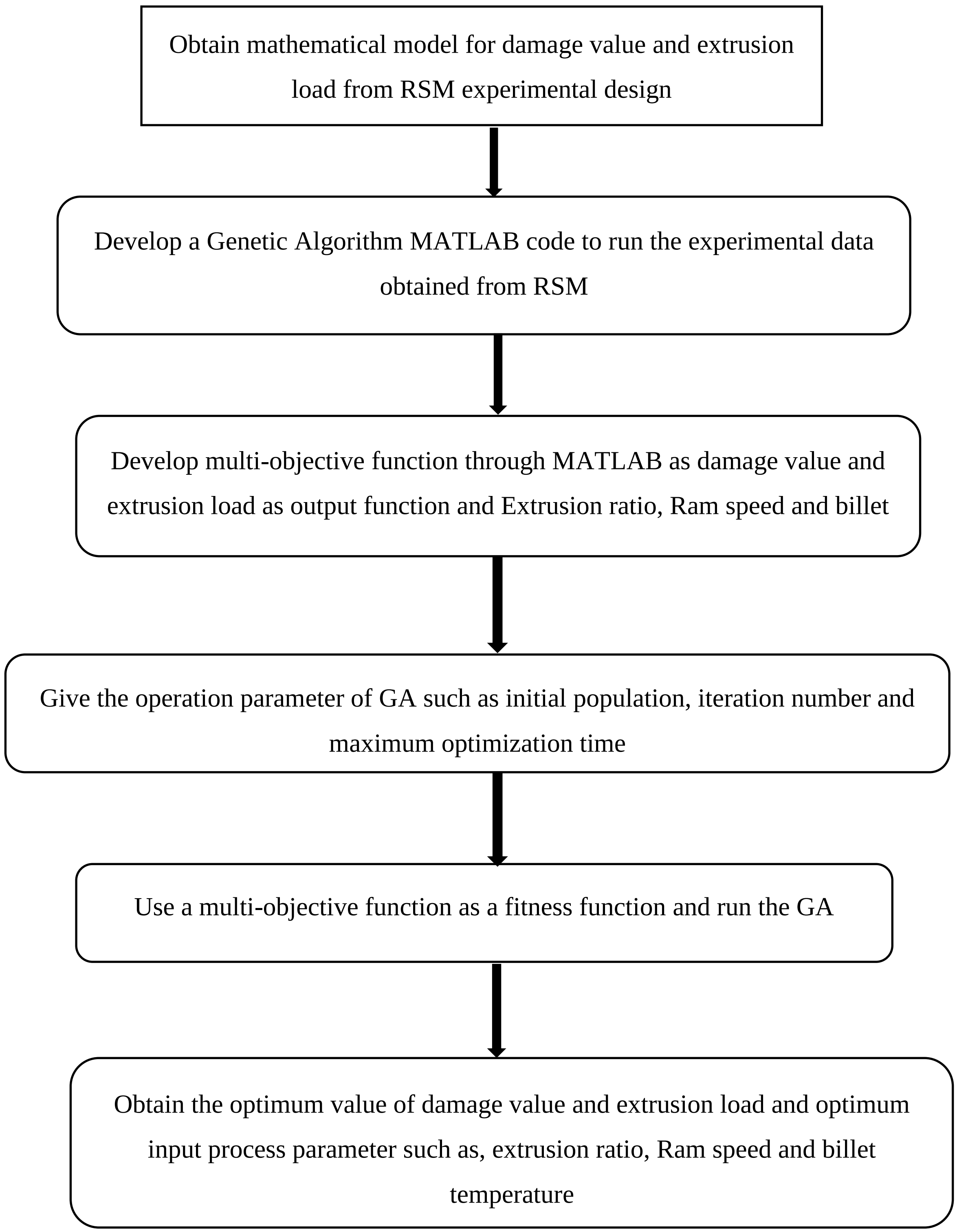

Figure 3.14 : GA flow chart

CHAPTER FOUR

4. RESULT AND DISCUSSION

4.1. Introduction

This section contains the primary analysis of the thesis's experimental results, as well as information on the prepared sample such as physical properties (density and porosity), mechanical properties (hardness, compression strength), wear and corrosion resistance tests, and microstructural characterization. Following the primary results, a sample with the best qualities was chosen for the post-deformation process. To predict the impact of the extrusion process parameters on the resulting hybrid composite, the sample was extruded by DEFORM 3D. The best value of (damage value and extrusion load) was found by analyzing and optimizing the data using RSM and GA. Finally, the obtained testing and characterization results were discussed in detail.

4.2. Design of the fabricated sample

Table 4.1 below shows the composition and sample designation of the developed hybrid composites through powder metallurgy fabrication technique at a constant process parameter compaction pressure(60MPa), sintering temperature(800 ℃) and sintering time(60min). The hybrid composite was fabricated mainly for the application of refrigeration and air-conditioning using oxygen-free copper (OFC) as a matrix and NiTi, Ti_3AlC_2, and Graphene as reinforcement materials.

Table 4.1: Sample designation of the developed composites

Sample Designation	Composition
S1	81%Cu+5%NiTi+10%Ti_3AlC_2+4%Graphene
S2	81%Cu+10%NiTi+5% Ti_3AlC_2+4%Graphene
S3	81%Cu+7.5%NiTi+7.5% Ti_3AlC_2+4%Graphene
S4	91%Cu+0%NiTi+5% Ti_3AlC_2+4%Graphene
S5	91%Cu+5%NiTi+0% Ti_3AlC_2+4%Graphene

4.3. Analysis of physical properties (density and porosity) of the developed sample

The density plot of the Oxygen-free copper matrix-based hybrid composite fabricated by varying the reinforcement weight fraction for five specimens is shown in Figure 4.1. the density of the developed composite was reduced because the densities of each reinforcement NiTi ($6.45 g/cm^3$), Ti_3AlC_2 ($4.25 g/cm^3$) and Graphene ($2.25 g/cm^3$) are less than the density of the base material which is ($8.90 g/cm^3$). (Ankur *et al.*, 2021) thought that density of copper matrix materials was decreased because low density of reinforcing materials over the matrix materials. (Ajagol *et al.*, 2018) reported that adding reinforcement materials to any base material creates a void in the synthesized sample due to reinforcing materials not uniformly dispersed throughout the matrix and the particle shape of the matrix and reinforcement being different and air entering between reinforcement and base materials during the fabrication process.

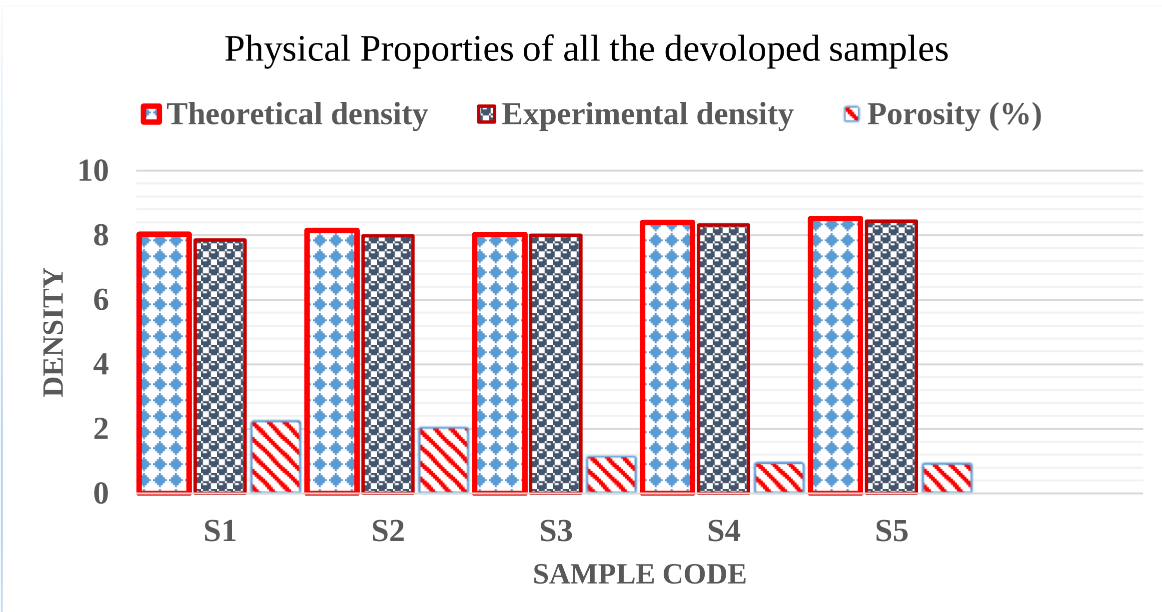

Figure 4.1: Physical properties of $Cu/NiTi/Ti_3AlC_2$/Graphene hybrid composite

Figure 4.1 shows that the theoretical density, experimental density and porosity of $Cu/NiTi/Ti_3AlC_2$/Graphene hybrid composite had been determined by equations (3.3,3.4 and 3.5). The density difference between theoretical and experimental values indicated the occurrence of voids and microholes on the fabricated sample. These voids and pores limit the mechanical and physical properties and performance of the hybrid composite(Reddy, 2007).

Table 4.2 shows the density of copper-based hybrid composites, both theoretical and experimental, along with their corresponding porosities, as determined by equations (3.3, 3.4, and 3.5) found in Chapter 3. Samples 4 and 5 had high densities because of their high copper contents, while sample 1 had low densities because of their high Ti_3AlC_2 (4.25g/cm3) composition. As the weight fraction of reinforcement grew, the produced sample's porosity increased as well. The porosity increase can be attributed to the possibility that during the manufacturing process, the reinforcing particles will serve as gas bubble nucleation sites. Because of their high reinforcement content (19) wt%, samples 1 and 2 exhibit high porosity values (3.349 and 4.135%), which are in line with reports by (Ajagol *et al*., 2018).

Table 4.2: Theoretical and experimental density and porosity of the developed sample

Sample	Theoretical density (g/cm^3)	Experimental density (g/cm^3)	Porosity (%)
S1	8.030	7.779	3.152
S2	8.151	7.822	4.042
S3	8.021	7.848	2.149
S4	8.394	8.230	1.954
S5	8.512	8.355	1.840

4.4. Hardness analysis for the developed hybrid material

Figure 4.2 shows the oxygen-free copper matrix reinforced with varying weight percentages of NiTi/ Ti_3AlC_2/Graphene reinforcement powder particles and its Vickers hardness value. Using a powder metallurgical processing method, five samples of Cu/NiTi/ Ti_3AlC_2/Graphene hybrid composite were prepared. The maximum and minimum Vickers hardness values were 132.3HV and 168.63HV, respectively. From Table (4.3) the Vickers hardness value of **sample 1** improved by 104.4% with the addition of 5wt% NiTi, 10wt% Ti_3AlC_2 and 4wt% Graphene reinforcement from the hardness value of pure copper this is due to the high reinforcement weight fraction of Ti_3AlC_2 particles which possess high hardness value 2.7 GPa (Ti *et al*., 2017). (Mazaheri *et al*., 2021) thought that an increase Ti_3AlC_2 MAX phase improved the hardness of pure copper metal matrix due to its hard ceramic and metallic properties.

According to the finding obtained by (Dadkhah *et al*., 2019), the micro-hardness of pure copper was enhanced because graphene enhanced the interfacial bonding between matrix and reinforcement. (Satishkumar *et al*., 2020) reported that the hardness value of copper-based composite increases by adding reinforcements. The result shows that the hardness value of Cu/ NiTi/Ti_3AlC_2/Graphene hybrid was maximum for S1 due to the high reinforcement continent (19%) and 10% of Ti_3AlC_2.

Table 4.3: Sample hardness at various trial values

Samples	Vickers hardness value (HV)				
	Trial 1	Trial 2	Trial 3	Mean value	%Improvement
S1	197.5	160.9	147.5	168.6	104.4
S2	127.2	157.6	112.2	132.3	60
S3	152.2	157.6	166.2	158.7	92.4
S4	151.3	150.1	142.3	147.9	79.3
S5	154.9	174.5	166.7	165.37	100.4

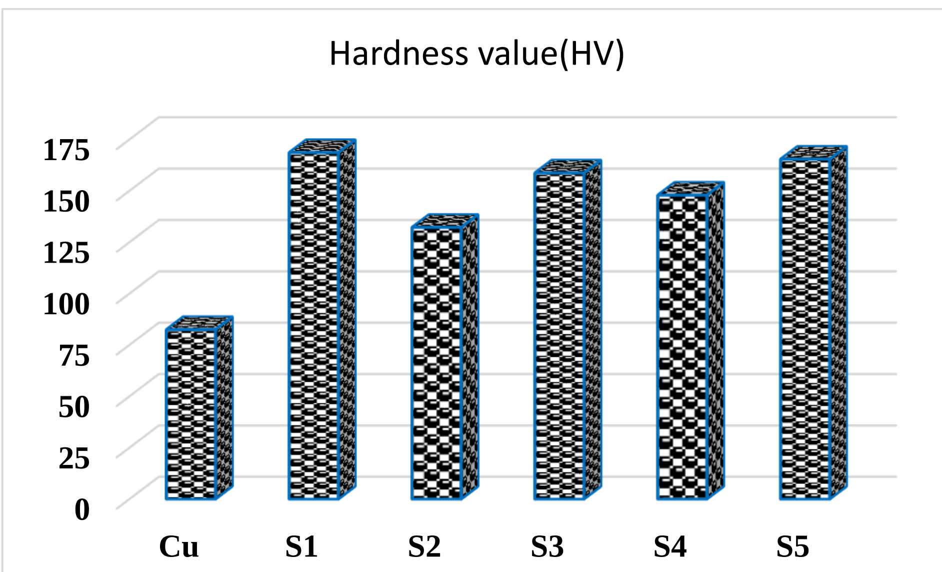

Figure 4.2: Hardness value of Cu/ NiTi/ Ti_3AlC_2/Graphene composite

The hardness improvement of the developed composite was calculated using equation (4.1), where HV_i = initial hardness value of Oxygen Free Copper which is 82.5HV and HV_f = Final hardness value of the developed hybrid composite. According to UNS C10200 has an average Vicker value which is HV_i = 82.5HV.

$$\text{Hardness improvement} = \frac{(HV_f - HV_i)*100\%}{HV_i} \quad (4.1)$$

4.5. Compression test

The developed sample was put through compression tests using the universal testing machine. Plotting of the compression strength result bar chart utilizing testing data is shown in Figure 4.3. The ultimate compressive strength for samples (1, 2, 3, 4, and 5) is 403.34, 392.38, 386.81, 365.07, and 386.25MPa respectively. This result shows that adding NiTi/Ti_3AlC_2/Graphene reinforcement particles significantly increases the compressive strength of pure copper which is (330MPa) by 22.2% due to hard ceramic particles of NiTi and Ti_3AlC_2 powders and Graphene powder enhancing the bonding between matrix and reinforcing particles. (Mazaheri *et al*., 2021) reported that the ultimate strength of pure copper reinforced with Ti_3AlC_2 MAX phase increased from 75-175%.

(Lu *et al*., 2022) thought that the compressive and tensile properties of copper matrix reinforced by Graphene improved because of the uniform distribution of graphene throughout the matrix. The result by (C. Chen *et al*., 2024) revealed that the compressive strength of pure copper was enhanced by the addition of Ti_3AlC_2 MAX by reducing the tendency for agglomeration and promoting a more uniform distribution of the reinforcing phase throughout the composite. From the test results, sample 1 has high compression strength due to the high content of Ti_3AlC_2 MAX phase which has high compression strength of 764 MPa (X. H. Wang & Zhou, 2002). And sample 4 has small compressive strength small percentage of reinforcements and 0% of Ti_3AlC_2.

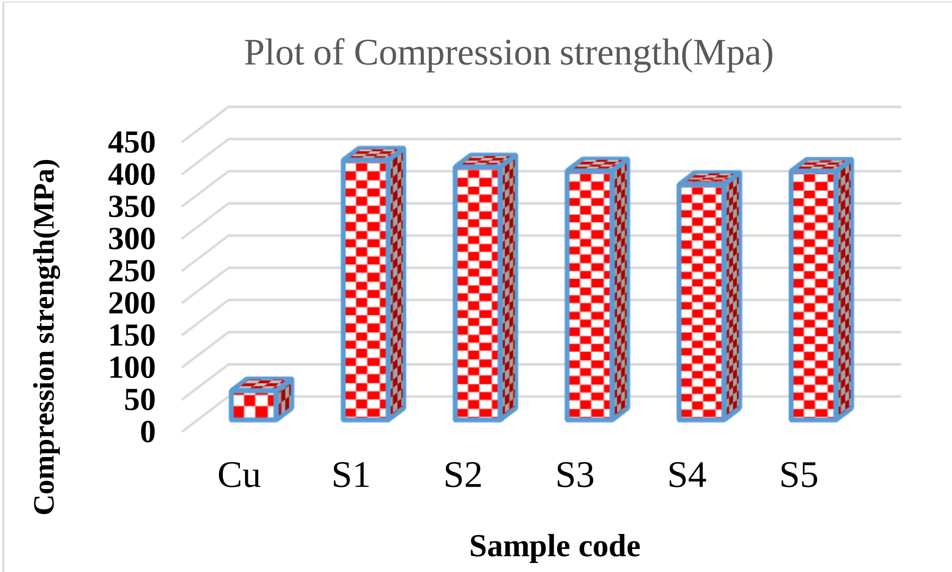

Figure 4.3: Compression strength of Cu/ NiTi/ Ti_3AlC_2/Graphene composite

Figure 4.4 shows the stress-strain curve of Cu/ NiTi/Ti_3AlC_2/Graphene composite implying that the maximum compression strength was around 400MPa.

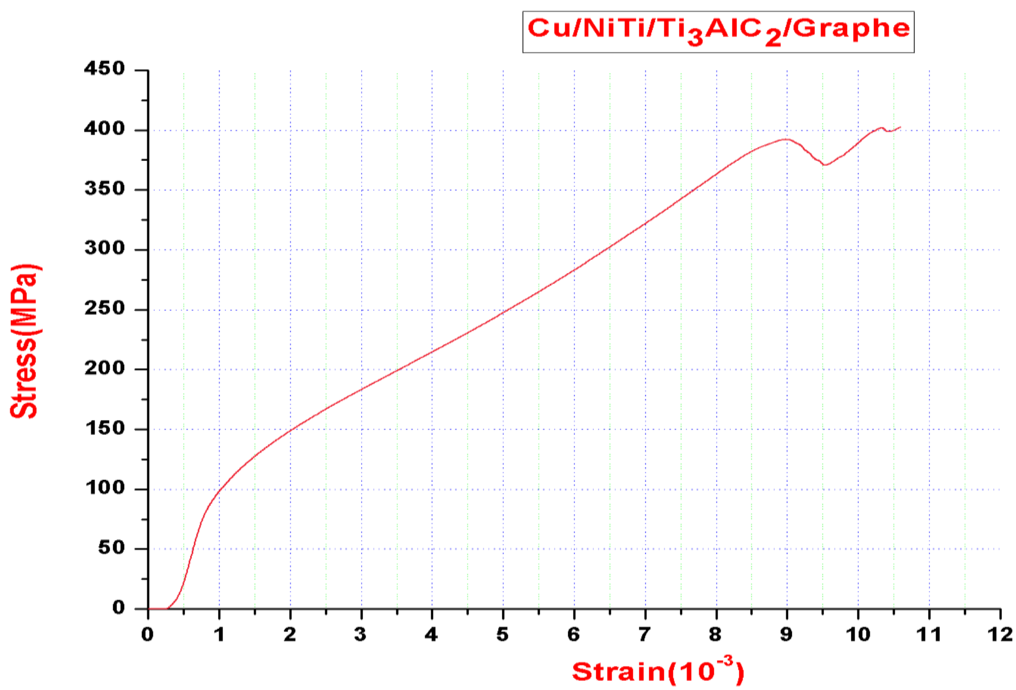

Figure 4.4: Stress-strain diagram for Cu/ NiTi/ Ti_3AlC_2/Graphene composite selected sample(S1)

4.6. Wear test

By weighing the specimen both before and after the test, the amount of wear can be determined. The quantity of material removed per unit of time is known as the wear rate. For this work pin on disk testing technique was used to test the wear mechanism of the developed copper hybrid composite under the recommended process parameters such as load, and sliding speed (20N and 200rpm) (Thankachan *et a*l., 2018) the time for each sample was 10 minutes (Haque *et al*., 2014). The result of (Geethendra Kumar *et al*., 2018) showed that Ti_3AlC_2 and Graphene enhance the wear rate and coefficient friction of copper matrix composite by forming a continuous, compact layer and lubricated layer on the worn surface.

(Akbarpour *et al*., 2022) reported that the presence of a self-lubricating Graphene and TiC within the matrix improves the composite's hardness, wear resistance and coefficient friction of a matrix. According to the findings of (Şap *et al*., 2021) increasing the weight percentage of Ti_3AlC_2 MAX has been positive on wear resistance. From Table (4.4) **sample 1** has smaller wear rate and coefficient of friction due to the high weight fraction of Ti_3AlC_2 the same (Jamshidi *et al*., 2019) reported that the wear rate and coefficient of friction of a matrix decreased with the addition of Ti_3AlC_2. (Lian *et al*., 2019) demonstrated that Graphene oxide with Ti_3AlC_2 minimizes the wear rate and COF of copper based composite. The addition of NiTi improves the tribological properties of a composite in spite of it shape memory effect and supper elasticity reported by (Abedini *et al*., 2009). Graphene oxide enhanced the wear rate and coefficient of friction of pure copper by forming a lubricant film on the surface of the composite (Nie *et al*., 2018).

Table 4.4: Tribological properties of Cu/NiTi/ Ti_3AlC_2/Graphene

Sample code	Initial weight(g)	Final weight(g)	Wear loss(g)	Sliding distance	Wear rate ($\times10^{-6} mm^3/Nm$)	Coefficient of friction (μ)
S1	1.2517	1.2489	0.00283	376.991	7.5188	0.29
S2	1.2692	1.2662	0.00306	376.991	8.1408	0.34
S3	1.3614	1.3582	0.00321	376.991	8.5146	0.32
S4	1.3936	1.3902	0.0033	376.991	8.9019	0.37
S5	1.2887	1.2854	0.0033	376.991	8.7671	0.35

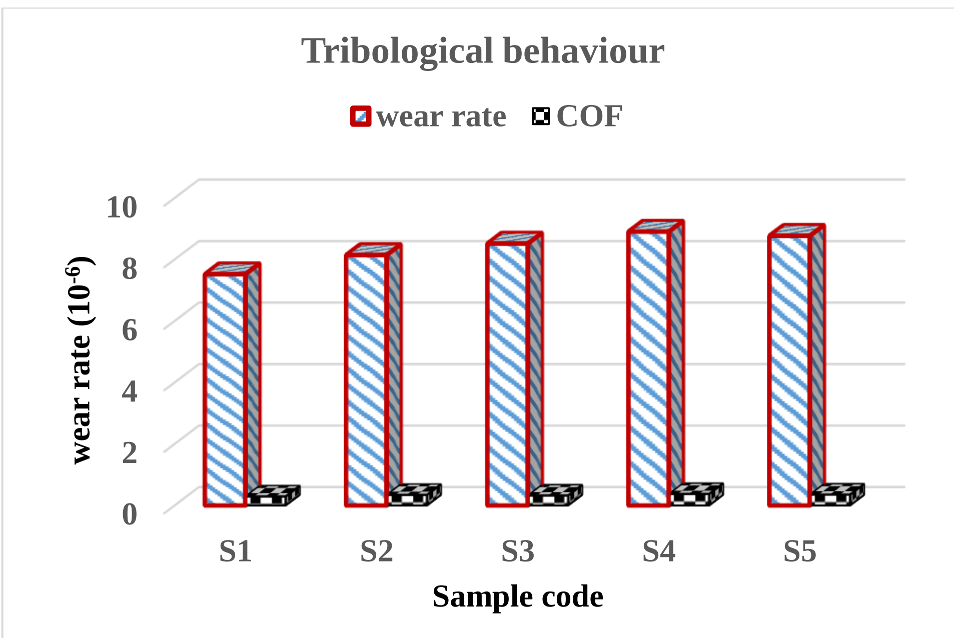

Figure 4.5: Wear rate and Coefficient of friction of (Cu/ NiTi/ Ti_3AlC_2/Graphene)

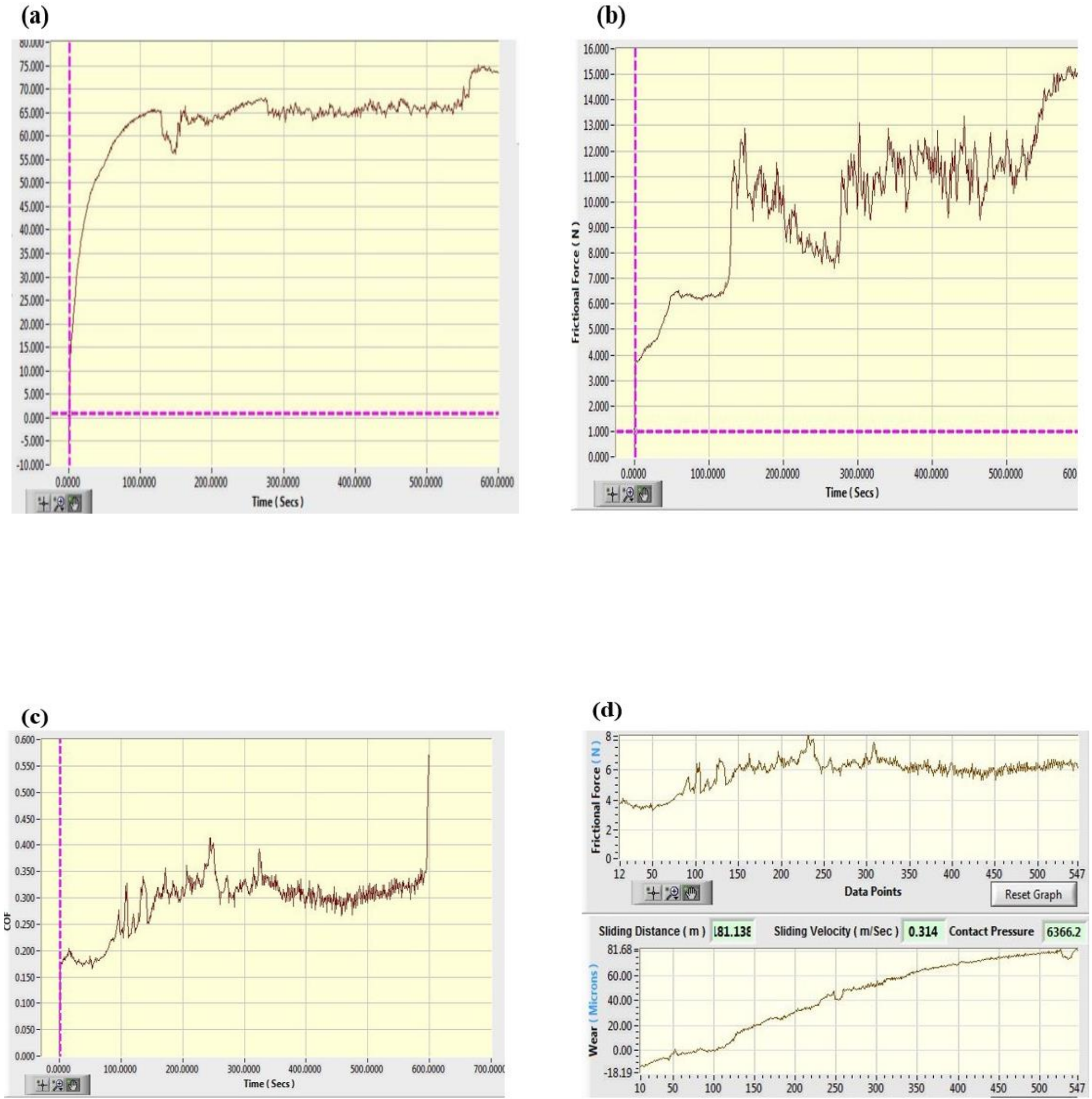

Figure 4.6: Plot from testing machine software (a) Wear in microns, (b) frictional force, (c) coefficient of friction and (d) wear and frictional force

4.7. Microstructural analysis of fabricated composite

Observing the microstructure was the fundamental aspect of the material characterization process. Analyzing observable patterns of microstructures made it possible to infer the actual properties of the examined specimens.

The current study provided a more detailed discussion of all synthesized specimens. The investigation of the particle distribution, morphology, phase, and microstructure of the composites was conducted using optical microscopy, scanning electron microscopy, and X-ray diffraction.

4.7.1. Optical microscopy

An optical microscope (OM) was used to examine the distribution of reinforcement particles within an oxygen-free copper matrix composite, as illustrated in Figure (4.6). To reveal the grain boundaries, the samples were etched by submerging them in a solution of 25ml $NH_4(OH)_2$, 10ml H_2O_2 and 25ml deionized water for 30 seconds to improve the contrast to visualize the microstructure easily. The grain size was determined through the ImageJ software line intercept approach on the optical microscope image. The value ranged between 22. 0μm and 192.0μm and the average grain size was 87.52 μm taking line intercepts from different directions.

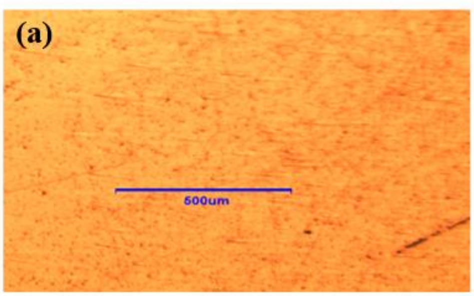

S1 before etching

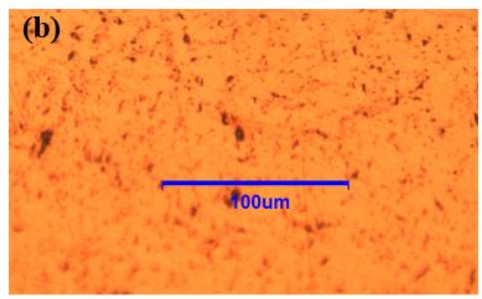

S1 after etching

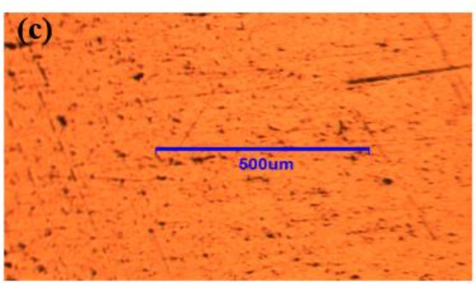

S2 before etching

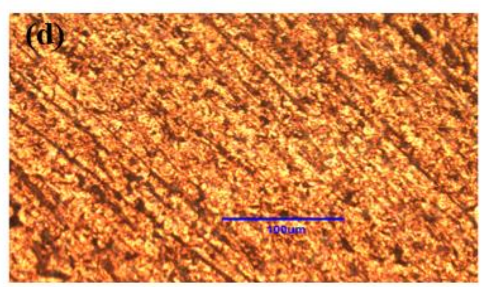

S2 after etching

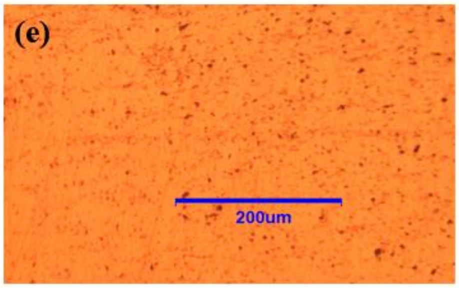

S3 before etching

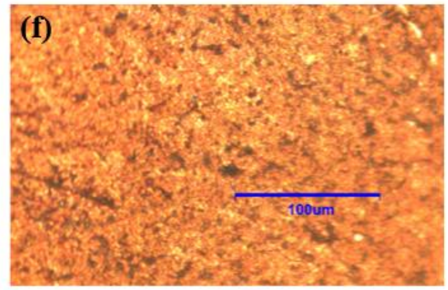

S3 after etching

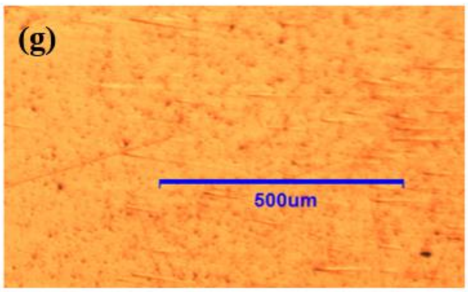

S4 before etching

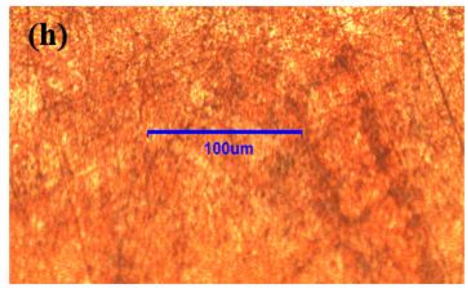

S4 after etching

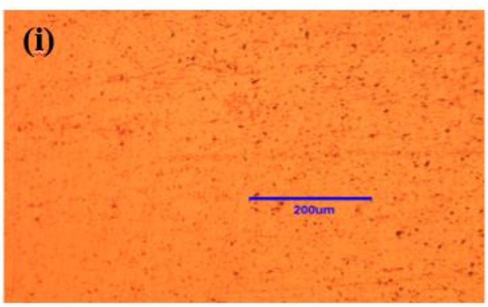

S5 before etching

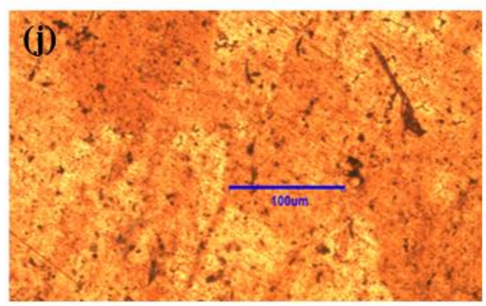

S5 after etching

Figure 4.7: Optical Microscope image of (S1, S2, S3, S4 and S5) before and after etching

The porosity level of the developed Cu/NiTi/Ti_3AlC_2/Graphene hybrid composite was calculated by using imagej software. Porosity percentages calculated for samples 1, sample 2, and sample 4 are 3.349%, 4.135%, and 2.474% respectively, which is a good agreement with the porosity level calculated using equation (3.5).

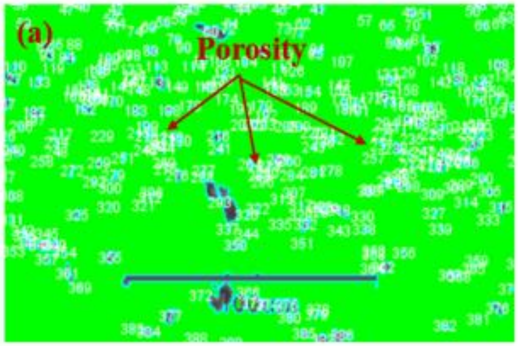

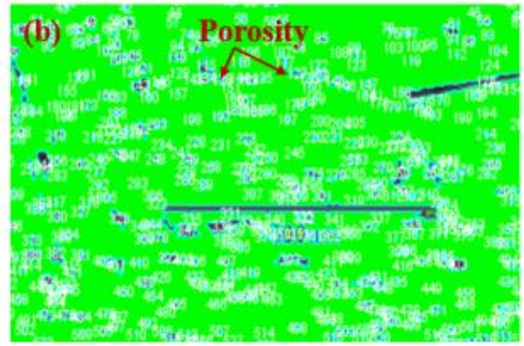

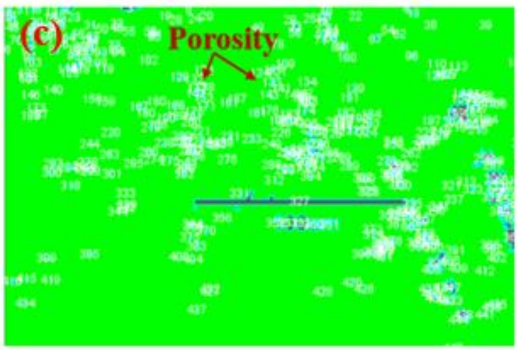

Sample code	Porosity(%)
S1	3.349
S2	4.135
S4	2.474

Figure 4.8: Porosity result through (a) S1, (b) S2 and (c) S4

4.7.2. Scanning Electron Microscopy (SEM)

SEM is a characterization method using a beam of electrons to scan a sample surface, causing the material to generate a signal that the microscope can detect. To analyze these signals, the surface of materials was imaged using SEM in fine detail. As shown in Figure (4.9) the reinforcements (NiTi/Ti_3AlC_2/Graphene) are homogeneously distributed in the Cu-based hybrid composite. Surface scanning of the sampled specimens also revealed the presence of micro holes and grooves, indicating the development of porosity and voids during the fabrication process and the shape of different reinforcement particles and density variation between the matrix and reinforcements form some heterogeneity on the developed materials (Jamwal *et al*., 2019). Figure (4.8) demonstrates the SEM morphology at different magnifications (300x, 600x and 1000x) analysis of the selected three samples (S1, S2 and S3). As shown in figure (4.8) some voids are observed due to different edges of reinforcement particles the same result was reported by(Şap et al., 2021). Reinforcement particles were observed in the SEM micrograph due to mixing defect and density variation between the matrix and reinforcements similar to the (Jamwal *et al*., 2019) reports.

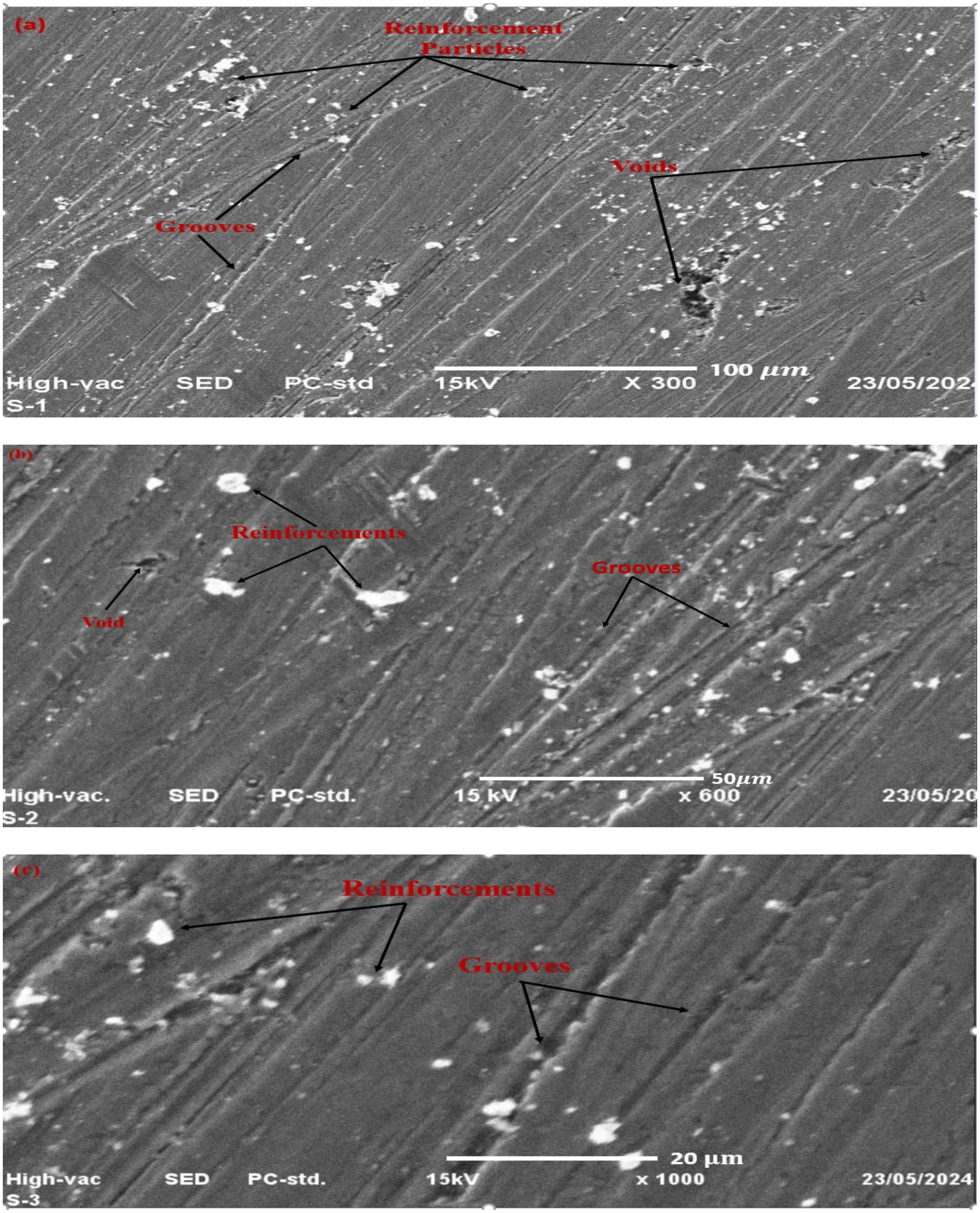

Figure 4.9: SEM micrographs of selected samples of (a) S1, (b) S2 and (c) S3

4.7.3. X-Ray Diffraction Microscopy (X-RD) Analysis

X-ray diffraction (XRD) of the selected three samples has been shown in the figure (4.10) at the angle range of (20°-2θ-80°) and scan speed of 3°/min using XRD-7000 X-RAY DIFFRACTOMETER model found at ASTU material science department. As shown in the below plot weak intensity peaks of NiTi/Ti_3AlC_2/Graphene reinforcement particles due to their low concentration in the developed composite. Weak oxide film and impurities were also observed they had been entered during the fabrication process. The reinforcing material of NiTi/Ti_3AlC_2/Graphene in the oxygen-free copper matrix was seen in small peaks in the XRD plots due to their small content in the composite. The XRD analysis identified distinct XRD-JCPDS signatures, indicating the presence of Oxygen Free Copper (with a high-intensity peak) and enhancements (including NiTi and Ti_3AlC_2) within the composite matrix(Mazaheri *et al.*, 2021). It has been observed that the tallest peaks, medium and smallest peaks of FCC pure copper phase were found at (2θ = 43.425°) and (111), (2θ =50.4°) and (200) and (2θ = 74.1°) and (220) from the (004-0836: JCPDS card number) similar result was reported by (Seo *et al.*, 2013) due to high composition of copper.

Table 4.5 Materials identified from X-RD results

Materials	PDF card number
Copper	00-004-0836
Nickel Aluminum Titanium Carbide	00-019-0035
Carbon	00-060-0053
Copper Nickel	00-047-1406

From Scherrer's equation (D = $\frac{k\lambda}{\beta \cos\theta}$). Where, D = crystal size, k = is shape factor can be 0.62-2.08, λ= XRD radiation of wavelength 0.15402nm), β = is line of boarding at FWHM in radians and θ= is Bragges angle in degree. The dislocation density and lattice strain were calculated using this formula (δ=$\frac{1}{D^2}$) and (ε = $\frac{\beta}{4\tan\theta}$).

Table 4.6: Crystalline size, dislocation density and lattice strain from the X-RD results

Data from obtained X-RD peaks in Figure (4.18) for S1,S2 and S3 respectively.			Calculated values through the Scherrer equation*(Seo et al.*, 2013).		
	$2\theta(°)$	FWHM β(Radian)	D (nm) = $\frac{K\lambda}{\beta\cos\theta}$	δ (μm $^{-2}$)=$\frac{1}{D^2}$	$\varepsilon = \frac{\beta}{4\tan\theta}$
S-1	43.425	0.01826	8.531	0.026	0.018
	50.4	0.02600	6.15	0.137	0.014
	74.1	0.01720	10.54	0.009	0.0057
Average value			**8.406**	**0.0573**	**0.0126**
S-2	43.52	0.01963	7.94	0.0158	0.0123
	50.66	0.02815	5.690	0.0287	0.0149
	74.3	0.01930	9.399	0.0113	0.006
Average value			**7.676**	**0.0186**	**0.0112**
S-3	43.4	0.01794	8.705	0.0132	0.0113
	50.54	0.02983	5.300	0.0356	0.0158
	74.18	0.01814	10.115	0.0098	0.0058
Average value			**8.03**	**0.0195**	**0.0110**

From the above Table (4.5) as crystal size increases dislocation density and lattice strain increase sample 1 (Cu-10% Ti_3AlC_2-5% NiTi-4% Graphene was higher average dislocation density (0.0573 μm $^{-2}$) and lattice strain (0.0126).

The average crystalline size for S1, S2 and were 8.460, 7.676 and 8.03nm respectively, approximately similar results are obtained by (LÓPEZ et al., 2021).

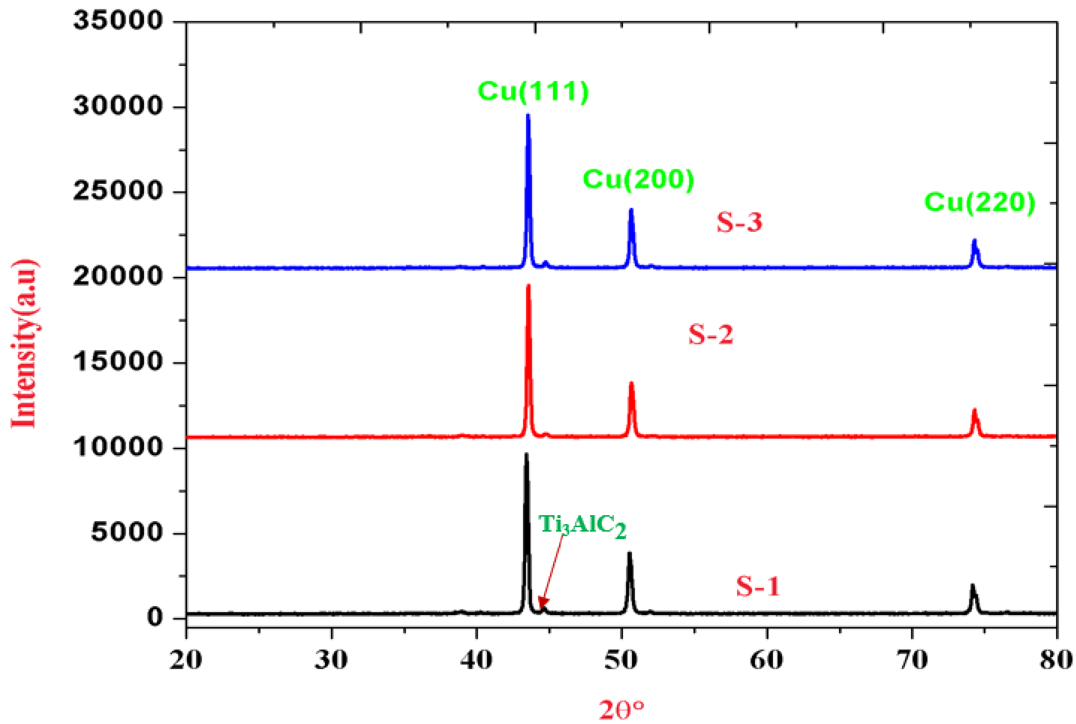

Figure 4.10: XRD spectrum of Cu/NiTi/ Ti_3AlC_2/Graphene for (S-1, S-2 and S-3)

From the X-RD test, some observed impurity materials were described below.

4.8. FT-IR analysis of Cu/NiTi/ Ti_3AlC_2/Graphene composite

FT-IR analysis provides valuable information about the composite composition and interaction at a molecular level. Reinforced Oxygen free copper was analyzed by FT-IR to confirm the existence of organic and inorganic peaks in the developed composite. The FTIR analysis of copper hybrid composite takes place at the beam of IR which contains many frequencies ranging between 500-4000Cm^{-1} used to detect the organic contaminates. The FTIR result obtained confirms that the relevant constitute peak of copper hybrid composite to the similar result obtained by several researchers. The formation of Peaks takes place at 663.14, 633.3, 603.49, 572.42, 546.69,519.85, 489.50, 461.58, 432.12 and 432.12 cm^{-1} similar to the report by (Dean *et al*., 1993) obtained that a peak between 610 to 440cm^{-1}. as shown in figure(4.11) (a). figure (4.11)(b) shows a copper peak which is 2360.74cm^{-1}.

The formation of CH_2 centered at 720cm^{-1} and The CH_3 asymmetric stretching vibration occurs at 2975-2950 cm^{-1}. bond vibration which occurred during compaction between 1500 to 2000Cm^{-1} (Jabinth & Selvakumar, 2021). the peak of graphene was observed at 3404Cm^{-1} (Ponraj *et al*., 2017). (Talabi *et al*., 2021) reported that nanoparticles are surrounded by different organic molecules.

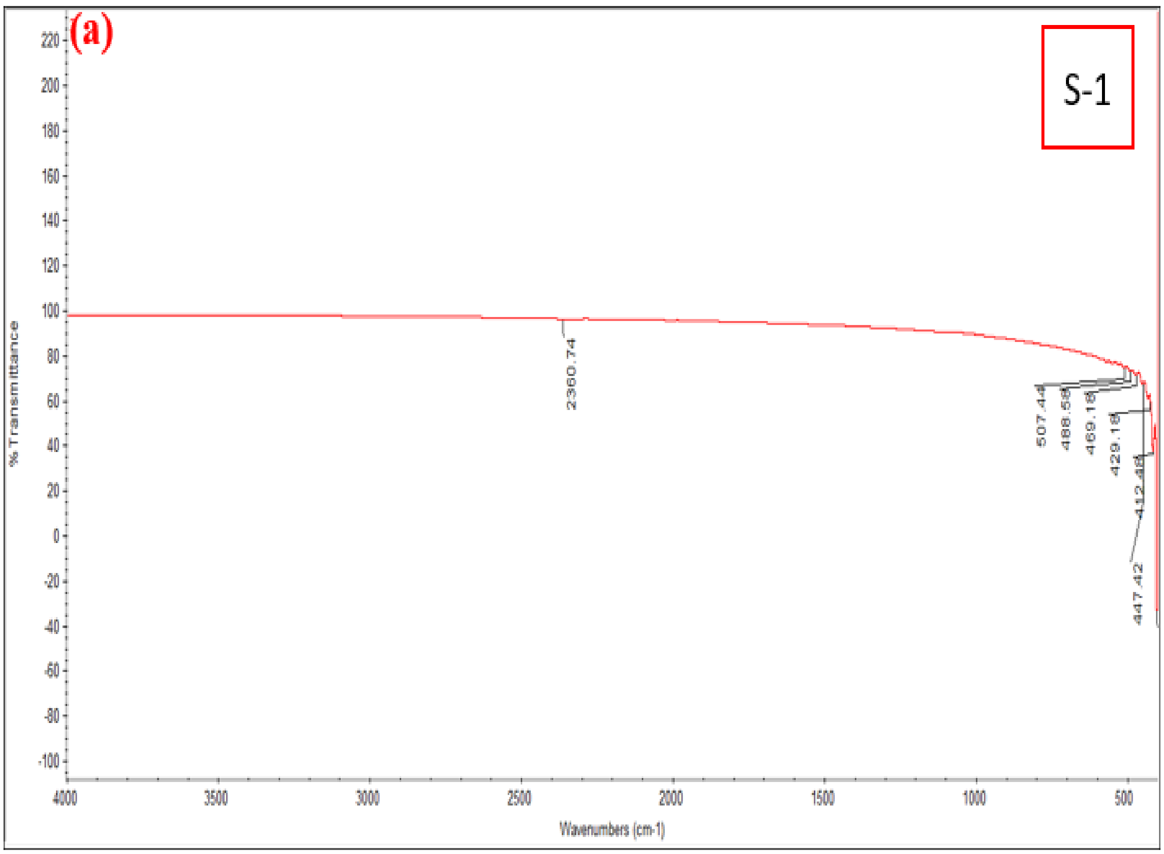

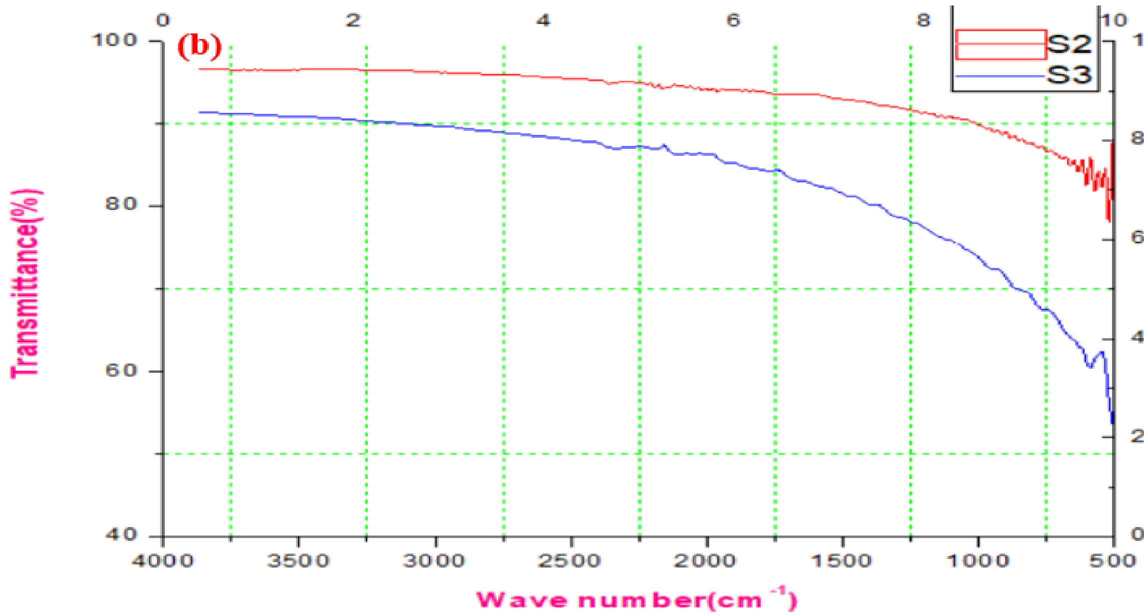

Figure 4.11: FTIR distribution of Cu/NiTi/ Ti_3AlC_2/Graphene for (a) sample 1 (b) sample 2 and 3

4.9. Analysis of corrosion

The corrosion rate of oxygen-free copper reinforced with NiTi/Ti_3AlC_2/Graphene was analyzed through a potentiodynamic curve by immersing the specimen in a 3.5% NaCl bath for 30 minutes. Measurement by Tafel plots provide an easy-to-use and quick electrochemical method for evaluating corrosion. The corrosion rate may potentially be determined using the corrosion current, which is obtained from the Tafel plot's intersection point between the catholic and anodic slopes. A potentiodynamic polarization scan was conducted at a scan rate of 1 mV/sec to capture curves within 250 mV. Tafel plots (corrosion potential on the Y-axis vs. logarithm of corrosion current on the X-axis) and Nyquist plots (real part of impedance on the X-axis vs. imaginary part of impedance on the Y-axis) from electrochemical impedance spectroscopy (EIS) were obtained and processed using origin8 software after the sample was immersed in a 3.5% NaCl solution for 30min. the corrosion rate was calculated using equation (3.7).

Table 4.7: Corrosion characteristics of $Cu/NiTi/Ti_3AlC_2$/Graphene hybrid composite

Samples	Corrosion potential (E_{corr})(V)	Corrosion current (I_{corr})(A/cm^2)	Corrosion rate (mm/year)
S1	-0.1745	1.24	0.250
S2	-0.2164	1.53	0.266
S3	-0.2206	1.980	0.405
S4	-0.2067	2.205	0.420
S5	-0.2143	2.014	0.372

Table (4.7) shows that the corrosion rate of $Cu/NiTi/Ti_3AlC_2$/Graphene for each fabricated sample was calculated based on corrosion potential and current density obtained from the test Tafel plot at 3.5% NaCl. the result shows that the addition of $NiTi/Ti_3AlC_2$/Graphene reinforcement particles enhanced the corrosion resistance of pure copper in harsh environments and high-temperature applications by forming a lubricated layer of Ti_3AlC_2 MAX phase and Nitinol (NiTi) on the surface of the composite. addition of Graphene into pure copper enhances corrosion resistance by increasing anodic dissolution (Hidalgo-Manrique *et al*., 2019). The report (Rondelli & Vicentini, 2002) demonstrated the corrosion rate is enhanced by forming in the case of Ni-Ti-Cu alloys in which Cu is substituted for Ni in orthodontic implants. (Jamwal *et al*., 2019) reported that the inclusion of reinforcement particles resides in the attack zone of the electrolytic reaction on the spaceman's surface and fills the defect region.

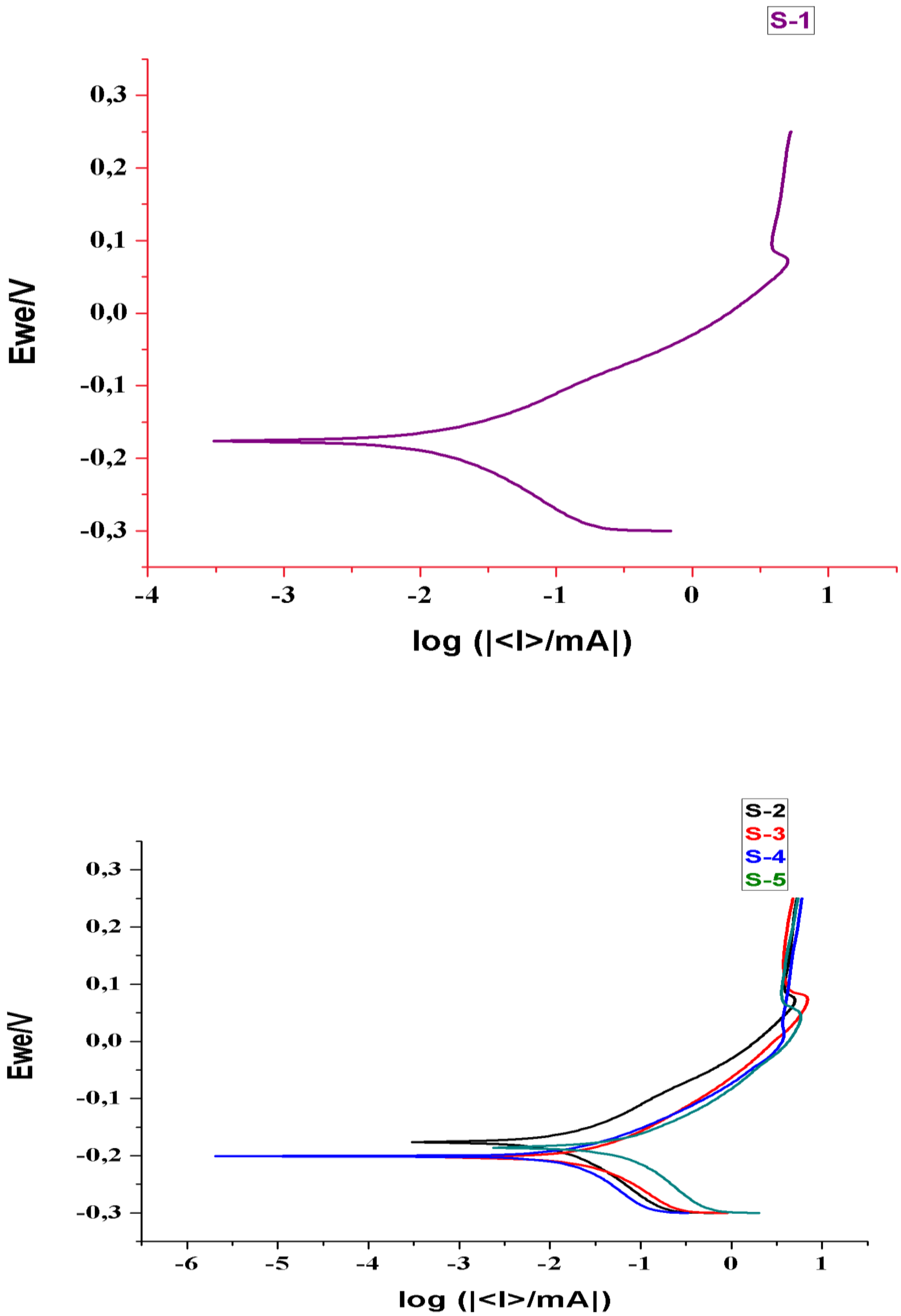

Figure 4.12: Tafel plot of Corrosion result for Copper hybrid composite

4.10. Sample selection for secondary operation (hot extrusion)

Taguchi-based Grey Relational Analysis and Signal to Noise Ratio (S/N) were utilized to identify the best sample of copper-based hybrid composite depending on the results of primary testing and characterization. Grey relational analysis was used to determine the multi-responses of the composite such as compression strength, hardness and corrosion rates of the Cu/NiTi/ Ti_3AlC_2/Graphene composite by converting the experimental results through S/N rations approach of the larger is the better for compression and hardness result and the smaller is the better for the corrosion rate and wear rate by using the equation of (3.11) and (3.12) despite the main goal of this study was to improve the compression strength and hardness and to reduce the corrosion and wear rate of the developed composite material. the S/N result was converted to Grey relational analysis based on the steps described in Chapter 3 to select the best sample for post-deform simulation. Table(4.8) shows the transformed experimental results of Grey relational analysis and S/N ratios using equations from (3.11) to (3.16).

Table 4.8: Experimental results and their S/N ratio of Cu/NiTi/Ti_3AlC_2/Graphene

Experimental Results				S/N ratio result		
Samples	Compression strength	Hardness	Wear rate(10^{-6})	Compression Strength	Hardness	Wear rate(10^{-6})
S1	403.34	132.3	7.5188	52.11343	42.4312	-17.523
S2	392.72	168.6	8.1408	51.88166	44.53715	-18.2133
S3	386.65	158.7	8.5146	51.74636	44.01154	-18.6033
S4	365.43	147.9	8.9019	51.25608	43.39936	-18.9897
S5	386.14	165.37	8.7671	51.7349	44.36913	-18.8571

Table (4.9) shows that the normalization data of the S/N through equation (3.11) the smaller is the better for wear rate and equation(3.12) the larger is the better for (compression strength and hardness). Normalization of the S/N ratio was done to uniformly distribute and scale the data to the acceptable ranges.

Table 4.9: Normalization data

Samples	Compression strength	Hardness	wear rate (10^{-6})
S1	1.0000	0.0000	1.0000
S2	0.7199	1.0000	0.5503
S3	0.5597	0.7273	0.2800
S4	0.0000	0.4298	0.0000
S5	0.5463	0.9110	0.0975

Table 4.10: Deviation sequence

Samples	Compression Strength	Hardness	Wear Rate(10^{-6})
S1	0.0000	1.0000	0.0000
S2	0.2801	0.0000	0.4497
S3	0.4403	0.2727	0.7200
S4	1.0000	0.5702	1.0000
S5	0.4537	0.0890	0.9025

Table(4.11) shows that the grey relational coefficient (GRC_i) at the identification coefficient was calculated using equation (3.15) and Gray relational Grade (GRG) was calculated by equation (3.16) and rank of all the sample properties.

Table 4.11: Grey relational coefficient, gray relational grade and rank at (δ = 0.5)

Samples	Compression Strength	Hardness	Wear Rate (10^{-6})	GRG_I	Rank
S1	**1**	**0.333333**	**1**	**0.777778**	**1**
S2	0.640913	1	0.526474	0.722462	2
S3	0.531772	0.647059	0.409844	0.529558	4
S4	0.333333	0.467181	0.333333	0.377949	5
S5	0.524271	0.848924	0.356497	0.576564	3

From Table(4.11) the largest gray relational grade and first rank was **sample 1** at 10%of Ti_3AlC_2, 5 % NiTi and 4% of Graphene. This sample was selected as the best sample from those five fabricated samples. simulation of the post-deformation took place at this selected sample (81%Cu-10% Ti_3AlC_2-5% NiTi-4% Graphene).

4.11. Result of simulation for secondary operation (hot extrusion)

The selected material of Cu/NiTi/Ti_3AlC_2/Graphene was simulated and analyzed through FEA DEFORM 3D software to predict the extrusion load, effective stress and the damage value of the developed hybrid composite. In this work, cosine die design was utilized and extrusion ratio, extrusion temperature and ram speed were determined as process parameters and optimized through the Design Expert based Response Surface Methodology (RSM) to model the multi-response regression and Genetic algorithm method to determine the optimal value of each process parameter and optimal response.

Table 4.12: Input variables for simulation of hot extrusion

Parameter and terms	Data used as input	Source
Material	Cu/NiTi/Ti_3AlC_2/Graphene	
Compression strength	403.34MPa	From compression test

Flow stress constitutive equation from (power law)	$\bar{\sigma} = C\bar{\varepsilon}^{n}\dot{\bar{\varepsilon}}^{m} + y$	DEFORM 3D flow stress equation selected for this material.
Constants used in power law C = material constants n = strain hardening exponent m = strain rate hardening exponents y = initial yield of the material	C = 1489.65MPa n = 0.468 m = 0.324 y = 173MPa	Constants calculated from equation () to () based on the result of the compression test of Cu/NiTi/Ti_2AlC/Graphene hybrid composite.
Coefficient of friction	$\mu = 0.3$	Assumption of DEFORM database for lubricated condition
Ram speed	1, 2, 3 m/s	
Initial and environmental temperature (℃)	20	
Thermal conductivity	562.33W/mK	

Response Surface Methodology (RSM) based ANOVA analysis was used to analyze the effect of each process parameter on hot extrusion of the developed composite. The genetic algorithm technique was used to optimize the multi-objective optimization process to determine the optimum level of each process parameter. for the minimum damage and extrusion load as a response of the optimization. The damage value and extrusion load of each combination of process parameters were predicted based on the input material data Table (4.12) from the result of the compression test.

4.10.1. Analysis of Damage Value

The damage value of each combination of process parameters was predicted through DEFORM 3D software. Response Surface Methodology (box Behnken design) 15 runs were conducted to determine the effect of extrusion ratio, extrusion temperature and ram speed and their interaction on the damage value of the developed composite.

The design of the experiment for each run was described as follows in Table (4.13) and by analyzing through RSM-based ANOVA analysis the multi-objective regression model determines the individual and interaction effect of each process parameter on the response of the simulation and the model was used as an objective function for the Genetic algorithm optimization technique. Because of lower damage value is required for the safe application of the fabricated sample then minimization of the objective function was conducted through GA. The experimental design of each simulation run is described in Table (4.13).

Table 4.13: Box-Behnken design of Cu/NiTi/Ti_3AlC_2/Graphene for damage value with DEFORM 3D results

Run	Extrusion ratio	Ram Speed (m/sec)	Billet Temperature (℃)	Damage Value
1	4	1	800	7.03
2	4	2	850	7.09
3	2	3	800	6.87
4	3	1	850	6.87
5	3	2	800	6.90
6	2	2	850	6.68
7	2	2	750	6.70
8	4	2	750	7.05

9	3	3	850	6.93
10	4	3	800	7.18
11	3	2	800	6.96
12	3	3	750	6.95
13	3	1	750	6.90
14	3	2	800	6.86
15	2	1	800	6.60

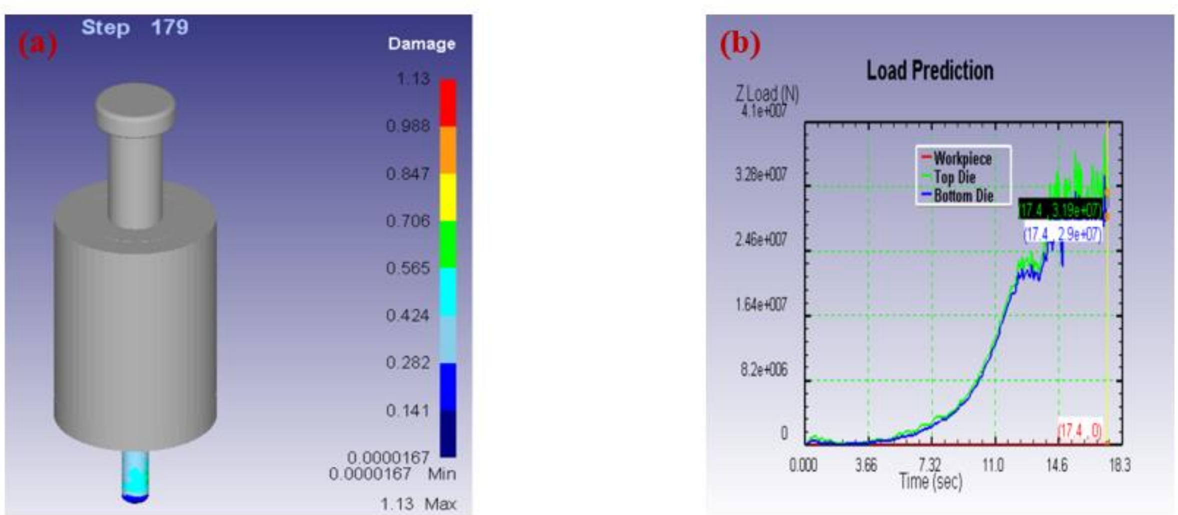

Figure 4.13: (a) Damage value and (b) load distribution

4.10.1.1. ANOVA analysis for damage value

The significance of each process parameter and their interaction on the damage value was investigated through ANOVA of the RSM experimental design using Design Expert software by taken into consideration of significance level of 5% and a confidence level of 95%. Table (4.14) shows the ANOVA of extrusion load where DOF = degree of freedom and F = F ratio.

Table 4.14: ANOVA results of damage value

Source	Sum of square	DOF	Mean of square	F-Value	P-Value	Significance
Model	3.24	9	0.3601	451.08	< 0.0001	
Extrusion ratio(X1)	2.30	1	2.30	2881.64	< 0.0001	
Ram speed(X2)	0.3160	1	0.3160	395.84	< 0.0001	
Billet Temperature(X3)	0.0450	1	0.0450	56.37	0.0007	
X1*X2	0.0072	1	0.0072	9.05	0.0298	
X1*X3	0.0196	1	0.0196	24.55	0.0043	
X2*X3	0.0169	1	0.0169	21.17	0.0058	
$X1^2$	0.2393	1	0.2393	299.76	< 0.0001	
$X2^2$	0.3314	1	0.3314	415.10	< 0.0001	
$X3^2$	0.0219	1	0.0219	27.48	0.0033	
Residual	0.0040	5	0.0008			
Lack of Fit	0.0029	3	0.0010	1.83	0.975	Insignificant
Pure Error	0.0011	2	0.0005			
Cor Total	3.24	14				

Table (4.14) shows the ANOVA analysis of damage value **P-values** for all factors (Extrusion ratio, Ram speed and billet temperature) and their interaction. **P-value** less than 0.0500 indicates model terms are significant. In this case, Extrusion ratio, Ram speed, billet temperature and their interaction are significant model terms that possess a great effect on the damage value. Values greater than 0.050 indicate the model terms are not significant. Extrusion ratio and ram speeds were the most significant factors with P-value ($P<0.0001$).

Figure (4.15) (a) implies the residual plot for the independent factors. As shown all the factors are normally distributed along the straight line thus confirming the model fit to the predict output. And (b) confirms the predicted values with the actual parameters which are totally the same.

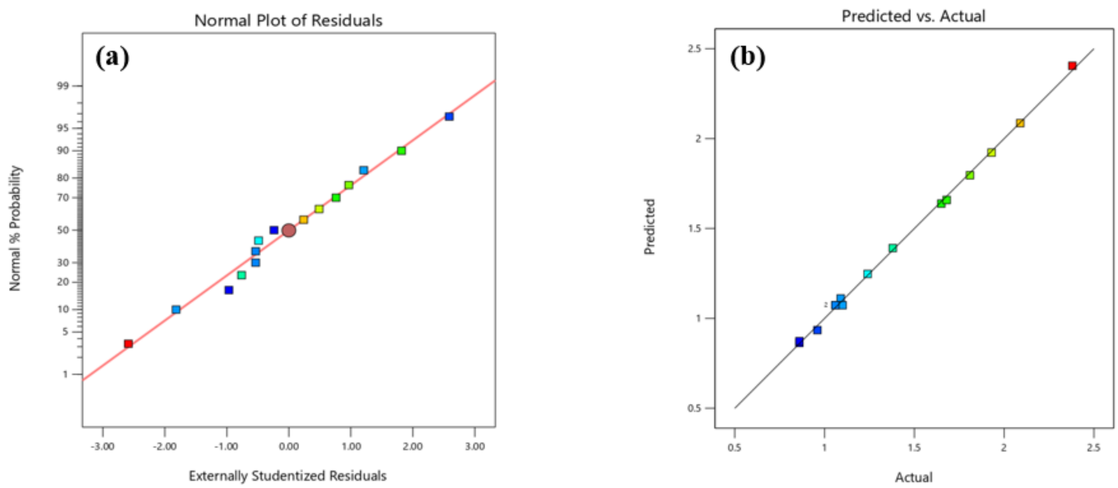

Figure 4.13: (a) Normal plot and (b) predicted vs actual value

4.10.1.2. Extrusion load analysis

The extrusion load of the hot extrusion was predicted through DEFORM 3D software from RSM15 run experimental design with extrusion ratio, ram speed and billet temperature as input process parameter and extrusion load as output parameter. Table (4.15) shows the experimental and simulation results of extrusion load at the given input process parameter. the effect of each process parameter at various levels was investigated in this study and the result showed that as the extrusion ratio increases the extrusion load also increases for the same material. A mathematical model was developed from this RSM experimental design and utilized as an objective function for the GA optimization process. Minimization of the objective function was used because a smaller extrusion load is necessary for the developed material in various engineering applications.

Table 4.15: Box-Behnken design of Cu/NiTi/Ti_3AlC_2/Graphene for extrusion load with DEFORM 3D results

Run	Extrusion ratio	Ram Speed (m/sec)	Billet Temperature (℃)	Extrusion Load (KN)
1	4	1	800	43800
2	4	2	850	44000
3	2	3	800	43700
4	3	1	850	44060
5	3	2	800	44500
6	2	2	850	44300
7	2	2	750	43600
8	4	2	750	46500
9	3	3	850	45500
10	4	3	800	46200
11	3	2	800	43700
12	3	3	750	44100
13	3	1	750	45200
14	3	2	800	44200
15	2	1	800	43600

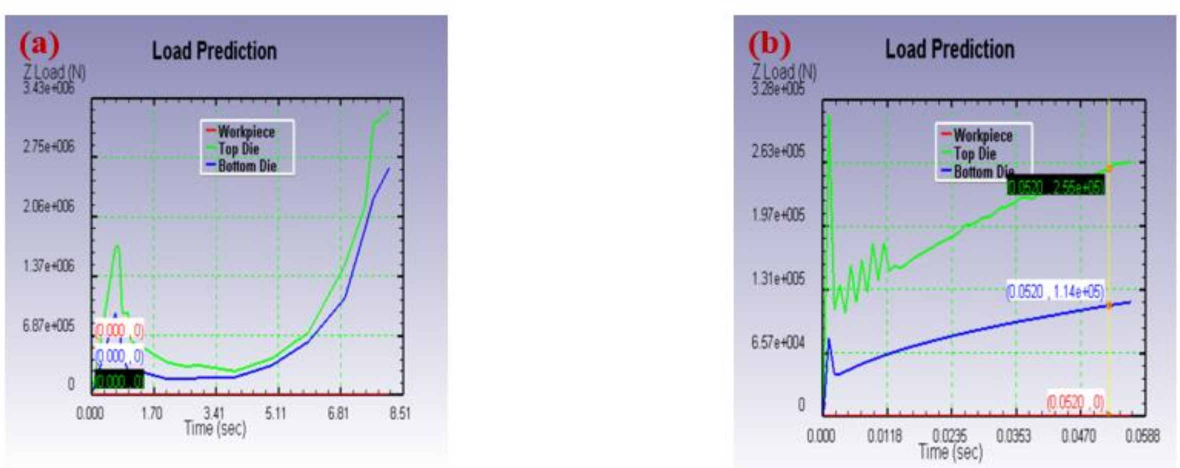

Figure 4.14: Load prediction result plot

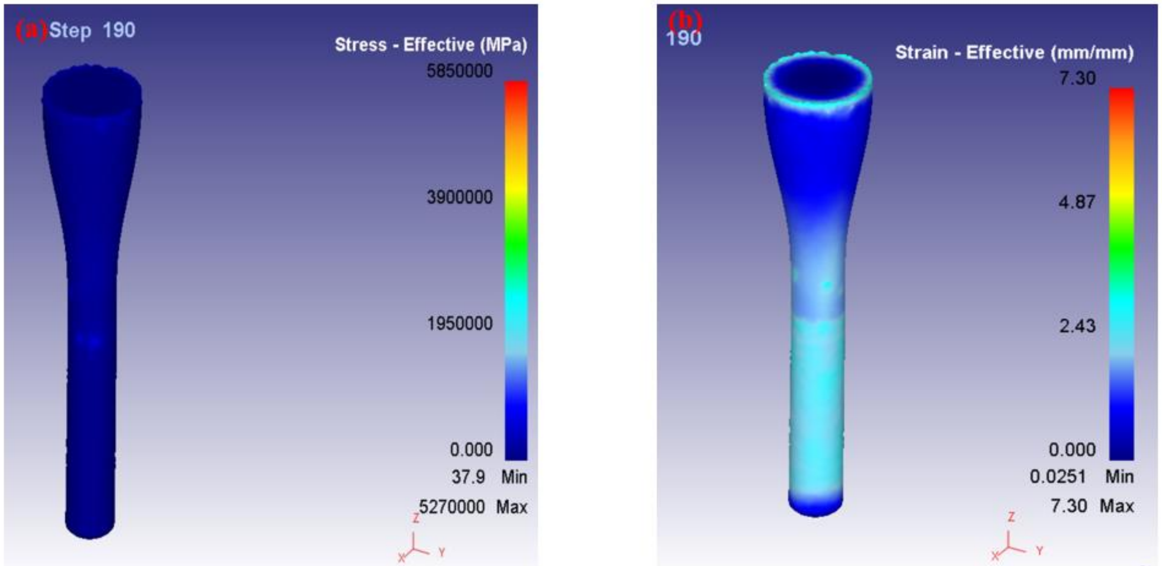

4.10.2. ANOVA analysis for extrusion load

The significance of each process parameter and their interaction on the extrusion load was investigated through ANOVA of the RSM experimental design using Design Expert software by taken into consideration of significance level of 5 % and a confidence level of 95 %. Table (4.16) shows the ANOVA of extrusion load where DOF = degree of freedom and F = F ratio.

Table 4.16: ANOVA of extrusion load

Source	Sum of square	DF	Mean of square	F-Value	P-Value	Significance
Model	1.558E+09	9	1.732E+08	548.83	< 0.0001	
Extrusion ratio(X1)	1.352E+09	1	1.352E+09	4285.26	< 0.0001	
Ram speed(X2)	2.531E+06	1	2.531E+06	8.02	0.0366	
Billet Temperature(X3)	1.711E+06	1	1.711E+06	5.42	0.0673	
X1*X2	2.025E+05	1	2.025E+05	0.6418	0.4594	
X1*X2	1.563E+06	1	1.563E+06	4.95	0.0766	
X2*X3	4.410E+06	1	4.410E+06	13.98	0.0134	

$X1^2$	1.572E+08	1	1.572E+08	498.26	< 0.0001	
$X2^2$	1.196E+07	1	1.196E+07	37.92	0.0016	
$X3^2$	2.496E+07	1	2.496E+07	79.11	0.0003	
Residual	1.577E+06	5	3.155E+05			
Lack of Fit	6.175E+05	3	2.058E+05	0.4288	0.965	Insignificant
Pure Error	9.600E+05	2	4.800E+05			
Cor Total	1.560E+09	14				

Table (4.16) shows the ANOVA analysis of extrusion load and **P-values** for the factors (Extrusion ratio, Ram speed), the interaction between ram speed and temperature and the quadratic value of all main parameters possess **P-value** less than 0.0500 indicates model terms had a significant effect on the extrusion load. Extrusion ratio($P<0.0001$) was the most significant factor on extrusion load.

Therefore extrusion load increased as extrusion ratio increased because the material deformation and surface area of contact increased. Figure (4.15) (a) implies the residual plot for the independent factors. As shown all the factors are normally distributed along the straight line thus confirming the model fit with predicted process parameters. And (b) confirms the predicted values best fit with the actual parameters.

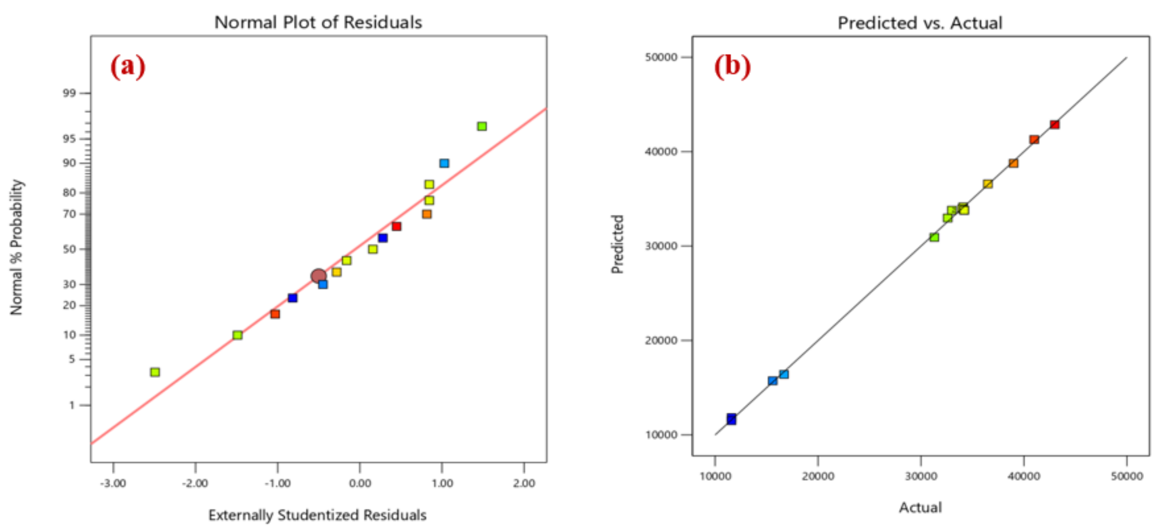

Figure 4.15: (a) residuals plot and (b) predicted vs actual

The mathematical model obtained from DOE was given by the following equation (4.2 and 4.3). As shown the equation below all the parameters, their quadratic formula and their interaction effect on the extrusion load takes in to consideration. Adjusted R-Square value (99.72%) and predicted R-Square value 99.23% indicate that the given data are very well correlated with the produced regression mathematical model.

4.10.3. Mathematical model

Regression analysis is a mathematical tool used for modeling and analyzing the data by considering the relationship between various input variables with the response variables in terms of linear or quadratic regression models. For this work, the regression model for damage value and extrusion load was described by equations (4.2) and (4.3).

These equations were employed as input objective functions for the GA optimization technique.

$$Y_1=-3.3+0.010X1-0.247X2+0.0104X3+0.0072X1^2+0.0625X2^2-0.0000077X3^2+0.0049X1*X2+0.000189X1*X3+0.000058X2*X3 \quad (4.2)$$

$$Y_2=34300+12900X1+812.5X2+37.5X3-6150X1^2+925X2^2-775X3^2+225X1*X2-525X1*X3+400.1X2*X3 \quad (4.3)$$

Where, X1=Extrusion Ratio, X2= Ram Speed, X3= Billet Temperature Y= Extrusion Load(Objective function)

4.10.4. Multi-response optimization for the developed materials

4.10.4.1: Genetic Algorithm Optimization Technique

In this approach, GA was used to optimize the mathematical model developed through the design of experiment-based Response Surface Methodology by developing quadratic regression model extrusion ratio, ram speed and billet temperature as independent variables and damage value and extrusion load as dependent variables. by using MATLABR2021a software. GA was employed under the constraints described as extrusion ratio ($2 \leq ER \leq 4$), Ram speed ($1\leq RS \leq 3$) m/s and billet temperature ($750 \leq BT \leq 850$) ℃. Table (4.17) describes the input for the GA optimization technique MATLAB Code.

Table 4.17: Optimization GA parameter for MATLAB Code

Variable		Value
Fitness function		Regression equations of (4.2) and (4.3)
Boundary condition	Lowe bound	(2, 1m/s and 750 ℃)
	Upper bound	(4, 3m.s and 850 ℃)
Total number of iterations		100
Population size		1000
Functional tolerance		10^{-6}
Constraint tolerance		10^{-6}

The optimum result (Damage value and extrusion load) was obtained at the iteration numbers 3 and 5 which found by GA, were 6.80618 and 4.3575x10^{8}KN as shown in Figures (4.16 to 4.18). The optimum parametric combinations obtained through the GA optimization technique were Extrusion ratio, Ram speed and Billet temperature (2, 1.5m/s and 850 ℃) respectively.

Table 4.18: OPtimum process parameter for extrusion load

Parameter	Extrusion ratio	Ram velocity	Billet temperature
Value	2	1.5m/s	850℃

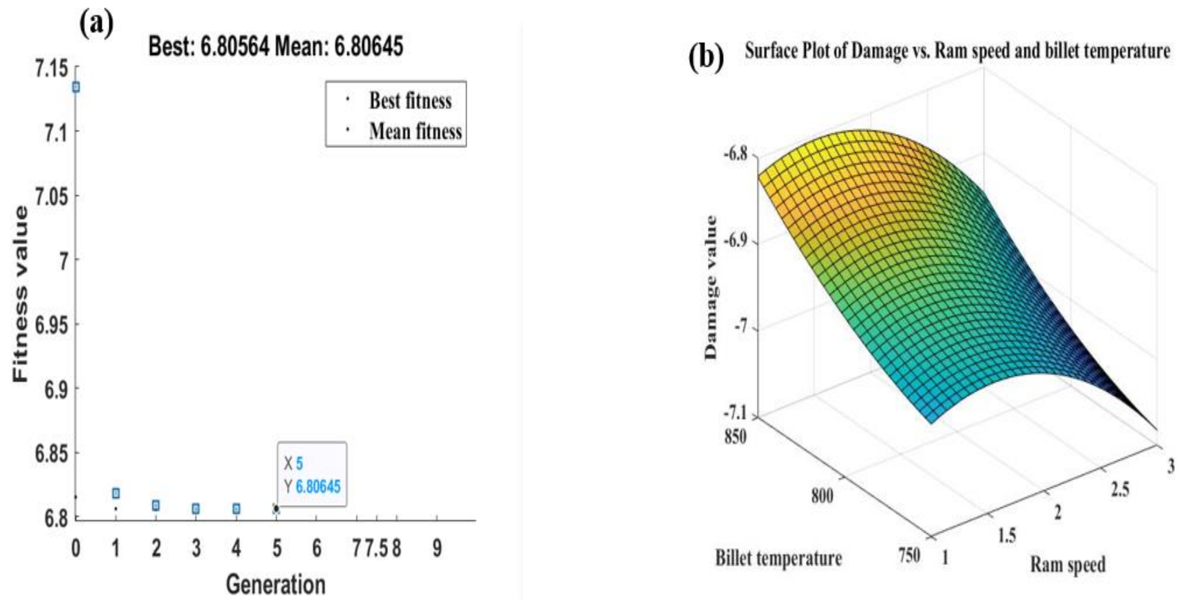

Figure 4.16: GA plot for the optimum Damage value

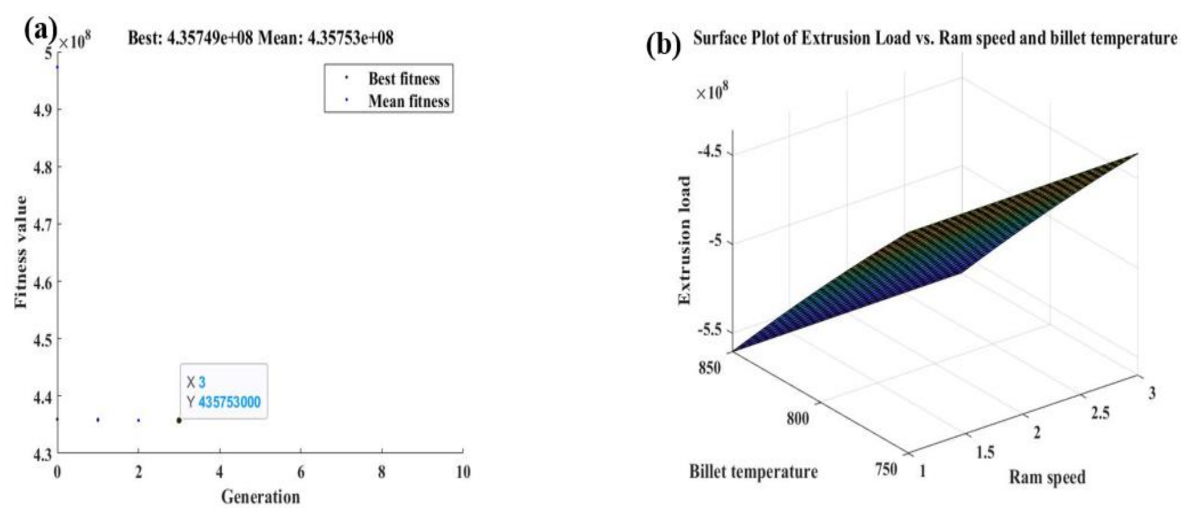

Figure 4.17: (a) GA plot for the Extrusion Load

4.10.5. Comparing the metallurgical properties of the developed sample for Refrigeration and Air Conditioning

Table 4.19: Comparison of properties

Properties	Previous materials	The developed materials	Improvement(%)
Corrosion rate (mm/year)	0.87 (Engineering, 2016)	0.250	248
Wear rate (mm^3/Nm)	34×10^{-6} (Koti, 2018)	$7.5188x10^{-6}$	353
Coefficient of Friction (μ)	0.604 (Koti, 2018)	0.29	108
Compression strength (MPa)	333.5(T. Zhang *et a*l., 2019)	403.34	22.22
Hardness (HV)	82.5(According to UNS C10200)	168.6	104.4

5. CONCLUSIONS AND RECOMMENDATION

5.1. Conclusion

Five samples were prepared for this thesis work using the powder metallurgy method, by varying weight percentages of each reinforcement. The reinforcements were NiTi (5, 10, 7.5, 5, 0) wt%, Ti_3AlC_2 (10, 5, 7.5, 0, 5) wt%, and Graphene (4%) at constant pressure of 60MPa, sintering temperature of 800 °C, and sintering time of 60min. The purpose of the experimental investigation was to examine the produced copper hybrid composite's microstructure behavior, Physical properties (density and porosity), Mechanical properties (hardness and compression strength) and Tribological qualities (wear and coefficient of friction),. Based on these primary findings, a sample with the optimum properties was chosen for post-deformation behavior. The deformation behaviors of this sample were then investigated using DEFORM 3D software, a finite element simulation tool, to examine the impact of process variables like extrusion ratio, ram speed, and billet temperature on the sample's damage value and extrusion load. The mathematical model for the regression was created using the Response Surface Methodology (RSM) design. The correlation between the input and output process parameters and the ideal process parameters were then examined using a Genetic algorithm (GA) that used the regression model as an objective function. The following findings can be drawn from the study.

- Cu/NiTi/ Ti_3AlC_2/Graphene was fabricated via powder metallurgy fabrication method at 24h blending time, 60Mpa compaction pressure and 60min sintering time.
- As a result of microstructural characterization homogenous particle distribution was observed by Optical micrograph. Some micro-holes and voids were observed by SEM micrograph. Impurity particles, crystalline size and dislocation density were determined through the X-RD.
- The density of the pure copper decreased from 8.90 g/cm^3 to 8.021g/cm^3 due to the addition of NiTi/ Ti_3AlC_2/Graphene which has a lower than the density of pure copper.
- The Vicker hardness value of the material was 168.67HV which is improved by 104.4% and the maximum compression strength was 403.34MPa with 22.2% improvement. these results showed that reinforcing oxygen-free copper with Ti_3AlC_2 max phase, nitinol (NiTi) and Graphene enhances the mechanical properties of the material.

- As a result of the wear and corrosion resistance tests the wear rate and coefficient of friction of the developed composite were obtained $7.5188x10^{-6}mm^3/Nm$ and 0.29 respectively, and 0.250 mm/year corrosion rate was calculated by the addition of 5% NiTi, 10% Ti_3AlC_2 and 4% Graphene.
- Sample 1 (81%Cu-10%Ti_3AlC_2-5% NiTi-4%Graphene) was selected by Gray Relational Analysis and S/N ratio optimization process for post deformation simulation.
- The predicted value of damage value and extrusion load was 6.806 and $4.357x10^8$KN at the optimum extrusion parameters extrusion ratio = 2, Ram speed = 1.5m/s and Billet temperature = 850 ℃ found by Genetic algorithm technique.

5.2. Recommendation

Based on the experimental results obtained and conclusions generated the following suggestions were generated to improve the properties of Oxygen-free copper material for different applications.

- Electrical and thermal conductivity tests could be done on the developed material.
- The mechanical properties (tensile and impact strength) of the Cu/NiTi/Ti_3AlC_2/Graphene composite can be analyzed.

5.3. Future Works

- The effect of powder metallurgy fabrication process parameters (blending time, compaction pressure and sintering time) ware not addressed by this research work and it can be optimized using different optimization techniques.
- Investigation of thermal properties of the developed sample was the limitation of this thesis work and it can be addressed by conducting different experimental testing such as TGA and thermal conductivity testing.
- The mechanical and physical properties of Hot extruded material was not investigated due to shortage of time and materials upcoming researchers can be done the experimental investigation on the post-deformation behavior of the developed material.

SPECIAL ACKNOWLEDEGMENT

This research work is funded by Adama Science and Technology University under the grant number ASTU/SM-R/104/24.

REFERENCES

Abedini, M., Ghasemi, H. M., & Nili Ahmadabadi, M. (2009). Tribological behavior of NiTi alloy in martensitic and austenitic states. *Materials and Design*, *30*(10), 4493–4497. https://doi.org/10.1016/j.matdes.2009.05.031

Adiloğlu, S., Fajardo, S., García-Galvan, R., F., Barranco, V., Galvan, J. C., & Batlle, S. F. (2016). We are IntechOpen, the world's leading publisher of Open Access books Built by scientists, for scientists TOP 1 %. *Intech*, *i*(tourism), 13. https://doi.org/http://dx.doi.org/10.5772/57353

Ajagol, P., Anjan, B. N., Marigoudar, R. N., & Preetham Kumar, G. V. (2018). Effect of SiC Reinforcement on Microstructure and Mechanical Properties of Aluminum Metal Matrix Composite. *IOP Conference Series: Materials Science and Engineering*, *376*(1). https://doi.org/10.1088/1757-899X/376/1/012057

Akbarpour, M. R., Sadeghi, N., & Aghajani, H. (2022). Nano TiC-Graphene-Cu composites fabrication by a modified ball-milling method followed by reactive sintering: Effects of reinforcements content on microstructure, consolidation, and mechanical properties. *Ceramics International*, *48*(1), 130–136. https://doi.org/10.1016/j.ceramint.2021.09.088

Alawadhi, M. Y., Sabbaghianrad, S., Wang, Y. C., Huang, Y., & Langdon, T. G. (2020). Characteristics of grain refinement in oxygen-free copper processed by equal-channel angular pressing and dynamic testing. *Materials Science and Engineering: A*, *775*, 16–18. https://doi.org/10.1016/j.msea.2020.138985

Albartouli, A. B. M., & Uzun, A. (2023). Mechanical and Electrical Properties of Graphene Nanosheet Reinforced Copper Matrix Composites Materials Produced by Powder Metallurgy Method. *Science of Sintering*, *55*(3), 399–411. https://doi.org/10.2298/SOS230415027A

Ali, R., Song, P., Khan, M., Ali, S., Kamli, M. R., Sabir, J. S. M., Huang, T., Deifalla, A., Shakeel, & Lu, J. (2023). Tribological and oxidation resistance performance of Ti2AlC MAX-phase generated by reactive spark plasma sintering. *Journal of Materials Research and Technology*, *26*, 8309–8326. https://doi.org/10.1016/j.jmrt.2023.09.110

ALIEMEKE, B. N. G., & OLADEİNDE, M. (2020). Box-Behnken Design Optimization of

Sand Casting Process Parameters. *International Journal of Engineering Technologies IJET*, *6*(2), 25–36. https://doi.org/10.19072/ijet.714473

Anil Kumar, B. K., Ananthaprasad, M. G., & GopalaKrishna, K. (2016). A review on mechanical and tribological behaviors of nickel matrix composites. *Indian Journal of Science and Technology*, *9*(2), 2658–2664. https://doi.org/10.17485/ijst/2016/v9i2/82868

Ankur, Bharti, A., Prasad, D., Kumar, N., & Saxena, K. K. (2021). A Re-investigation: Effect of various parameter on mechanical properties of copper matrix composite fabricated by powder metallurgy. *Materials Today: Proceedings*, *45*, 4595–4600. https://doi.org/10.1016/j.matpr.2021.01.009

Bellah, M., Nosonovsky, M., & Rohatgi, P. (2023). Shape Memory Alloy Reinforced Self-Healing Metal Matrix Composites. *Applied Sciences (Switzerland)*, *13*(12). https://doi.org/10.3390/app13126884

Benitez, R., Kan, W. H., Gao, H., O'Neal, M., Proust, G., Srivastava, A., & Radovic, M. (2020). Mechanical properties and microstructure evolution of Ti2AlC under compression in 25–1100 °C temperature range. *Acta Materialia*, *189*, 154–165. https://doi.org/10.1016/j.actamat.2020.02.057

Bharat, N., & Bose, P. S. C. (2021). An overview on the effect of reinforcement and wear behaviour of metal matrix composites. *Materials Today: Proceedings*, *46*(xxxx), 707–713. https://doi.org/10.1016/j.matpr.2020.12.084

Casati, R., & Vedani, M. (2014). Metal matrix composites reinforced by Nano-Particles—A review. *Metals*, *4*(1), 65–83. https://doi.org/10.3390/met4010065

Chen, C., Zhai, Z., Sun, C., Wang, Z., & Li, D. (2024). Mechanical Properties of Ti3AlC2/Cu Composites Reinforced by MAX Phase Chemical Copper Plating. *Nanomaterials*, *14*(5). https://doi.org/10.3390/nano14050418

Chen, Y., Li, J., Liu, H., Li, Z., & Zeng, C. (2016). Microstructures and mechanical, electrical, high-temperature properties of Cu/Ti2AlC FGM fabricated by hot-pressing. *Journal Wuhan University of Technology, Materials Science Edition*, *31*(6), 1250–1254. https://doi.org/10.1007/s11595-016-1521-6

Dadkhah, M., Saboori, A., & Fino, P. (2019). An overview of the recent developments in metal matrix nanocomposites reinforced by graphene. *Materials*, *12*(7). https://doi.org/10.3390/ma12172823

Dean, D. R., Scawthorn, C., O'Rourke, T. D., Blackburn, F. T., Whitney, D. J., Lindell, M. K., Nguyen, H. H. D., Kenner, S. J., Segall, P., Ellsworth, W. L., Lindh, A. G., Prescott, W. H., Herd, D. G., Park, S. M., Al, E. E. T., Ager, P., Eriksson, K., Hansen, C. W., Lønstrup, L., &)1993. (ا, غلامرضا. No Titleمتداولترین گیاهای. *Explorations in Economic History*, *24*(6), ETG 5-1-ETG 5-17. https://doi.org/10.1080/00033799300200371

Endra, M. A. H., & Pachalasiya, S. (2013). *Modeling of Extrusion Through Curve Die Modeling of Extrusion*. *2176*(June).

Engineering, O. (2016). *CORROSION AND HARDNESS BEHAVIOUR OF COPPER METAL MATRIX COMPOSITE*. *2*(12), 81–85.

Farber, E., Zhu, J. N., Popovich, A., & Popovich, V. (2019). A review of NiTi shape memory alloy as a smart material produced by additive manufacturing. *Materials Today: Proceedings*, *30*(xxxx), 761–767. https://doi.org/10.1016/j.matpr.2020.01.563

Gao, X., Yue, H., Guo, E., Zhang, H., Lin, X., Yao, L., & Wang, B. (2016). Mechanical properties and thermal conductivity of graphene reinforced copper matrix composites. *Powder Technology*, *301*, 601–607. https://doi.org/10.1016/j.powtec.2016.06.045

Garg, P., Jamwal, A., Kumar, D., Sadasivuni, K. K., Hussain, C. M., & Gupta, P. (2019). Advance research progresses in aluminium matrix composites: manufacturing & applications. *Journal of Materials Research and Technology*, *8*(5), 4924–4939. https://doi.org/10.1016/j.jmrt.2019.06.028

Gautam, Y. K., Somani, N., Kumar, M., & Sharma, S. K. (2018). A review on fabrication and characterization of copper metal matrix composite (CMMC). *AIP Conference Proceedings*, *2018*(Cmmc). https://doi.org/10.1063/1.5058254

Geethendra Kumar, E., Ahasan, M., Venkatesh, K., & Sastry, K. S. B. S. V. S. (2018). Design, fabrication of Powder Compaction Die and Sintered behavior of Copper Matrix Hybrid Composite. *International Research Journal of Engineering and Technology*, 876–882. www.irjet.net

Guler, O., & Bagci, N. (2020). A short review on mechanical properties of graphene reinforced metal matrix composites. *Journal of Materials Research and Technology*, *9*(3), 6808–6833. https://doi.org/10.1016/j.jmrt.2020.01.077

Hamada, A. S., Khosravifard, A., Kisko, A. P., Ahmed, E., & Porter, D. A. (2016). High temperature deformation behavior of a stainless steel fiber-reinforced copper matrix composite. *Materials Science and Engineering: A*, *669*, 469–479. https://doi.org/10.1016/j.msea.2016.03.084

Haque, S., Ansari, A. H., & Bharti, P. K. (2014). Effect of process parameters on wear rate of Al 6061-Cu reinforced SiCp metal matrix composites. *Journal of Materials and Environmental Science*, *5*(5), 1485–1489.

He, B., & Bin, W. (2012). Development and application of 16MnR Materials database of pressure vessel in software DEFORM-3D. *Applied Mechanics and Materials*, *189*, 465–469. https://doi.org/10.4028/www.scientific.net/AMM.189.465

Henry Ononiwu, N., Akinlabi, E. T., & Ozoegwu, C. G. (2019). Sustainability in Production and Selection of Reinforcement particles in Aluminium Alloy Metal Matrix Composites: A Review. *Journal of Physics: Conference Series*, *1378*(4). https://doi.org/10.1088/1742-6596/1378/4/042015

Hidalgo-Manrique, P., Lei, X., Xu, R., Zhou, M., Kinloch, I. A., & Young, R. J. (2019). Copper/graphene composites: a review. *Journal of Materials Science*, *54*(19), 12236–12289. https://doi.org/10.1007/s10853-019-03703-5

Huanchao Liua, Xinying Tenga, Huanchao Liua, Xinying Tenga. (2018). Authors : Ac ce d M us pt. *2D Materials*, 0–23. https://iopscience.iop.org/article/10.1088/2053-1583/abe778

Jabinth, J., & Selvakumar, N. (2021). Enhancing the mechanical, wear behaviour of copper matrix composite with 2V-Gr as reinforcement. *Proceedings of the Institution of Mechanical Engineers, Part J: Journal of Engineering Tribology*, *235*(7), 1405–1419. https://doi.org/10.1177/1350650120960573

Jahani, A., Jamshidi Aval, H., Rajabi, M., & Jamaati, R. (2023). Effects of Ti2SnC MAX Phase on Microstructure, Mechanical, Electrical, and Wear Properties of Stir-Extruded Copper Matrix Composite. *Advanced Engineering Materials*, *25*(9), 1–14.

https://doi.org/10.1002/adem.202201463

Jamshidi, R., Heidarpour, A., Aghamohammadi, H., & Eslami-Farsani, R. (2019). Improvement in the mechanical and tribological behavior of epoxy matrix with the inclusion of synthesized Ti3AlC2 MAX particles. *Journal of Composite Materials*, *53*(26–27), 3819–3827. https://doi.org/10.1177/0021998319848140

Jamwal, A., Mittal, P., Agrawal, R., Gupta, S., Kumar, D., Sadasivuni, K. K., & Gupta, P. (2020). Towards sustainable copper matrix composites: Manufacturing routes with structural, mechanical, electrical and corrosion behaviour. *Journal of Composite Materials*, *54*(19), 2635–2649. https://doi.org/10.1177/0021998319900655

Jamwal, A., Prakash, P., Kumar, D., Singh, N., Sadasivuni, K. K., Harshit, K., Gupta, S., & Gupta, P. (2019). Microstructure, wear and corrosion characteristics of Cu matrix reinforced SiC–graphite hybrid composites. *Journal of Composite Materials*, *53*(18), 2545–2553. https://doi.org/10.1177/0021998319832961

Jebarose Juliyana, S., & Udaya Prakash, J. (2020). Drilling parameter optimization of metal matrix composites (LM5/ZrO2) using Taguchi Technique. *Materials Today: Proceedings*, *33*(xxxx), 3046–3050. https://doi.org/10.1016/j.matpr.2020.03.211

Jomah, A. J., Subhi, A., & A. Hashim, F. (2022). Properties of Welded Copper Tubes Fabricated Via Friction crush Welding. *Engineering and Technology Journal*, *40*(6), 840–847. https://doi.org/10.30684/etj.v40i6.2292

Kalepu, S., & Nallu, R. (2021). Experimental Investigation and Optimization of Mechanical Properties of Nitinol Reinforced Composites. *Composites Theory and Practice*, *2021*(4), 154–160.

Karthick et al. (2019). Experimental investigation on mechanical properties and microstructure of hybrid copper matrix composites through microwave sintering process. *Indian Journal of Science and Technology*, *12*(6), 1–8. https://doi.org/10.17485/ijst/2019/v12i6/141892

Karuppiah, I., Poovaraj, R. K., Veeramani, A., Shanmugam, S., Manickam, R., & Rangasamy, R. (2017). Synthesis, characterization and forming behavior of hybrid copper matrix composites produced using powder metallurgy. *International Journal of Materials Research*, *108*(7), 586–591. https://doi.org/10.3139/146.111510

Katoch, S., Chauhan, S. S., & Kumar, V. (2021). A review on genetic algorithm: past, present, and future. In *Multimedia Tools and Applications* (Vol. 80, Issue 5). Multimedia Tools and Applications. https://doi.org/10.1007/s11042-020-10139-6

Khuri, A. I., & Mukhopadhyay, S. (2010). Response surface methodology. *Wiley Interdisciplinary Reviews: Computational Statistics*, *2*(2), 128–149. https://doi.org/10.1002/wics.73

Koti, V. (2018). *attributed to uniform dispersion of carbon nanotubes and formation of carbonaceous layer on the d M us*.

Krinitcyn, M. (2022). *Structure, Phase Composition, and Properties of Ti 3 AlC 2 —Nano-Cu Powder Composites*. 1–11.

Kumar, A., Vichare, O., Debnath, K., & Paswan, M. (2020). Fabrication methods of metal matrix composites (MMCs). *Materials Today: Proceedings*, *46*(xxxx), 6840–6846. https://doi.org/10.1016/j.matpr.2021.04.432

Kumar, J., & Mondal, S. (2018). Microstructure and properties of graphite-reinforced copper matrix composites. *Journal of the Brazilian Society of Mechanical Sciences and Engineering*, *40*(4), 1–10. https://doi.org/10.1007/s40430-018-1115-7

Kumar, N., Bharti, A., Dixit, M., & Nigam, A. (2020). Effect of Powder Metallurgy Process and its Parameters on the Mechanical and Electrical Properties of Copper-Based Materials: Literature Review. *Powder Metallurgy and Metal Ceramics*, *59*(7–8), 401–410. https://doi.org/10.1007/s11106-020-00174-1

Kumar, S., Singh, R., & Hashmi, M. S. J. (2020). Metal matrix composite: a methodological review. *Advances in Materials and Processing Technologies*, *6*(1), 13–24. https://doi.org/10.1080/2374068X.2019.1682296

Kumar Singh, M., Kumar Gautam, R., Prakash, R., & Ji, G. (2018). Mechanical and corrosion behaviors of developed copper-based metal matrix composites. *IOP Conference Series: Materials Science and Engineering*, *330*(1). https://doi.org/10.1088/1757-899X/330/1/012021

Lachowicz, M. M. (2020). A metallographic case study of formicary corrosion in heat exchanger copper tubes. *Engineering Failure Analysis*, *111*(January), 104502. https://doi.org/10.1016/j.engfailanal.2020.104502

Lian, W., Mai, Y., Wang, J., Zhang, L., Liu, C., & Jie, X. (2019). Fabrication of graphene oxide-Ti3AlC2 synergistically reinforced copper matrix composites with enhanced tribological performance. *Ceramics International*, *45*(15), 18592–18598. https://doi.org/10.1016/j.ceramint.2019.06.082

Lomakin, I., Castillo-Rodríguez, M., & Sauvage, X. (2019). Microstructure, mechanical properties and aging behavior of nanocrystalline copper-beryllium alloy. *Materials Science and Engineering: A*, *744*, 206–214. https://doi.org/10.1016/j.msea.2018.12.011

LÓPEZ, R., NAMIGTLE, J., & MASTACHE, J. (2021). Structural characterization of copper oxide by X-ray diffraction. *Handbooks Engineering Science and Technology TIX*, 70–96. https://doi.org/10.35429/h.2021.9.1.70.96

Lu, R., Liu, B., Cheng, H., Gao, S., Li, T., Li, J., & Fang, Q. (2022). Microstructure and Properties of a Graphene Reinforced Cu–Cr–Mg Composite. *Materials*, *15*(17). https://doi.org/10.3390/ma15176166

Mahapatra, T. R., Panda, S. K., & Kar, V. R. (2016). Geometrically nonlinear flexural analysis of hygro-thermo-elastic laminated composite doubly curved shell panel. *International Journal of Mechanics and Materials in Design*, *12*(2), 153–171. https://doi.org/10.1007/s10999-015-9299-9

Malghan, R. L., Rao, K. M. C., Shettigar, A. K., Rao, S. S., & D'Souza, R. J. (2017). Application of particle swarm optimization and response surface methodology for machining parameters optimization of aluminium matrix composites in milling operation. *Journal of the Brazilian Society of Mechanical Sciences and Engineering*, *39*(9), 3541–3553. https://doi.org/10.1007/s40430-016-0675-7

Marashi, J., Yakushina, E., Xirouchakis, P., Zante, R., & Foster, J. (2017). An evaluation of H13 tool steel deformation in hot forging conditions. *Journal of Materials Processing Technology*, *246*, 276–284. https://doi.org/10.1016/j.jmatprotec.2017.03.026

Matli, P. R., Manakari, V., Parande, G., Mattli, M. R., Shakoor, R. A., & Gupta, M. (2020). Improving mechanical, thermal and damping properties of niti (Nitinol) reinforced aluminum nanocomposites. *Journal of Composites Science*, *4*(1), 18–21. https://doi.org/10.3390/jcs4010019

Mazaheri, Y., Bahiraei, M., Jalilvand, M. M., Ghasemi, S., & Heidarpour, A. (2021). Improving mechanical and tribological performances of pure copper matrix surface composites reinforced by Ti2AlC MAX phase and MoS2 nanoparticles. *Materials Chemistry and Physics*, *270*(May), 124790. https://doi.org/10.1016/j.matchemphys.2021.124790

Meignanamoorthy, M., & Ravichandran, M. (2018). Synthesis of metal matrix composites via powder metallurgy route: A review. *Mechanics and Mechanical Engineering*, *22*(1), 65–75. https://doi.org/10.2478/mme-2018-0007

Mohapatra, S. K., & Maity, K. P. (2016). Parametric Optimization of Simulated Extrusion of Square to Square Section Through Linear Converging Die. *IOP Conference Series: Materials Science and Engineering*, *115*(1). https://doi.org/10.1088/1757-899X/115/1/012031

Nagavally, R. R. (2016). Composite Materials - History, Types, Fabrication Techniques, Advantages, and Applications. *International Journal of Mechanical And Production Engineering*, *2*, 25–30.

Nazeer, F., Ma, Z., Gao, L., Wang, F., Khan, M. A., & Malik, A. (2019). Thermal and mechanical properties of copper-graphite and copper-reduced graphene oxide composites. *Composites Part B: Engineering*, *163*, 77–85. https://doi.org/10.1016/j.compositesb.2018.11.004

Nie, H., Fu, L., Zhu, J., Yang, W., Li, D., & Zhou, L. (2018). Excellent tribological properties of lower reduced graphene oxide content copper composite by using a one-step reduction molecular-level mixing process. *Materials*, *11*(4). https://doi.org/10.3390/ma11040600

Nwobi-Okoye, C. C., & Uzochukwu, C. U. (2020). RSM and ANN modeling for production of Al 6351/ egg shell reinforced composite: Multi objective optimization using genetic algorithm. *Materials Today Communications*, *22*(August), 100674. https://doi.org/10.1016/j.mtcomm.2019.100674

Özgün, & Bulut, C. (2020). A novel mixing method for powder metallurgy copper-carbon nanotube composites. *Materialwissenschaft Und Werkstofftechnik*, *51*(7), 982–991. https://doi.org/10.1002/mawe.201900149

Panwar, N., & Chauhan, A. (2018). Fabrication methods of particulate reinforced Aluminium metal matrix composite-A review. *Materials Today: Proceedings*, *5*(2), 5933–5939. https://doi.org/10.1016/j.matpr.2017.12.194

Patel, M., Pardhi, B., Prasad Sahu, D., & Sahu, S. K. (2021). Different Techniques Used for Fabrication of Aluminium Metal Matrix Composites. *International Journal of Engineering and Techniques*, *7*(1), 1–8. https://doi.org/10.29126/23951303/ijet-v7i1p1

Ponraj, N. V., Azhagurajan, A., Vettivel, S. C., Sahaya Shajan, X., Nabhiraj, P. Y., & Sivapragash, M. (2017). Graphene nanosheet as reinforcement agent in copper matrix composite by using powder metallurgy method. *Surfaces and Interfaces*, *6*, 190–196. https://doi.org/10.1016/j.surfin.2017.01.010

Rajak, D. K., Pagar, D. D., Kumar, R., & Pruncu, C. I. (2019). Recent progress of reinforcement materials: A comprehensive overview of composite materials. *Journal of Materials Research and Technology*, *8*(6), 6354–6374. https://doi.org/10.1016/j.jmrt.2019.09.068

Rajeswari, B., & Amirthagadeswaran, K. S. (2018). Study of machinability and parametric optimization of end milling on aluminium hybrid composites using multi-objective genetic algorithm. *Journal of the Brazilian Society of Mechanical Sciences and Engineering*, *40*(8), 1–15. https://doi.org/10.1007/s40430-018-1293-3

Reddy, A. C. (2007). *CMC Effect of Clustering Induced Porosity on Micromechanical Properties of AA6061 / Titanium Oxide Particulate Metal Matrix Composites*. *June*, 149–154.

Reza Rezaie, H., Beigi Rizi, H., Rezaei Khamseh, M. M., & Öchsner, A. (2020). Application of the Finite Element Method in Dentistry. *Advanced Structured Materials*, *123*, 211–224. https://doi.org/10.1007/978-3-030-48931-1_7

Riswanto, F. D. O., Rohman, A., Pramono, S., & Martono, S. (2019). Application of response surface methodology as mathematical and statistical tools in natural product research. *Journal of Applied Pharmaceutical Science*, *9*(10), 125–133.

https://doi.org/10.7324/JAPS.2019.91018

Rondelli, G., & Vicentini, B. (2002). Effect of copper on the localized corrosion resistance of Ni-Ti shape memory alloy. *Biomaterials*, *23*(3), 639–644. https://doi.org/10.1016/S0142-9612(01)00142-9

Saber, D., El-Aziz, K. A., Felemban, B. F., Alghtani, A. H., Ali, H. T., Ahmed, E. M., & Megahed, M. (2022). Characterization and performance evaluation of Cu-based/TiO2 nano composites. *Scientific Reports*, *12*(1), 1–14. https://doi.org/10.1038/s41598-022-10616-y

Sahu, P. S., & Banchhor, R. (2016). Fabrication methods used to prepare Al metal matrix composites- A review. *International Research Journal of Engineering and Technology*, *03*(10), 123–132.

Sajan, S., & Philip Selvaraj, D. (2021). A review on polymer matrix composite materials and their applications. *Materials Today: Proceedings*, *47*(xxxx), 5493–5498. https://doi.org/10.1016/j.matpr.2021.08.034

Samal, P., Tarai, H., Meher, A., Surekha, B., & Vundavilli, P. R. (2023). Effect of SiC and WC Reinforcements on Microstructural and Mechanical Characteristics of Copper Alloy-Based Metal Matrix Composites Using Stir Casting Route. *Applied Sciences (Switzerland)*, *13*(3). https://doi.org/10.3390/app13031754

Şap, S., Uzun, M., Usca, Ü. A., Pimenov, D. Y., Giasin, K., & Wojciechowski, S. (2021). Investigation on microstructure, mechanical, and tribological performance of Cu base hybrid composite materials. *Journal of Materials Research and Technology*, *15*, 6990–7003. https://doi.org/10.1016/j.jmrt.2021.11.114

Satishkumar, P., Mahesh, G., Meenakshi, R., & Vijayan, S. N. (2020). Tribological characteristics of powder metallurgy processed Cu-WC/SiC metal matrix composites. *Materials Today: Proceedings*, *37*(Part 2), 459–465. https://doi.org/10.1016/j.matpr.2020.05.449

Selvam, J. D. R., Dinaharan, I., & Rai, R. S. (2021). Matrix and Reinforcement Materials for Metal Matrix Composites. *Encyclopedia of Materials: Composites*, *2*(February), 615–639. https://doi.org/10.1016/B978-0-12-803581-8.11890-9

Seo, J. Y., Kang, H. W., Jung, D. S., Lee, H. M., & Park, S. Bin. (2013). One-step synthesis of copper nanoparticles embedded in carbon composites. *Materials Research Bulletin*, *48*(4), 1484–1489. https://doi.org/10.1016/j.materresbull.2012.12.070

Sharma, A. K., Bhandari, R., Aherwar, A., & Pinca-Bretotean, C. (2020). A study of fabrication methods of aluminum based composites focused on stir casting process. *Materials Today: Proceedings*, *27*, 1608–1612. https://doi.org/10.1016/j.matpr.2020.03.316

Sharma, D. K., Mahant, D., & Upadhyay, G. (2019). Manufacturing of metal matrix composites: A state of review. *Materials Today: Proceedings*, *26*, 506–519. https://doi.org/10.1016/j.matpr.2019.12.128

Singh, K., Khanna, V., Sonu, Singh, S., Bansal, S. A., Chaudhary, V., & Khosla, A. (2023). Paradigm of state-of-the-art CNT reinforced copper metal matrix composites: processing, characterizations, and applications. *Journal of Materials Research and Technology*, *24*, 8572–8605. https://doi.org/10.1016/j.jmrt.2023.05.083

Singh, M. K., & Gautam, R. K. (2018). Mechanical and tribological properties of plastically deformed copper metal matrix nano composite. *Materials Today: Proceedings*, *5*(2), 5727–5736. https://doi.org/10.1016/j.matpr.2017.12.168

Singh, M. K., & Gautam, R. K. (2019). Structural, Mechanical, and Electrical Behavior of Ceramic-Reinforced Copper Metal Matrix Hybrid Composites. *Journal of Materials Engineering and Performance*, *28*(2), 886–899. https://doi.org/10.1007/s11665-019-3860-x

Singh, R., Sharma, A. K., & Sharma, A. K. (2021). Physical and mechanical behavior of NiTi composite fabricated by newly developed uni-axial compaction die. *Materials Research*, *24*(3). https://doi.org/10.1590/1980-5373-MR-2020-0549

Situmorang, R. S., & Kawai, H. (2018). Investigating the mechanism behind “ant nest” corrosion on copper tube. *Materials*, *11*(4), 18–20. https://doi.org/10.3390/ma11040533

Slowik, A., & Kwasnicka, H. (2020). Evolutionary algorithms and their applications to engineering problems. *Neural Computing and Applications*, *32*(16), 12363–12379. https://doi.org/10.1007/s00521-020-04832-8

Srirekha, A., & Bashetty, K. (2010). Infinite to finite: An overview of finite element analysis. *Indian Journal of Dental Research*, *21*(3), 425–432. https://doi.org/10.4103/0970-9290.70813

Talabi, H. K., Adewuyi, B. O., Olaniran, O., & Ayekusibe, P. O. (2021). Reinforcement Efficiency of Copper Nanoparticles on Epoxy Matrix Bactericide Composite. *Journal of Chemical Technology and Metallurgy*, *56*(2), 321–326.

Tanaka, T., Sugioka, T., Kobayashi, T., Shohji, I., Shimada, Y., Watanabe, H., & Kamakoshi, Y. (2021). Low cycle fatigue characteristics of oxygen-free copper for electric power equipment. *Materials*, *14*(15). https://doi.org/10.3390/ma14154237

Thankachan, T., Soorya Prakash, K., & Kamarthin, M. (2018). Optimizing the Tribological Behavior of Hybrid Copper Surface Composites Using Statistical and Machine Learning Techniques. *Journal of Tribology*, *140*(3). https://doi.org/10.1115/1.4038688

Ti, A., Composites, A., Strength, H., & Conduc-, H. (2017). Ag/Ti3AlC2 Composites with High Hardness, High Strength and High Conductivity. *Materials Letters*. https://doi.org/10.1016/j.matlet.2017.11.038

Tiwari, A., Kumar, N., & Banerjee, M. K. (2024). Applications of genetic algorithm in prediction of the best achievable combination of hardness and tensile strength for graphene reinforced magnesium alloy (AZ61) matrix composite. *Results in Control and Optimization*, *14*. https://doi.org/10.1016/j.rico.2023.100334

Tokutomi, J., Uemura, T., Sugiyama, S., Shiomi, J., & Yanagimoto, J. (2015). Hot extrusion to manufacture the metal matrix composite of carbon nanotube and aluminum with excellent electrical conductivities and mechanical properties. *CIRP Annals - Manufacturing Technology*, *64*(1), 257–260. https://doi.org/10.1016/j.cirp.2015.04.083

Venkatesh, B., & Harish, B. (2015). MECHANICAL PROPERTIES OF METAL MATRIX COMPOSITES (Al/SiCp) PARTICLES PRODUCED BY POWDER METALLURGY. *International Journal of Engineering Research and General Science*, *3*(1), 1277–1284.

Wang, N., Chen, Y. N., Zhang, L., Li, Y., Liu, S. S., Zhan, H. F., Zhu, L. X., Zhu, S. D., & Zhao, Y. Q. (2019). Isothermal diffusion behavior and surface performance of Cu/Ni coating on TC4 alloy. *Materials*, *12*(23). https://doi.org/10.3390/ma122333884

Wang, X. H., & Zhou, Y. C. (2002). Microstructure and properties of Ti3AlC2 prepared by the solid-2002.pdf. *Acta Materialia*, *50*, 3141–3149.

Workie, F., & Tesfaye, A. (2021). *Analytical and Numerical Analysis of Extrusion Force , Stress and Strain Development During Extrusion Al6063-SiC Composite*. *5*(1), 1–16. https://doi.org/10.11648/j.cm.20200501.11

Yoganandam, K., Mohanavel, V., Vairamuthu, J., & Kannadhasan, V. (2020). Mechanical properties of titanium matrix composites fabricated via powder metallurgy method. *Materials Today: Proceedings*, *33*(xxxx), 3243–3247. https://doi.org/10.1016/j.matpr.2020.04.569

Zainuddin, F. A., & Samad, M. F. A. (2020). A review of crossover methods and problem representation of genetic algorithm in recent engineering applications. *International Journal of Advanced Science and Technology*, *29*(6), 759–769.

Zhang, T., Wang, Z., Wang, Y., & Chen, Z. (2019). Experimental study on the mechanical properties of oxygen-free copper used in high energy physics detectors and accelerators. *Nuclear Instruments and Methods in Physics Research, Section A: Accelerators, Spectrometers, Detectors and Associated Equipment*, *935*(April), 8–16. https://doi.org/10.1016/j.nima.2019.04.112

Zhang, X., Xu, Y., Wang, M., Liu, E., Zhao, N., Shi, C., Lin, D., Zhu, F., & He, C. (2020). A powder-metallurgy-based strategy toward three-dimensional graphene-like network for reinforcing copper matrix composites. *Nature Communications*, *11*(1), 1–13. https://doi.org/10.1038/s41467-020-16490-4

Zheng, Z., Yang, A., Tao, J., Li, J., Zhang, W., Li, X., & Xue, H. (2022). Mechanical and Conductive Properties of Cu Matrix Composites Reinforced by Oriented Carbon Nanotubes with Different Coatings. *Nanomaterials*, *12*(2). https://doi.org/10.3390/nano12020266

APPENDIXS

APPENDIX 1: MATLAB Code for Damage Value

```
clear all
clc
close all

%% Define Objective Function and Constraints
POWER = @(x) +(3.3+0.010.*x(1)-
0.247.*x(2)+0.0104.*x(3)+0.0072.*x(1).*x(1)+0.0625.*x(2).*
x(2)-
0.0000077.*x(3).*x(3)+0.0049.*x(1).*x(2)+0.000189.*x(1).*x
(3)+0.000058.*x(2).*x(3)); % maximize objective function
g1 = @(x) x(1) - 4; % constraint 4
g2 = @(x) x(2) - 3; % constraint 2
g3 = @(x) x(3) - 850; % constrain

%% Define Genetic Algorithm Parameters
nvars = 3; % number of decision variables
lb = [2, 1, 750]; % lower bounds of decision variables
ub = [4, 3, 850]; % upper bounds of decision variables
options = optimoptions('ga', 'Display', 'iter',
'PopulationSize', 1000, ...
    'MaxGenerations', 100, 'FunctionTolerance', 1e-6,
'PlotFcn', @gaplotbestf);

%% Run Genetic Algorithm
[x, fval] = ga(POWER, nvars, [], [], [], [], lb, ub, ...
    @(x) deal([g1(x), g2(x), g3(x)], []), options);

%% Display Results
disp('Optimization Results:')
disp(['Damage value: ', num2str(-fval)])
disp(['OPTIMUM VALUE OF ER, RS, BT: ', num2str(x)])

%% Generate Surface Plot
% Define range of values for decision variables 1 and 2
n = 30; % number of points
d_range = linspace(lb(2), ub(2), n);
h_range = linspace(lb(3), ub(3), n);
[d_grid, h_grid] = meshgrid(d_range, h_range);

% Evaluate objective function at each point in the range
```

```
f_grid = zeros(size(d_grid));
for i = 1:numel(d_grid)
    x = [x(1), d_grid(i), h_grid(i), x(3)];
    f_grid(i) = POWER(x);
end

% Create surface plot
figure();
surf(d_grid, h_grid, -f_grid);
xlabel('Ram speed');
ylabel('Billet temperature');
zlabel('Damage value');
title('Surface Plot of Damage vs. Ram speed and billet temperature');
```

Appendix2:MATLAB Code for Extrusion Load

```
clear all
clc
close all

%% Define Objective Function and Constraints
POWER = @(x) -(34300+12900.*x(1)+812.5.*x(2)+37.5.*x(3)-
6150.*x(1).*x(1)+925.*x(2).*x(2)-
775.*x(3).*x(3)+225.*x(1).*x(2)-
525.*x(1).*x(3)+400.1.*x(2).*x(3)); % maximize objective
function
g1 = @(x) x(1) - 4; % constraint 4
g2 = @(x) x(2) - 3; % constraint 2
g3 = @(x) x(3) - 850; % constrain

%% Define Genetic Algorithm Parameters
nvars = 3; % number of decision variables
lb = [2, 1, 750]; % lower bounds of decision variables
ub = [4, 3, 850]; % upper bounds of decision variables
options = optimoptions('ga', 'Display', 'iter',
'PopulationSize', 1000, ...
    'MaxGenerations', 100, 'FunctionTolerance', 1e-6,
'PlotFcn', @gaplotbestf);

%% Run Genetic Algorithm
[x, fval] = ga(POWER, nvars, [], [], [], [], lb, ub, ...
    @(x) deal([g1(x), g2(x), g3(x)], []), options);

%% Display Results
```

```matlab
disp('Optimization Results:')
disp(['Extrusion load In (N): ', num2str(-fval)])
disp(['OPTIMUM VALUE OF ER, RS, BT: ', num2str(x)])

%% Generate Surface Plot
% Define range of values for decision variables 1 and 2
n = 30; % number of points
d_range = linspace(lb(2), ub(2), n);
h_range = linspace(lb(3), ub(3), n);
[d_grid, h_grid] = meshgrid(d_range, h_range);

% Evaluate objective function at each point in the range
f_grid = zeros(size(d_grid));
for i = 1:numel(d_grid)
    x = [x(1), d_grid(i), h_grid(i), x(3)];
    f_grid(i) = POWER(x);
end

% Create surface plot
figure();
surf(d_grid, h_grid, -f_grid);
xlabel('Ram speed');
ylabel('Billet temperature');
zlabel('Extrusion load');
title('Surface Plot of Extrusion Load vs. Ram speed and
billet temperature');
```

APPendix3: Hardness (HV) results of (a) sample 2 and (b) sample 3

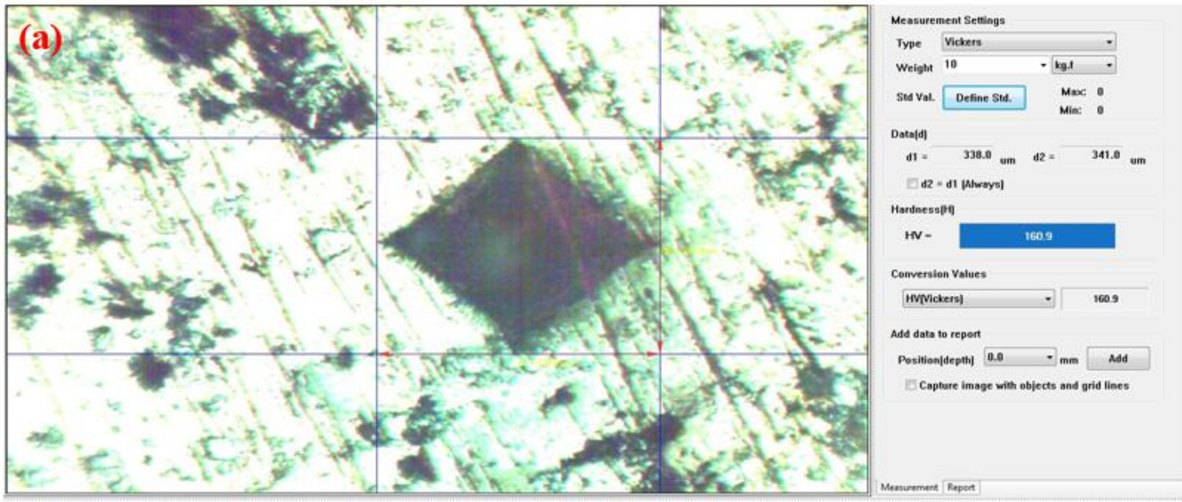

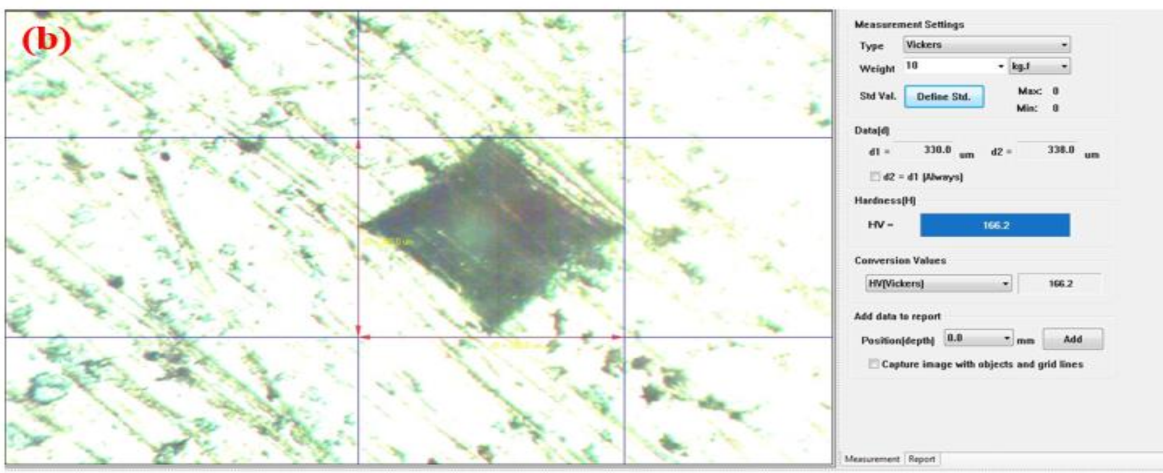

Appendix4: Wear and fractional force graph of (a) Sample 3 and (b) Sample 4

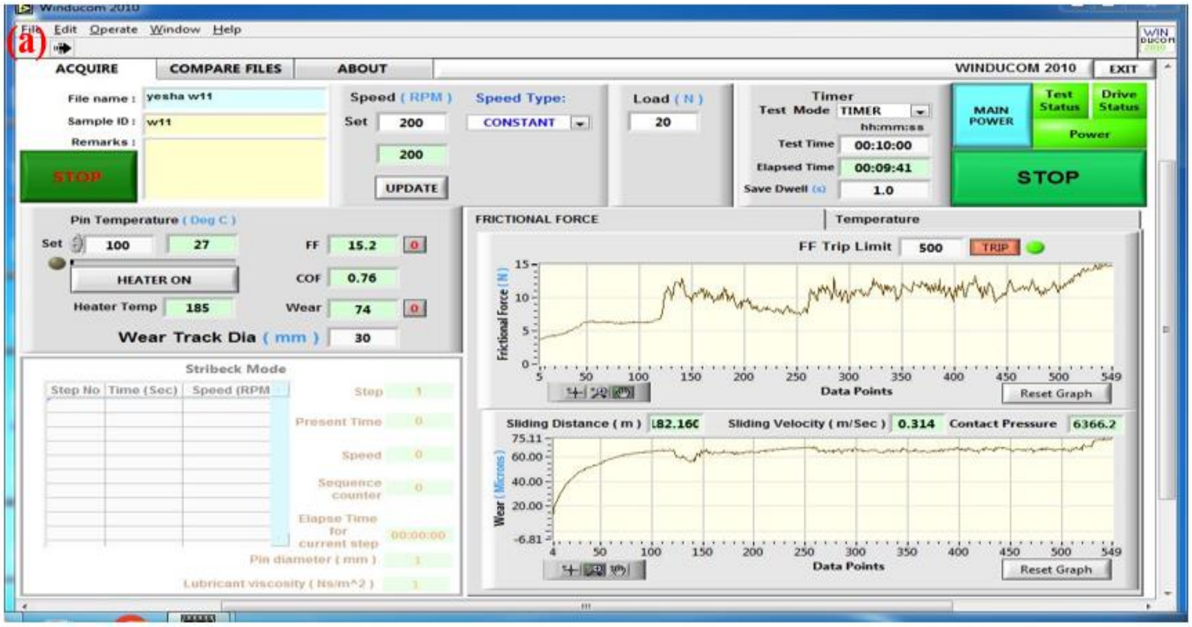

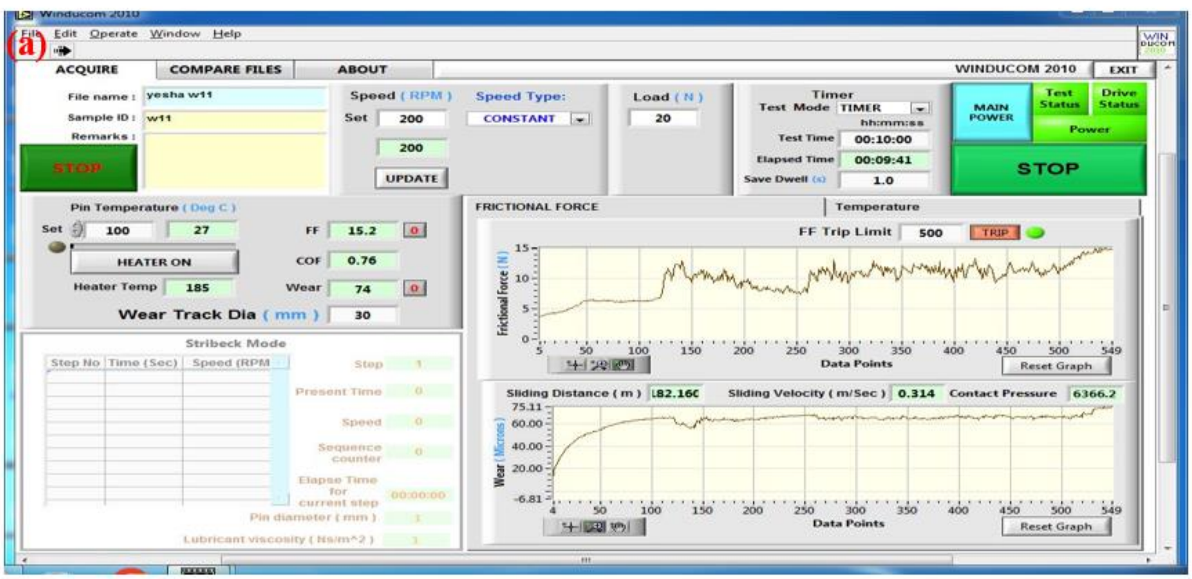

Appendix5: Stress-strain graph for Sample 3

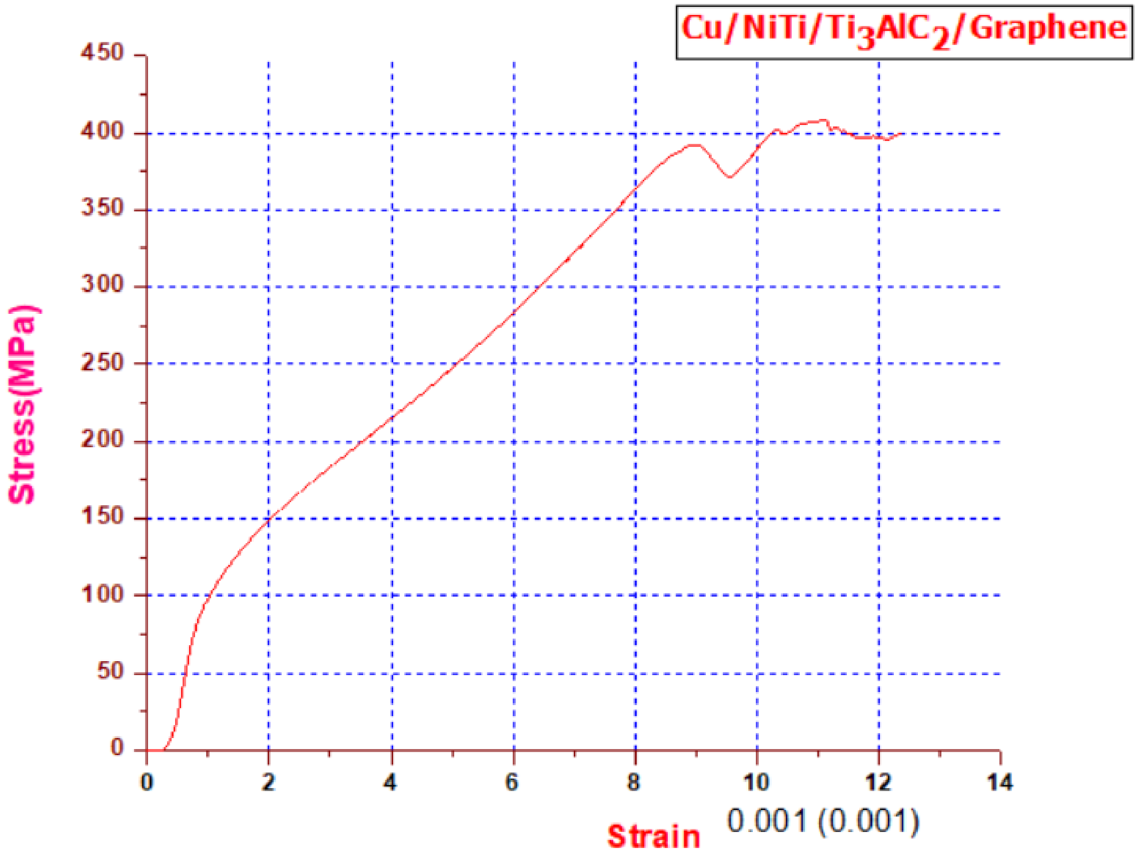

Appendix7: Distribution of (a) effective strain (b) damage value and (c) extrusion ratio of Cu/NiTi/Ti_3AlC_2/Graphene

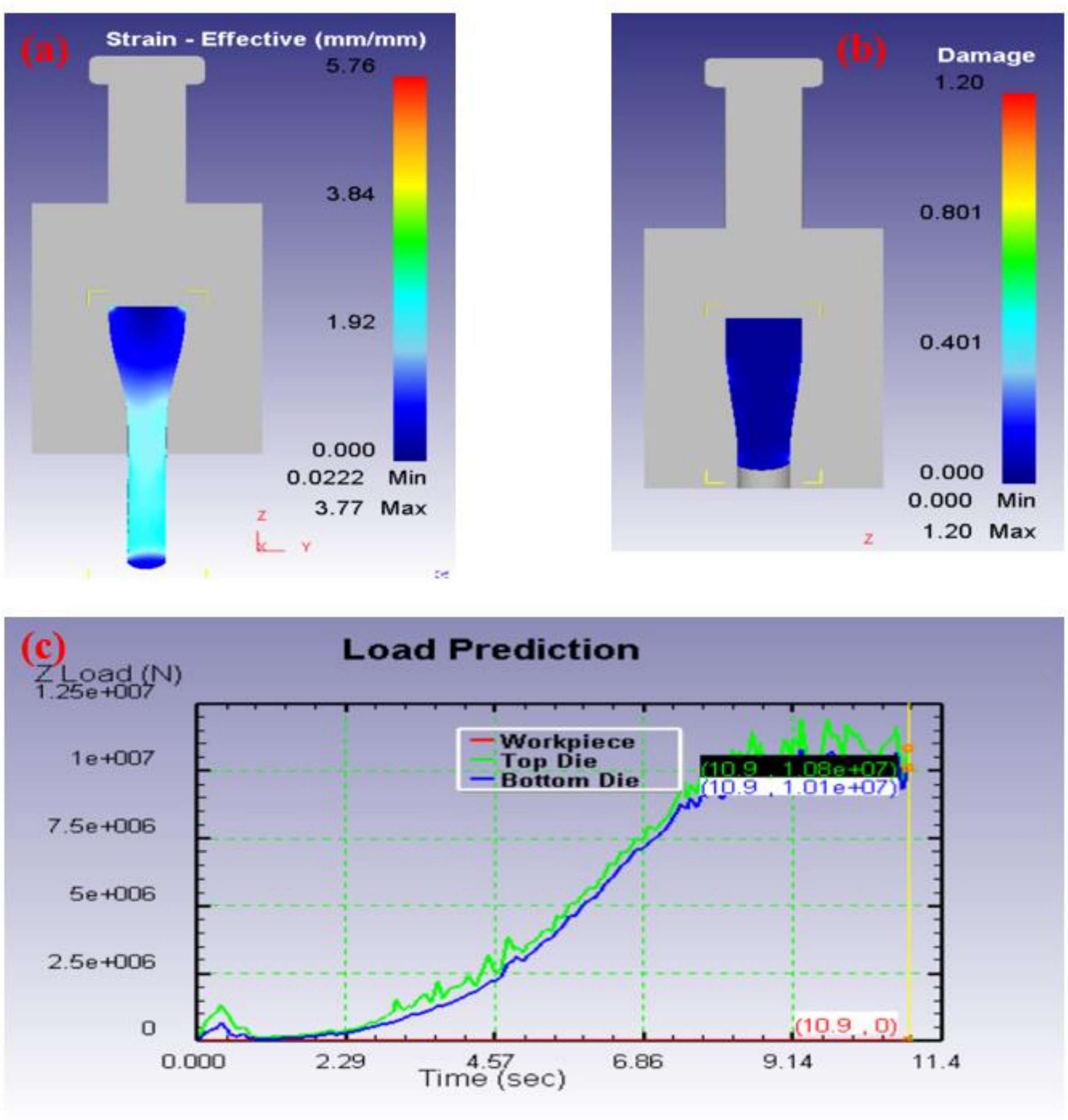

Appendix8: Tafel plot analysis